

*SCIENCO*  
**SOUTHERN BRAZILIAN JOURNAL  
OF CHEMISTRY**

**ISSN 0104-5431**

**AN INTERNATIONAL FORUM FOR THE RAPID PUBLICATION  
OF ORIGINAL SCIENTIFIC ARTICLES DEALING WITH CHEMISTRY AND  
RELATED INTERDISCIPLINARY AREAS**

**VOLUME FIVE, NUMBER FIVE**

**DECEMBER 1997**

## EDITOR

LAVINEL G. IONESCU, Departamento de Química, CENE, Universidade Luterana do Brasil, Canoas, RS & Instituto de Química, Pontifícia Universidade Católica do Rio Grande do Sul, Porto Alegre, RS, BRASIL

## EDITORIAL BOARD

- D. BALASUBRAMANIAN, Centre for Cellular and Molecular Biology, Hyderabad, INDIA  
HÉCTOR E. BERTORELLO, Departamento de Química Orgánica, Facultad de Ciencias Químicas, Universidad Nacional de Córdoba, Córdoba, ARGENTINA  
AÉCIO P. CHAGAS, Instituto de Química, UNICAMP, Campinas, SP, BRASIL  
JUAN JOSÉ COSA, Departamento de Química y Física, Facultad de Ciencias Exactas, Universidad Nacional de Río Cuarto, Río Cuarto, ARGENTINA  
GLENN A. CROSBY, Department of Chemistry, Washington State University, Pullman, WA, USA  
VITTORIO DEGIORGIO, Dipartimento di Elettronica, Sezione di Fisica Applicata, Università di Pavia, Pavia, ITALIA  
JOSÉ C. TEIXEIRA DIAS, Departamento de Química, Universidade de Coimbra, Coimbra, PORTUGAL  
XORGE A. DOMÍNGUEZ, Departamento de Química, Instituto Tecnológico y de Estudios Superiores de Monterrey, Monterrey, N.L., MÉXICO  
OMAR A. EL SEUDI, Instituto de Química, Universidade de São Paulo, São Paulo, SP, BRASIL  
ERNESTO GIESBRECHT, Instituto de Química, Universidade de São Paulo, São Paulo, SP, BRASIL  
FERNANDO GALEMBECK, Instituto de Química, UNICAMP, Campinas, SP, BRASIL  
NISSIM GARTI, Casali Institute of Applied Science, Hebrew University of Jerusalem, Jerusalem, ISRAEL  
GASPAR GONZALEZ, Centro de Pesquisa, CENPES-PETROBRAS, Ilha do Fundão, Rio de Janeiro, RJ, BRASIL  
YOSHITAKA GUSHIKEM, Instituto de Química, UNICAMP, Campinas, SP, BRASIL  
WILLIAM HASE, Department of Chemistry, Wayne State University, Detroit, MI, USA  
I. B. IVANOV, Laboratory of Thermodynamics and Physico-chemical Hydrodynamics, Faculty of Chemistry, University of Sofia, Sofia, BULGARIA  
IVAN IZQUIERDO, Departamento de Bioquímica, Universidade Federal do Rio Grande do Sul, Porto Alegre, RS, BRASIL  
V.A. KAMINSKY, Karpov Institute of Physical Chemistry, Moscow, RUSSIA  
MICHAEL LAING, Department of Chemistry, University of Natal, Durban, SOUTH AFRICA  
EDUARDO LISSI, Departamento de Química, Universidad de Santiago de Chile, Santiago, CHILE  
WALTER LWOWSKI, Department of Chemistry, New Mexico State University, Las Cruces, N.M., USA  
C. MANOHAR, Bhabha Atomic Research Centre, Chemistry Division, Bombay, INDIA  
AYRTON FIGUEIREDO MARTINS, Departamento de Química, Universidade Federal de Santa Maria, Santa Maria, RS, BRASIL  
FRED MENCER, Department of Chemistry, Emory University, Atlanta, GA, USA  
MICHAEL J. MINCH, Department of Chemistry, University of the Pacific, Stockton, CA, USA  
E. L. MITTAL, IBM Corporate Technical Institutes, Thornwood, N.Y., USA  
ARNO MÜLLER, Escola de Engenharia, Universidade Federal do Rio Grande do Sul, Porto Alegre, RS, BRASIL  
JOSE MIGUEL PARRERA, Instituto de Investigaciones en Catalisis y Petroquímica, Universidad Nacional del Litoral, Santa Fe, ARGENTINA  
LARRY RIMSTED, Department of Chemistry, Rutgers University, Piscataway N.J., USA  
GILBERTO FERNANDES DE SA, Departamento de Química Fundamental, Universidade Federal de Pernambuco, Recife, PE, BRASIL  
DIMITRIOS SAMIOS, Instituto de Química, Universidade Federal do Rio Grande do Sul, Porto Alegre, RS, BRASIL  
DIOGENES DOS SANTOS, Department of Molecular Biology, Oxford University, Oxford, ENGLAND  
JOSEPH A. SCHUFLÉ, Department of Chemistry, New Mexico Highlands University, Las Vegas, N.M., USA  
BEN K. SELINGER, Department of Chemistry, Australian National University, Canberra, AUSTRALIA  
KORO SHINODA, Department of Applied Chemistry, Faculty of Engineering, Yokohama National University, Yokohama, JAPAN  
CRISTOFOR I. SIMIONESCU, Academia Română, Filială Iasi, Iasi, ROMANIA  
UMBERTO TONELLATO, Dipartimento di Chimica Organica, Università degli Studi di Padova, Padova, ITALIA  
DIETER VOLLMER, Max Planck Institut für Kolloid und Grenzflächenforschung, Berlin, GERMANY  
RADUL ZANA, Institut Charles Sadron, CRM-EAHP, Strassbourg, FRANCE

# SOUTHERN BRAZILIAN JOURNAL OF CHEMISTRY

ISSN 0104-5431

VOLUME FIVE, NUMBER FIVE

DECEMBER 1997

## CONTENTS / CONTEÚDO

ANDRÉS MANUEL DEL RIO, DISCOVERER OF VANADIUM Lavinel G. Ionescu .....	1
STUDY OF SOME ENVIRONMENTAL IMPLICATIONS DUE TO THE DISPOSAL OF ASHES FROM THE SÃO JERONIMO POWER STATION-RS Haidi D. Fiedler, Manuel Carneiro and Elba C. Teixeira ...	7
X-RAY STUDIES ON $Tl_2HgI_4$ , $PbHgI_4$ , $CdHgI_4$ AND $Au_2HgI_4$ INORGANIC COMBINATIONS Tudor Rosu, Lidia Paruta, Mirela Calinescu and Anca Emandi .....	21
SOLID SUBSTRATE FERMENTATION OF CACTUS PULP BY ASPERGILLUS NIGER Arnaldo D.S. Júnior, Rosangela B. Garcia, Dina G. Rodrigues and Jorge Nozaki .....	35
SOME NEW N-BENZOYL-N'-SUBSTITUTED PHENYL THIOUREA COMPLEXES OF COPPER(II) Tudor Rosu, Viorel Cărcu, Maria Negoiu, Ovidiu Maior and Niculina Badicu .....	43
THE PÉRCIO DE MORAES BRANCO COLLECTION OF RARE MINERALS OF THE UNIVERSIDADE LUTERANA DO BRASIL (ULBRA) Paulo César Pereira das Neves, Pércio de Moraes Branco and Paulo Anselmo Mاتيoli .....	51
TRANSITION METAL COMPLEXES OF THE FORMYL VANILLINE DERIVATIVES LIGAND FAMILY Tudor Rosu, Angela Kriza, Viorel Cărcu and Anca Nicolae .....	67
SORPTION AND SEPARATION OF Cu(II), Co(II) AND Ni(II) ON 1(4'-AZOBENZYLCELLULOSE)-2-NAPHTHOL Tinca Onofrei, Cecilia Arsene and Carmen Mita .....	79
COORDINATION COMPOUNDS OF Cu(II) AND Ni(II) WITH SCHIFF BASES DERIVED FROM FORMYL CARVONE AND o,p-AMINOBENZOIC ACID Adalgiza Ciobanu, Florica Zalaru, D. Albinescu and Christina Zalaru .....	87
REACTIVE EXTRACTION OF DICARBOXYLIC ACIDS. I. MECHANISM, LIMITING STEPS AND KINETICS Dan Cascaval, Radu Tudose and Corneliu Oniscu .....	97
THE PHOTODEGRADATION REACTION OF SOME PORPHYRINS Rodica Mariana Ion and Cristina Mandravel .....	111
CHARACTERIZATION OF SOME NODULAR CAST IRONS BY THERMAL ANALYSIS Dumitru Fatu and Maria Muscalu .....	131
AUTHOR INDEX .....	143

## **ANDRÉS MANUEL DEL RIO, DISCOVERER OF VANADIUM**

Lavinel G. Ionescu

Departamento de Química Pura, Instituto de Química  
Pontifícia Universidade Católica do Rio Grande do Sul - PUCRS  
Porto Alegre, RS BRASIL 90610-900

&

Departamento de Química, Centro de Ciências Naturais e Exatas  
Universidade Luterana do Brasil - ULBRA  
Canoas, RS BRASIL 92420-280

### **ABSTRACT**

*Andrés Manuel Del Rio was born in Madrid in 1764 and died in Mexico City in 1849. He studied mineralogy, geology, metallurgy and mining engineering at the Royal Academy of Mines of Almadén and the Patriotic Seminary of Vergara. In 1871, with a stipend from the Spanish Crown, he continued his studies in Paris, Freiberg, Chemnitz and other scientific centers throughout Europe, particularly in metallurgy. In 1794 at the invitation of Don Fausto Delhuyar, who together with his brother Juan José Delhuyar discovered tungsten in 1783, Andrés Manuel Del Rio went to Mexico where he was professor at the School of Mines for more than fifty years, until his death. In 1801, while analyzing a lead mineral from Zimpán, Hidalgo, Mexico, he discovered a new element that he called panchromium or erythronium, because of the red colors, characteristic of its salts. In 1831, the Swedish chemist Nils Gabriel Serfström rediscovered erythronium in an iron ore from Taberg, Småland, Sweden and named it vanadium in honor of the Scandinavian goddess Vanadis.*

### **RESUMO**

*Andrés Manuel Del Rio nasceu em Madrid em 1764 e morreu na Cidade do México em 1849. Estudou mineralogia, geologia, metalurgia e engenharia de minas na Real Academia de Minas de Almadén e no Seminário Patriótico de Vergara. Em 1781, com uma bolsa de estudos da Coroa Espanhola, viajou para Paris, Freiberg, Chemnitz e outros centros metalúrgicos da Europa para trabalhos de especialização. A pedido de Don Fausto Delhuyar, que junto com o seu irmão Juan José descobriu o tungstênio em Vergara em 1781, Andrés Manuel Del Rio foi para México a ocupar o cargo de professor na Escola de Minas onde trabalhou por mais de cinquenta anos, até a sua morte. Em 1801, enquanto analisava um minério de chumbo de Zimpán, Hidalgo, México, descobriu o elemento que ele chamou de pancromo ou eritrônio, devido as cores vermelhas, características de seus sais. Em 1831, o químico sueco Nils Gabriel Serfström redescobriu o eritrônio num minério de ferro proveniente de Taberg, Småland, Suécia e o chamou de vanádio em homenagem à deusa escandinava Vanádia.*

**KEYWORDS** History of Chemistry, Vanadium, Erythronium, Panchromium, Discovery of the Elements.

Contrary to general belief in certain circles, many scientists that were born, lived or worked in Latin America, made important contributions to chemistry. Among them are Bartolomé de Medina who set up amalgamation as an industrial process; Antonio De Ulloa, who was the first to take platinum to Europe; Fausto and Juan José Delhuyar, discoverers of tungsten; Andrés Manuel Del Río, discoverer of vanadium; José Luis Casaseca, founder of the Cuban Institute of Chemical Research in 1848; Alvaro Reynoso, father of modern sugar technology and Luis Frederico Leloir, Nobel laureate in chemistry. Significant contributions were also made by Horacio Damianovich in noble gas chemistry, Gustavo Fester, Xorge Alejandro Dominguez and Otto Gottlieb in natural products and Ernesto Giesbrecht in the chemistry of lanthanides.<sup>1-14</sup> In 1995 the Mexican chemist Mario Molina was awarded the Nobel Prize in Chemistry together with Paul Crutzen and F. Sherwood Rowland for their work on the ozone layer.

Andrés Manuel Del Río was born in Madrid on November 10, 1764 and passed away in Mexico City on March 23, 1849. He studied mineralogy, geology, metallurgy and mining engineering at the Royal Academy of Mines of Almadén and the Patriotic Seminary of Vergara. It was at the School of Mines of Vergara that Fausto and Juan José Delhuyar discovered tungsten or wolfram in 1783.

After completing studies in Spain, Del Río received a stipend from the Spanish Crown and in 1781 travelled to Paris and later Freiberg, Chemnitz (Schemnitz) and other scientific centers throughout Europe. He returned to Spain, more than a decade later, in 1793. In Paris, he studied chemistry with Darcet and acquired experience in porcelain and ceramics manufacturing and processing. In Chemnitz, Freiberg and various metallurgic centers in France, England and other European countries, Del Río specialized in metallurgy and mining engineering. While in Freiberg, he was a devoted student of Abraham Gottlob Werner and became fascinated by mineralogy.

Soon after his return to Spain, at the invitation of Don Fausto Delhuyar, Andrés Manuel Del Río went to Mexico where he was appointed professor at the School of Mines (*Colegio de Minería*). He arrived in Mexico on December 18, 1794. There he lived and worked, with few interruptions, for almost half a century, until his death in 1849.

From 1820 to 1823 he represented Mexico as a deputy in the Spanish Cortes and from 1829 to 1832 he lived in exile in Philadelphia, United States. In 1820 he pleaded for Mexico's independence in the Cortes and in 1829, when the Mexican Government expelled the Spanish (although he was not included among them) he went to exile in Philadelphia, in solidarity with his fellow countrymen.

At the Colegio de Minería (School of Mines), Del Río taught mineralogy, French, geology, mining engineering and metallurgy. He wrote many textbooks including *Arte de las Minas*,



*Geometría Subterránea*, *Tratado de Vetas* (Treatise on Lodes or Mineral Veins) and *Elementos de Orictognosia* (Elements of Fossil Science and Mineralogy). He also translated various manuals including the *New Mineral System of Berzelius*, a *Textbook of Geology*, extracted from *Lethae Geognosticae* by Bronn and annotated, translated and commented Karsten's Mineralogical Tables (*Tablas Mineralógicas de Karsten*).

*Elementos de Orictognosia*, by far the most important work, was first published in two volumes in Mexico in 1795 and 1805. The second expanded edition was divided into two parts, practical and theoretical. The practical part, that Del Río considered more important and included the description of many minerals from Mexico, was published in Philadelphia in 1832 during his exile in the United States. The second or theoretical part was published after his return to Mexico and a thorough revision in 1846. Alexander von Humboldt said that it was the best book on mineralogy in Spanish and Guyton de Morveau considered it the best book on mineralogy in all languages.<sup>11,15</sup>

On the more practical side, Del Río developed a pump for draining water from mines, was the manager of the first formal iron and steel foundry of Latin America in Coalcomán, Michoacán, Mexico from 1805 to 1809, director of the Casa de Moneda (Public Mint), deputy in the Mining Tribunal and honorary councilman of Mexico City.

His main research interest was the study of minerals found in Mexico and in particular of vanadinite,  $\text{PbCl}_2 \cdot 3\text{Pb}_3(\text{VO}_4)_2$ . He published a large number of papers dealing with minerals and geology in the main European journals and also in scientific periodicals from Mexico and the United States.

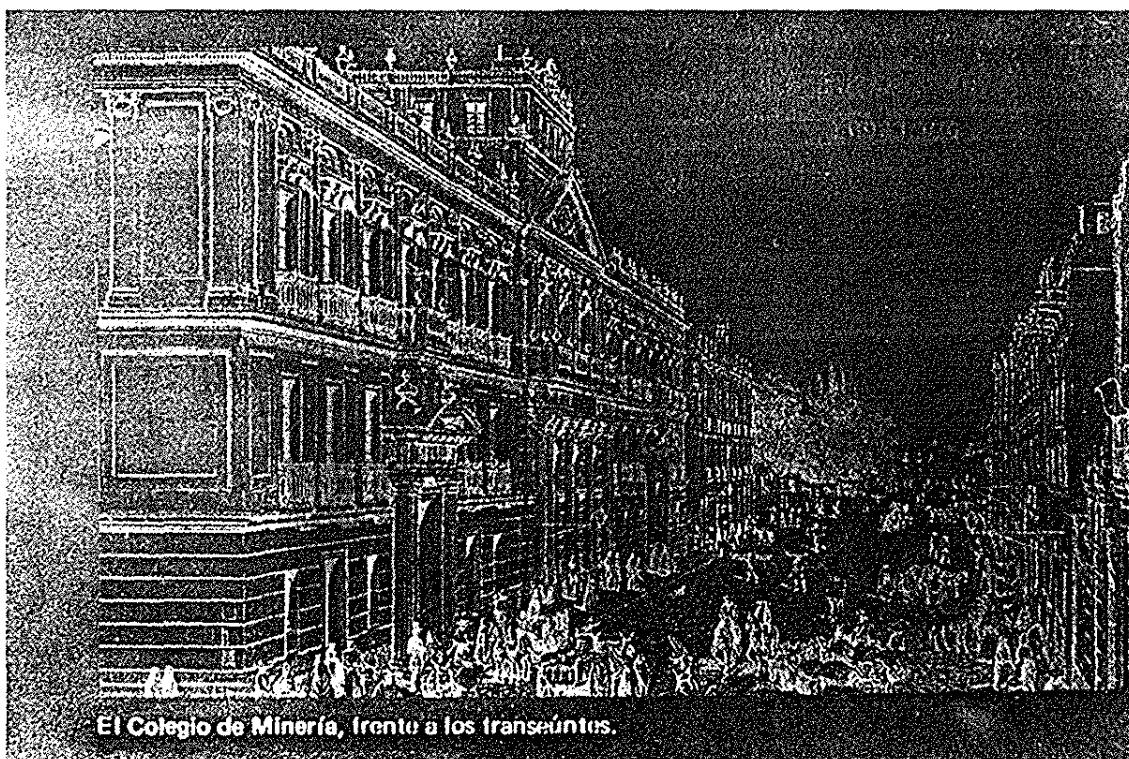
It was in 1801, while analyzing the grey lead mineral vanadinite from Zimapan, Hidalgo, Mexico that Andrés Manuel Del Río discovered a new element that he at first called *panchromium*, because of the many colors of its oxides and later *erythronium*, because of the characteristic red colors of its salts. On September 26, 1802 he communicated his discovery to Don Antonio Cavanilles (Cavanilles), who published it in the *Anales de Ciencias Naturales de Madrid* in May of 1803 (volume VI, Number 16).<sup>16-18</sup>

The discovery, as described by Del Río himself in a footnote on page 61 of *Tablas Mineralógicas de Karsten* published in 1804 is given below,<sup>11,16</sup>

"Habiendo destilado tres ó cuatro veces media onza (de la mena de Zimapan) en polvo con ácido sulfúrico diluido y lavado el residuo a cada vez, tuve una disolución verde, que saturada con exceso de amonía me dio a los pocos días costras compuestas de agujas en la superficie del líquido o estrellitas compuestas de pirámides muy agudas en las paredes de la copilla. Estos cristallitos, que eran blancos, lavados en muy poca agua, porque se disuelven en frío y secados al aire libre, tomaron el más bello roxo de escarlata inmediatamente que tocaron una sola gota de ácido concentrado; quando estaba diluido, se ponían primero amarillos y luego rojos. Estos ácidos los disolvía sin descomponerlos. Lo mismo sucedió con la potasa, la sosa, la cal, etc., excepto que los



ANDRÉS MANUEL DEL RÍO (1764-1849),  
DISCOVERER OF VANADIUM.



El Colegio de Minería, frente a los transeúntes.

THE SCHOOL OF MINES OF MEXICO IN AN ENGRAVING OF THE TIME.

rombitos que dio la potasa solo se volvieron amarillos. Saturando el exceso de amonia con ácido nítrico, y concentrado un poco por evaporación, obtuve despues prismitas de sabor algo punzante y metálico y de un bello roxo de aurora, qu parecían quadrangulares rectángulos apuntados con cuatro caras puestas sobre las aristas. Haciendo lo mismo con la sosa, me dio cristalitos rojos de aurora, que parecían tablas quadrangulares oblicuángulas, y con la potasa, tablitas quadrangulares rectángulas amarillas. Poniendo 17,75 granos de las agujas formadas por la amonia baxo la mufla de un tiesto de porcelana, tomaron el más bello roxo, sin perder su figura, y luego se fundieron en una masa opaca de color entre pardo de hígado y gris plomo, con muy finas estrellitas en la superficie de lustre semimetálico, que pesó 11,75 granos. No sufrió alteración alguna al fuego de la fragua en hora y media que se tuvo en un crisolito con carbón; es verdad que la cantidad era muy poca; solo la materia ennegrecida con el carbón y con 1,25 granos de aumento. Se metió en una retorta con ácido nítrico; hubo vapores rojos al fin, y la substancia se puso roxa; se repitió dos veces lo mismo; se aumentó al fin al fuego para desprender todo ácido, y echando agua fría se volvió emulsiva. Aclarada la emulsión con el tiempo, no enrojecía la tintura de rábano, aunque daba precipitados amarillos con disoluciones nítricas de plata, mercurio y plomo, no con la muriática del último; precipitaba verde esmeralda el prusiato calizo, y ponía verde oscura la tintura de agallas. El sedimento verde aceituna que se había formado se puso roxo instantáneamente con un poco de ácido nítrico, y la disolución amarillenta precipitaba un óxido verde con el zinc y el hierro. Al soplete con borax tomaba también el vidrio un color verde hierba. La proporción de las partes por quintal de plomo pardo es de 80,72 de óxido amarillo de plomo y de 14,80 de esta nueva substancia (eritronio), siendo por lo demás un poco de arsénico, óxido de hierro y ácido muriático. Su combinación con la amonia no se amalgamó con el mercurio. Pareciéndome nueva esta substancia, la llamé pancromo por la universalidad de colores de sus óxidos, disoluciones, sales y precipitados, y después *eritronio* por formar con los álcalis y las tierras sales que se ponían rojas al fuego y con los ácidos”

As can be seen from the description above, Del Rio did a series of exhaustive analyses and had no doubt that he had discovered a new substance. During Baron Alexander von Humboldt's visit to Mexico, Del Rio also communicated to him the discovery of the new element. Von Humboldt, for his own reasons, believed that the new element was chromium. Upon his departure from Mexico, Del Rio, who considered von Humboldt a friend, gave him a sample of the brownish-gray lead mineral from Zimpán as well as a copy in French describing the discovery. As Del Rio stated in 1832 (See *Elementos de Orictognosia*, 2nd edition, J. F. Hurtel, Philadelphia, 1832, pp. 484-485), von Humboldt did not even bother to show a copy the experiments to H.V. Collet-Descotils<sup>19</sup>, a renowned French analytical chemist, who identified the mineral as lead chromate. Del Rio was forced to admit that he was mistaken and that the mineral from Zimpán contained 80.72% lead oxide and 14.80% chromic acid.

In 1831 the Swedish chemist Nils Gabriel Serfström, working in Berzelius's laboratory rediscovered erythronium in an iron ore from Taberg, Småland, Sweden and named it vanadium in honor of the Scandinavian goddess Vanadis.



Soon afterwards, F. Wöhler also discovered vanadium in a sample of the mineral from Zimpán given to him by Baron A. von Humboldt and proved that Del Rio was correct in his original analysis. It is interesting to read the correspondence between Berzelius and Wöhler and the latter's lines to Liebig. They offer some astonishing clues about the side-scenes and the development of science. <sup>20</sup> Be it as it may, the discovery of vanadium can be considered an outstanding accomplishment for science in Mexico and Latin America. The next discovery of an element in a laboratory of the United States took place almost one and a quarter century later.

Andrés Manuel Del Rio's more than fifty years of service to science in Mexico has been duly recognized. The highest prize awarded by the Mexican Chemical Society bears his name.

## REFERENCES

1. M. Roche, *Science*, 194, 806 (1976).
2. G. Weinberg, *Interciencia*, 3(2), 72 (1978).
3. J. A. Schufle and L. G. Ionescu, *J. Chem. Educ.*, 53, 174 (1976).
4. L. G. Ionescu and J. A. Schufle, *J. Chem. Educ.*, 55, 583 (1978).
5. L. G. Ionescu and J. A. Schufle, *N. Mex. J. Science*, 21(1), 41 (1978).
6. L. G. Ionescu, R. A. Yunes and J. A. Schufle, *J. Chem. Educ.*, 59, 304 (1982).
7. L. G. Ionescu, R. A. Yunes and J. A. Schufle, *N. Mex. Highlands Univ. J.*, 4(1), 32 (1983).
8. L. G. Ionescu, *South. Braz. J. Chem.*, 2, 1 (1994).
9. L. G. Ionescu and C. A. Perazzolo, *South Braz. J. Chem.*, 3, 1 (1995).
10. L. G. Ionescu, *South. Braz. J. Chem.*, 4, 1 (1996).
11. R. Osorio O., *"Historia de la Química en Colombia"*, Publ. Geol. Esp., Ingeminas, Bogotá, Colombia, 1982.
12. M. Bargalló, *"La Amalgamación de los Minerales de Plata en Hispanoamérica Colonial"*, Compañía Fundidora de Fierro y Acero de Monterrey, Mexico, D.F., 1969.
13. M. Bargalló, *La Minería y Metalurgia en la América Española durante la Época Colonial*, Fondo de Cultura Económica, Mexico, D.F., 1955.
14. M. E. Weeks, *"Discovery of the Elements"*, Published by Journal of Chemical Education, Easton, Pa, USA, 1945.
15. A. von Humboldt, *"Essai Politique sur le Royaume de la Nouvelle Espagne"*, Schoell, Paris, 1811.
16. A. M. Del Rio, *"Tablas Mineralógicas de Karsten"*, Mexico, 1804.
17. A. Cabanilles, *Anal. Cienc. Nat. Madrid*, 6, 16 (1803).
18. A. von Humboldt, *Gilb. Ann.*, 78, 118 (1804).
19. H. V. Collet-Descotils, *Ann. Chim. Phys.*, (1), 53, 268 (1805).
20. O. Wallach, *"Briefwechsel zwischen J. Berzelius und F. Wöhler"*, Vols. 1, 2, Verlag Wilhelm Engelmann, Leipzig, 1901.

**STUDY OF SOME ENVIRONMENTAL IMPLICATIONS DUE TO THE  
DISPOSAL OF ASHES FROM THE SÃO JERÔNIMO POWER STATION - RS**

Haidi D. Fiedler\*<sup>1</sup>, Manuel Carneiro  
Pontifícia Universidade Católica do Rio Grande do Sul- Instituto de Química.  
Laboratório de Pesquisa em Química Analítica.  
Av. Ipiranga, Porto Alegre-RS. Brasil.  
CEP.: 90619-900

Elba C. Teixeira\*  
Fundação Estadual de Proteção Ambiental do Rio Grande do Sul.  
Rua Carlos Chagas, 55. Porto Alegre-RS. Brasil.  
CEP.: 90030-020

**ABSTRACT**

*The residues (ash agglomerates from combustion) generated at the São Jerônimo Power Station (UTSJ) were characterized with the main objective of evaluating, in pre-established conditions, the release of Cd, Co, Cu, Pb, Ni, Zn, Mn, Al and Fe to the environment. Results revealed that, at different pH values, Fe, Zn, Mn and Al were present in higher contents. In surface waters, for all sites analyzed, Fe and Al surpass the environmental standards imposed by Brazilian Legislation for class II surface waters. Surface sediments at the sites studied are basically composed by ashes from UTSJ and a cumulative effect of deposition of the metals on the river sediments was verified. The experimental results, are strongly indicative of an imperative need for a change in criteria in relation to the final disposal of residues from UTSJ. Otherwise there is a high risk that the environmental impact in the short term will irreversibly damage the environment.*

**KEYWORDS:** Residue analysis, coal ash, extractable metals, surface waters, sediments.

**RESUMO**

*Os resíduos gerados (cinzas aglomeradas provenientes da combustão) da Usina Termoeletrica de São Jerônimo (USTJ) foram analisados com o objetivo principal de avaliar, em condições pré-estabelecidas, a liberação de Cd, Co, Cu, Pb, Ni, Zn, Mn e Fe ao ambiente. Os resultados mostraram que a diferentes valores de pH, o Fe, Zn, Mn e Al apresentaram teores mais elevados. Nas águas superficiais, em todos os pontos analisados, o Fe e o Al excedem os padrões ambientais estabelecidos pela legislação brasileira para águas de classe II. Os sedimentos de margem dos pontos estudados, se compõem basicamente por cinzas da USTJ e ainda existe um efeito acumulativo de deposição de metais sobre os sedimentos do rio. Os resultados experimentais são fortemente indicativos da necessidade urgente de alteração dos critérios de deposição final dos rejeitos da USTJ. Se providências não forem tomadas, existe um elevado risco de que o impacto ambiental atual se torne, a curto prazo, irreversivelmente prejudicial ao meio ambiente.*

<sup>1</sup> Present Address : Departamento de Química, Universidade Federal de Santa Catarina, Florianópolis, SC. CEP: 88.000-970

## INTRODUCTION

Residues are generally defined as substances present in any environment and whose properties affect environmental characteristics (quality) (ISO - International Organization for Standardization)<sup>1</sup>. In this context, associating this idea to coal processing, it is relevant to report that the major coal application in the state of Rio Grande do Sul (RS) is the combustion in power stations for energy generation. About 2 million ton/year are consumed by thermoelectricity and about 1 million ton/year by cement and petrochemical industries, among others.

Most thermoelectrical power stations (Usinas Termoeletricas - UT) located in Rio Grande do Sul burn pulverized coal, except for Usina Termoelétrica São Jerônimo (UTSJ) that uses a combustion system on grate furnace. This small-sized power station, when compared to others located in Southern Brazil, e.g. Usina Termoelétrica Presidente Medici at Candiota generates agglomerated residues due to ash sintering inside the combustion chamber. Ashes from combustion on grates are generally made up of high contents of organic matter when compared with pulverized coal and this ashes content metals (Ni, Co, Pb, Zn, etc.), the concentrations varying according to coal origin<sup>2-4</sup>. The organic matter persists after combustion because the coal is burned without previous processing.

Environmental problems brought about from residue disposal depend on its characteristics and the pH found in the environment. It is well-known that ash agglomerates induce less-critical environmental effects than ash from pulverized coal combustion, which presents smaller particle size and is more readily subjected to the environmental action and subsequent metal release.

Some kind of ashes produce acidic pH values in contact with water, while others result in alkaline ones. Several studies have been done on metallic extraction of ashes from coal combustion, to evaluate metal mobility in these residues. Some of them are outstanding, such as Sanchez et al.<sup>5,6</sup>, Teixeira et al.<sup>7</sup>, Eary et al.<sup>8</sup> and Roy et al.<sup>9</sup>. These studies establish that the type of process, the nature of ashes, the metallic enrichment on particle surface are factors that contribute to metal mobility.

Environmental problems induced by ash disposal have been observed in certain regions in Rio Grande do Sul, where the presence of significant amounts of this residue, inadequately disposed<sup>10</sup>. In spite of the fact that inadequate disposal of ashes has been verified in the areas of Charqueadas and São Jerônimo, the behavior of the pollutants due to weathering has not been clearly elucidated. The ashes from the two locations present different characteristics that are due to coal type and different combustion processes. Ashes have been used in pavement of highways and as landfill on private properties. Many of the deposits and landfills found in these two areas are within the Jacuí River Flood plain. In both cases, the landfills as well as significant quantities of ashes launched without defined guidelines along roads or highways present serious problems to the environment<sup>10</sup>.

The aim of this study is to characterize residues generated by Usina Termoeletrica São Jerônimo-UTSJ, with the use of different extraction techniques, to evaluate in "pre-established conditions" the release (mobility) of metals (Cd, Co, Cu, Pb, Ni, Zn, Mn and Fe) in the environment. This type of study is important since due to the increase in use of coal, the Environmental Protection Agency of the State of Rio Grande do Sul should encourage the adoption of proper techniques for the disposal of residues generated in all steps of coal processing. The destination of areas for residue disposal, protection of

surface and ground waters, coal preparation and processing, damage to the environment and economic issues are all important factors to be considered.

## EXPERIMENTAL

### Origin of coal ashes and sampling

Ashes studied come from the São Jerônimo Power Station -UTSJ that are disposed in areas surrounding it. Sampling procedures followed the ISO Norm <sup>11</sup>. The sampling site is shown in Figure 1. Samples were carried to the laboratory (in Porto Alegre, RS-Brazil) in suitable polyurethane bags. A manual quartering followed, until four equal one-kilogram portions, representative of the global sample, were obtained. Finally, samples were comminuted to a particle size smaller than 149  $\mu\text{m}$  (total fraction).

Water and sediments were collected according to standard procedures<sup>12</sup>. Water samples were placed in adequate bottles, cold-stored (in a box with ice) until arrival to the laboratory. There, they were stored in cold chamber at - 4°C up to the time of analysis. Samples destined for analysis of specific elements were preserved adequately in the moment of sampling, to maintain the activity of each element. Sediment samples were packed in plastic bags at low temperature and transported to the laboratory for further homogenization, quartering, drying (temperature up to 60°C) and size reduction in porcelain mortar (< 149  $\mu\text{m}$  particle size).

Sampling points for water are shown in Figure 1 and are the following: Point 1: Porteira Stream, under the bridge of the RS Road 105; Point 2: Jacuí River, close to the coal discharge site; Point 3: water put in puddles close to the point of embarkation of the boat to General Câmara, along the RS Road 105.

Figure 1 also illustrates sampling sites for sediments: on the banks of Porteira Stream, close to the bridge of the RS Road 105 (Point 1) and in the Jacuí River's bank, by the site of coal discharge (Point 2).

### Methodology

**Ashes :** Total extractions were made with hydrofluoric and hydrochloric acids. Partial extractions were done with a preliminary calcination of 1 g sample at 450°C for 24 hours. Afterwards, the sample was dissolved in 5 ml of concentrated  $\text{HNO}_3$  (analytical grade, Merck) and taken to dryness in a water bath. Again it was dissolved in 5 ml aqua-regia ( $\text{HCl}:\text{HNO}_3$ , 3:1) and dried ( $T = 250^\circ \text{C}$ ). The residue was dissolved in 5ml of  $\text{HNO}_3$  (conc.) and diluted to a volume of 50ml. To check the chosen method, another aliquot of sample was dried at 85°C for 12 hours. From it, 1g was weighted and digested with 10ml of aqua regia. The solution was heated at 250°C and evaporated to dryness. A second 10-ml aliquot of aqua regia was added. This procedure was followed until the complete elimination of coal matter from the sample. Three blanks were prepared, containing the same concentration of acids used in the sample preparation for both digestion methods.

**Dissolution of metallic elements.** Two methodologies of analysis were applied for this test:

- 1°) method A – was proposed for the characterization of residue's harmfulness by EPA-USA and corresponds to the ABNT 10005 Norm and to the Leaching Test - CETESB<sup>13</sup>;
- 2°) method B – was proposed by the Instituto of Pesquisas Hidráulicas of the Universidade Federal of Rio Grande do Sul (IPH-UFRGS) to determine the behavior of a determined residue when disposed in a natural environment.<sup>14</sup>

In both methods the samples of residues (ashes) were tested also "in natura" as in size range < 149 µm. This smaller particle size aimed to increase the surface of contact and to make the residues characteristics more uniform. We tested the two procedures described below to determine the more adequate conditions for analysis.

The following procedures were adopted for both size ranges:

- 1) Without agitation : a) For a relatively short period of time (48 hours) to avoid that bacterial cultures develop in the test medium or other effects, and b) For a long period of time (7, 14, 30, 60 days) to achieve conditions of better equilibrium;
- 2) With agitation: The adopted systematics was the same as described in the item above for 12 hours at 60°C, using a portion of 1g of sample; 10ml deionized water at a constant pH value (= 5) during the test<sup>13</sup>. The other consisted of 25g of sample in 125ml of distilled deionized water (20% pulp); the pH wasn't adjusted, its changes were monitored.

In each step, after the adequate interval of time, an aliquot was taken for the analysis of dissolved metals.

Extractable metals (those that are not a part of the crystalline lattice) were determined from ashes. The procedure of analysis adopted consisted of changing the pH to 6.0, 4.0 and 1.5. For these tests, 25g of "in natura" sample were treated with a solution of aqua regia and sufficient HNO<sub>3</sub> to achieve the desired pH value. This solution was left for 3 hours under agitation in a semi-turbulent flow regime. Samples were prepared in duplicate for analysis of metals (final volume of 100ml). Afterwards 5% (volume proportion) of nitric acid was added and concentrated to complete dryness. Finally the residue was dissolved in 20 mL of a 10% HNO<sub>3</sub> solution.

The determination of metals (Ni, Pb, Fe, Cu, Zn) in all extracts was performed by Flame Atomic Absorption Spectrometry (FAAS).

**Waters:** parameters determined were: pH, Hg (cold vapor technique), and Cd, Co, Pb, Fe, Ni, Zn, Mn, Al and Mg, by FAAS techniques. These elements were determined in both dissolved and total forms, following procedures recommended by Standard Methods<sup>12</sup>.

**Sediments:** chemical analyses on "margin sediments" were performed for the determination of extractable metals in a certain level of acidity, at pH values of 6.0, 4.0 and 1.5. The technique applied was the treatment of a solution, 1g sample in 10 ml distilled deionized water, with HNO<sub>3</sub> up to the desired acidity, followed by stirring in a semi-turbulent regime for 3 hours. After heating (250°C) up to almost complete dryness, 2.5 ml of HNO<sub>3</sub> were added and the solution was again heated to a small reflux. It was then diluted to a volume of 25 ml for the determination of Cd, Co, Cu and Pb.

At the present time, the poor sensibility of FAAS for the determination of such levels of metals is widely known. However, the time when the experimental part of this study was done (1987), this was the only technique available at the institution where it was carried out. Today, in the particular case of analysis of metals in sediments, exist scientifically safer methods that permit a study of metallic mobility. They are recognized

by ISO Scientific Committees for their analytical rigor. They were given certified reference materials (CRM) specific for the study of metallic mobility in sediments<sup>15,16</sup>.

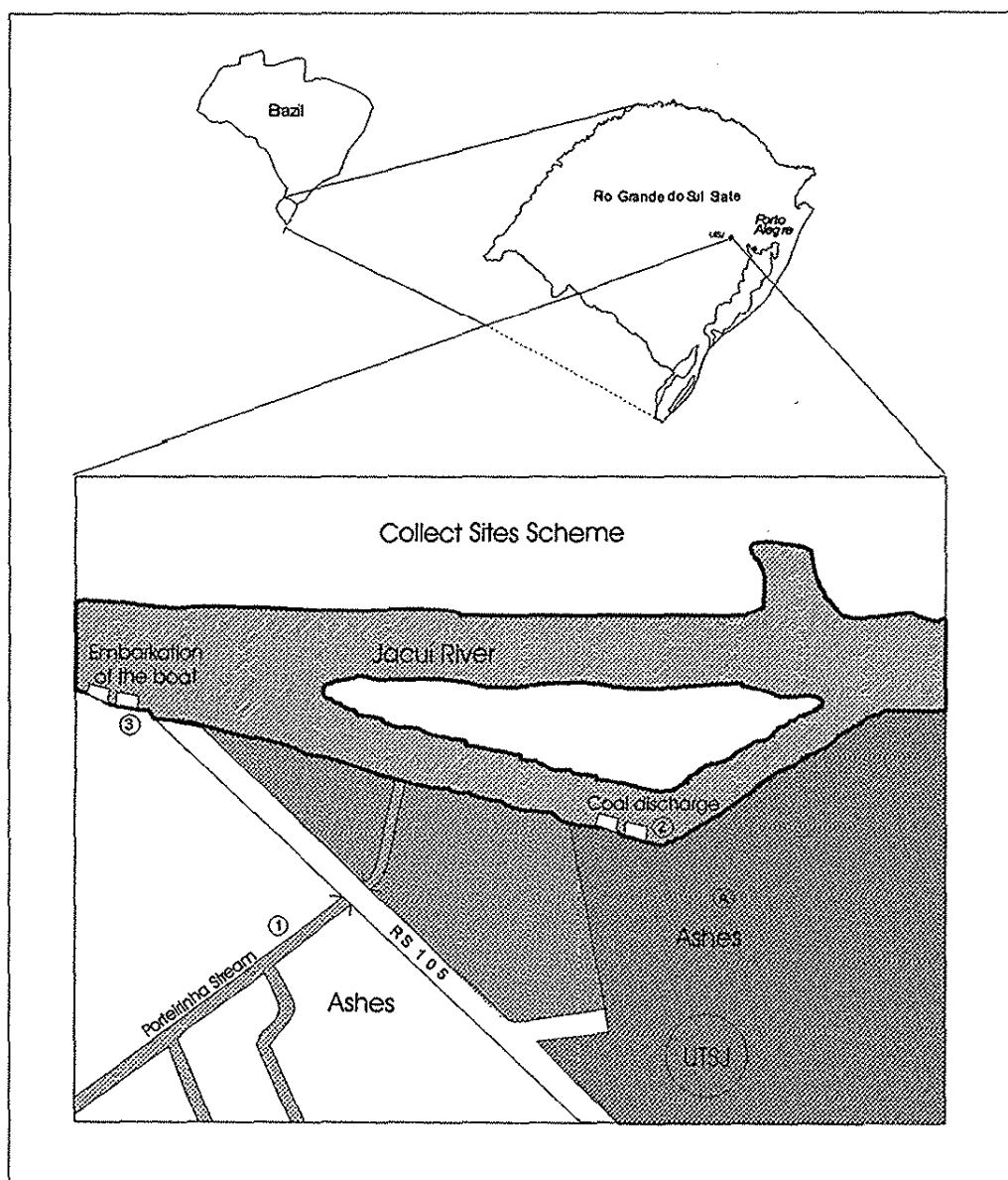


Figure 1. Scheme of the sampling points



## RESULTS AND DISCUSSIONS

## Ashes

Table I presents the results of total and partial extraction of metallic elements (Cd, Co, Cu, Pb, Fe, Ni, Zn and Mn) present in ashes produced by Usina Termoeletrica São Jerônimo. The difference between those values obtained in total and partial extractions can be explained by distinct associations of metals to the residual organic and inorganic fractions that, depending on environmental conditions, release them in greater or lesser degree in the environment. Nearly 40% results showed low indices of partial extraction (< 20% in relation to the total fraction) indicating that the elements Mn, Cd, Pb, Fe and Co are mostly likely to be associated to the aluminossilicate fraction. However, the other elements (Ni, Zn and Cu) showed a higher degree of dissolution. This indicates that they are present in greater amount in the form of oxides and sulfates, and more significant concentrations of them are likely to appear in aqueous environment <sup>17</sup>.

Ashes from UTSJ present basic pH values (pH~9), confirming data reported by other authors that reported an alkaline character for residues from coal combustion <sup>5</sup>.

Table II shows the concentration of metals extracted from ashes, varying the pH of the extracting solution. Data revealed a more significant mobility of metals in ashes in extremely acidic medium (pH=1.5), in agreement with results presented by other authors<sup>6,7,9,18,19</sup>. Meanwhile, it was verified that elements presented, even at pH=1,5, low mobility when compared to results obtained in the total extraction. With pH values of 4 and 6, extraction is practically negligible, because metals are below the analytical detection limit of the method (see explanation above referring to analysis of sediments).

Table I: Concentration and partial extraction percentage of metallic elements in ashes

	Concentration ( $\mu\text{gg}^{-1}$ )		%
	Total Extraction (TE)	Partial Extraction (PE)	
Cd	2.0	0.3	15
Co	8.0	3.0	38
Cu	29	22	76
Pb	37	7.0	19
Fe	12000	4000	33
Al	--	5000	--
Ni	28	16	57
Zn	26	15	58
Mn	107	12	11

Table II : Concentration of metals from ashes as a function of the pH of the extracting solution.

	Concentration of metal ( $\mu\text{gg}^{-1}$ )		
	pH = 6.0	pH = 4.0	pH = 1.5
Cd	< 0.002	< 0.002	< 0.003
Co	< 0.006	< 0.006	0.092
Cu	< 0.004	0.005	0.275
Pb	< 0.012	< 0.012	0.073
Al	< 0.111	< 0.111	36.4
Fe	0.064	0.141	85.9
Ni	< 0.006	< 0.006	0.302
Zn	0.014	0.017	0.407
Mn	0.004	0.006	1.28

Figure 2 a, b, c, d shows the results of the mobility studies for Zn, Ni, Mn and Fe from ashes in different systems (in aqueous medium as a function of time, using different methods of extraction). Method A presented a higher efficiency for the extraction of Mn, Zn, Ni from "in natura" ashes in relation to method B. This can be attributed to the pH correction and the maintenance of an acidic medium (pH=5), favoring the release of these elements. Meanwhile, method B with agitation was the most efficient in the 20-day period of iron extraction. The mobility curves for Ni and Zn show two subsequent increases. This can be explained by the stirring to which the sample was submitted, that could lead to fragmentation of the residue and a subsequent growth in the surface area allowing a closer contact of the aqueous medium with the unreleased metals.

Method A without agitation was also more efficient in the release of metals in the aqueous medium, when 24 hours was the period used for maximum solubilization, while for method B a longer period was required (10 days). In both cases, Ni, Zn and Mn presented similar behaviors.

In relation to particle size, the fraction with size < 149  $\mu\text{m}$  presented a higher index of release of metals in the aqueous medium, generally showing higher concentrations than "in natura" ashes for both methods (Figure 3 a, b, c, d). These results can be attributed to the finer particle size that enhances metallic release in aqueous medium in more significant amounts.

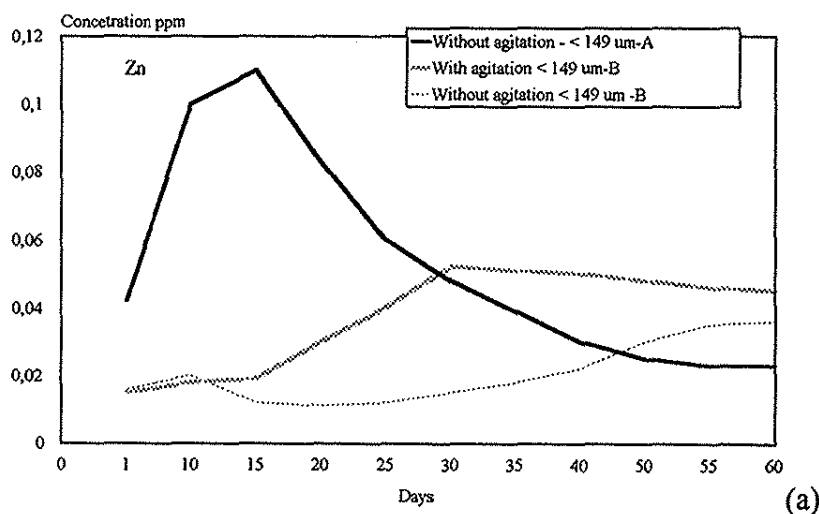


Figure 2a : Study of the mobility of Zn in ashes in function of time in different systems.

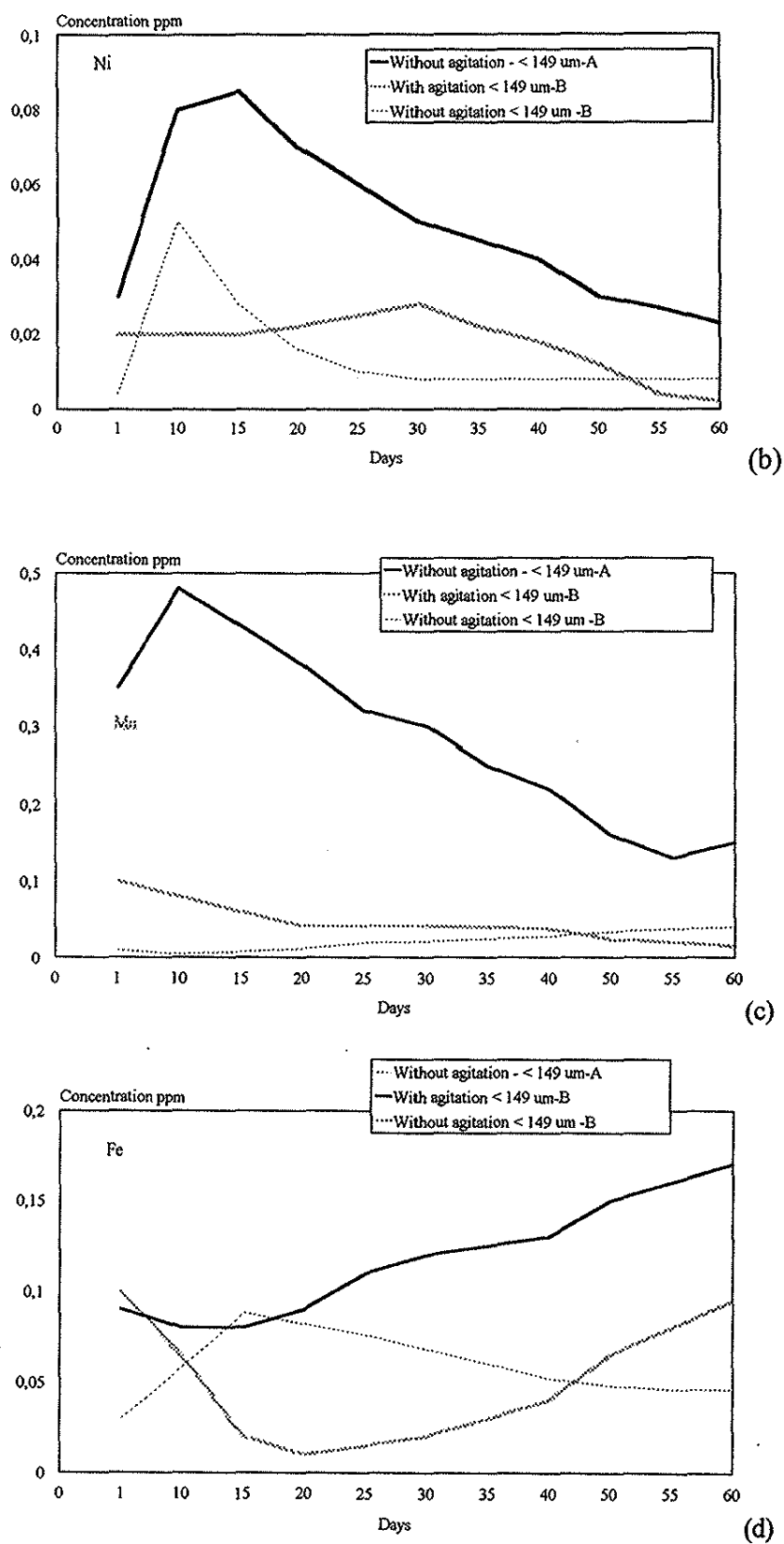


Figure 2 b,c,d: Study of the mobility of Ni, Mn and Fe in ashes in function of time in different systems.

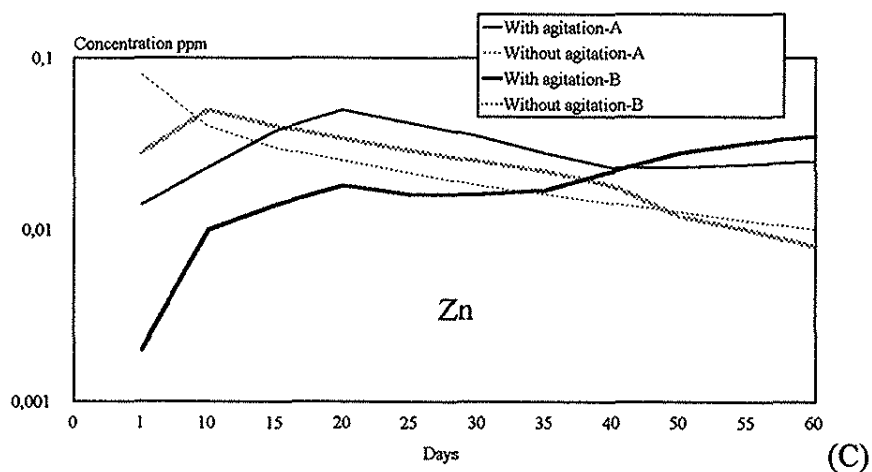
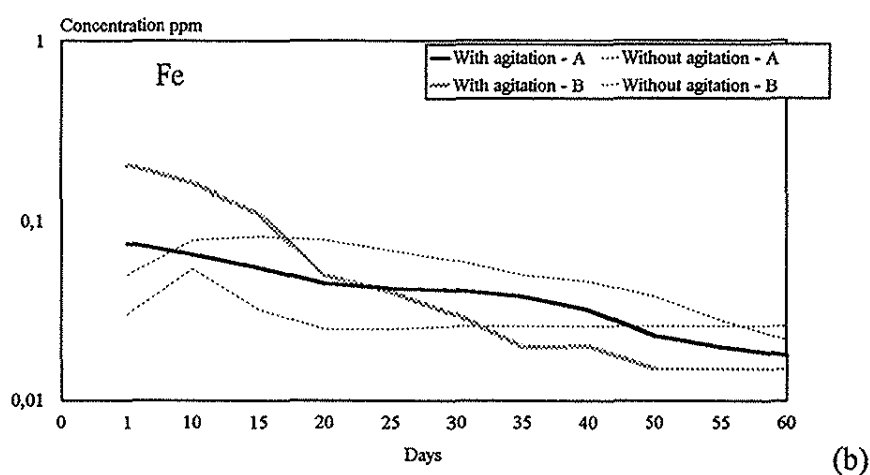
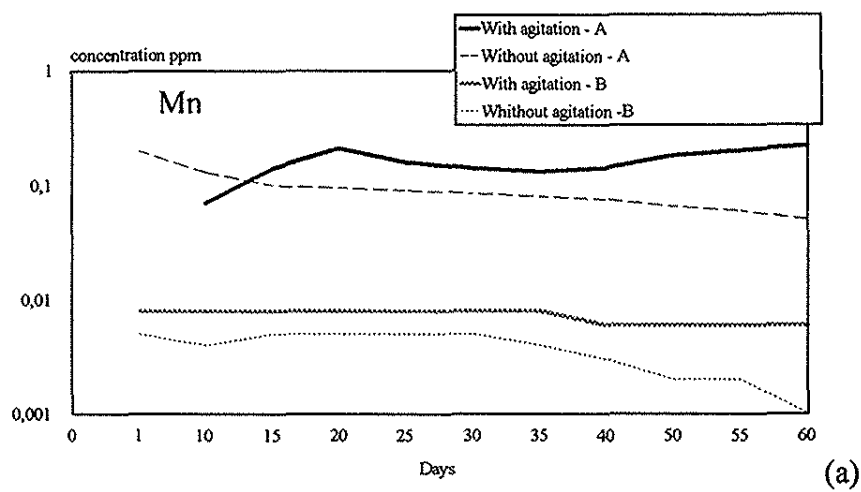


Figure 3 a, b, c : Study of the mobility of Mn, Fe and Zn in ashes of particle size less than 149  $\mu\text{m}$  as a function of time, using two different methods of extraction.

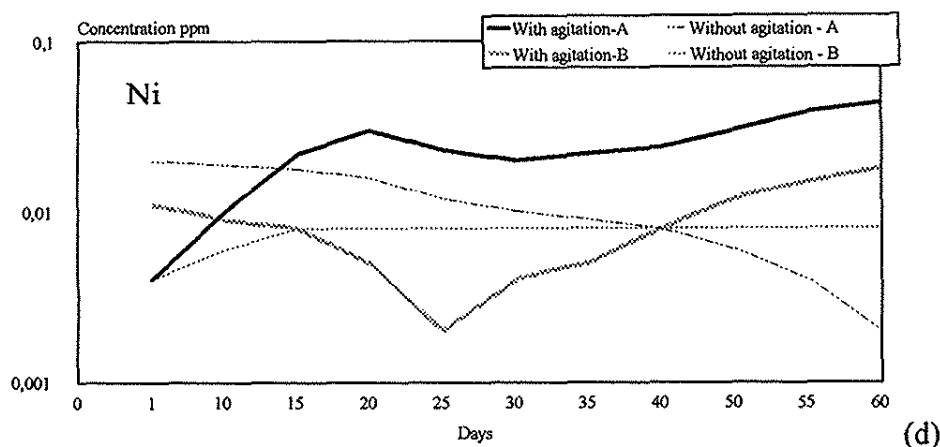


Figure 3 d : Study of the mobility of Ni in ashes of particle size less than 149  $\mu\text{m}$  as a function of time, using two different methods of extraction.

### Surface waters

In three sites close to the São Jerônimo Power Station, where the contamination by ashes was visible, pH and total and dissolved metals (Cd, Co, Cu, Ni, Pb, Zn, Cr, Mn and Fe) were determined in surface waters (Figure 4). The pH at these sites was close to neutral, ranging between 6.2 and 6.4. The results of metallic contents were below the detection limit of the method for Cd, Co and Ni. The concentrations of the other elements, except for Fe, were inferior to the values recommended by Brazilian Legislation of the Conselho Nacional de Meio Ambiente (CONAMA) for class II water courses (CONAMA, Resolution nº020/86). These elements did not present variations between total and dissolved concentrations, except for Pb and Mn, because of the ease with which these elements associate to suspended particles and Fe because of its elevated content in ashes (Figure 2) and also in sediments of the Jacuí River<sup>20</sup>.

### Sediments

In sites of the Jacuí River banks, metals extractable from sediments were determined, with variations in pH and the results are shown in Figure 4. A relation between these data and those obtained for metals extractable from ashes (Figure 5) is verified, leading to the conclusion that the collected sediments are basically made up of residues from the power station, as visually observed.

The elevation of pH from 6.0 to 6.4 and from 4.0 to 6.3 at sampling points 2 and 3, respectively, indicates the presence of ashes in these sites, with alkaline characteristics. At low pH (1.5) the concentrations of metal ions is much higher indicating again that the coal ashes are alkaline in character.

When the results of extractable metals from sediments (Figure 5) and ashes (Table I) are compared, one can notice that data from the latter are lower than those values obtained for sediments. This can be attributed to a cumulative effect of element deposition in sediments at the sampling point 1, and to this effect the presence of coal fines should be added, as it's visually confirmed at the point 2.

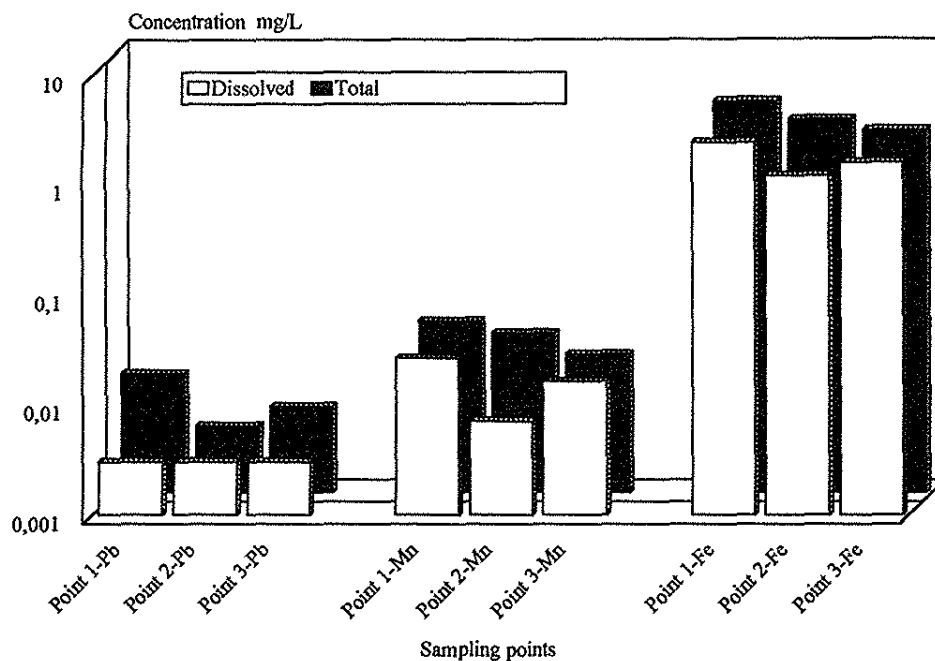


Figure 4 : Concentration of dissolved and total metals in surface water

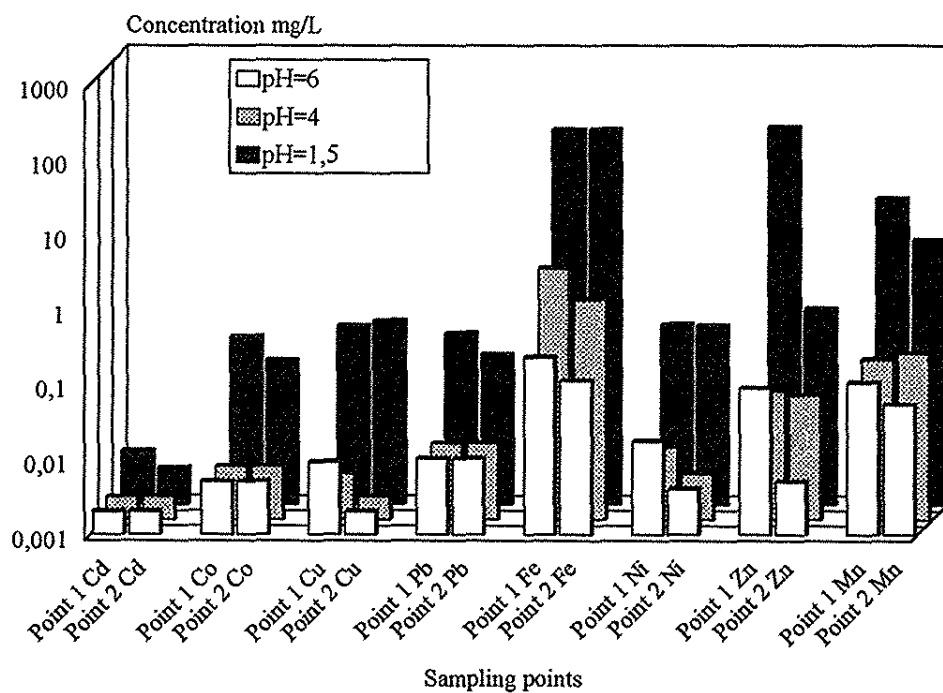


Figure 5: Efficiency of extraction of metals from sediments with variation of the pH of the medium



The experimental results obtained permit us to conclude that the bottom ashes from the São Jerônimo power station present a basic character and the release of Ni, Pb, Cd, Zn, Cu, Mn and Fe from this residue is much more significant at low pH.

From the methods studied in this work, that in which an acidic pH in the medium is corrected and maintained throughout all the experiment (method A), favored the release of Zn, Ni and Mn. The concentrations of such elements increased with the time of extraction, reaching a maximum value in 20 days, while Fe presented a highest value in the earlier phase of the experiment, 24 hours.

At Jacuí River's banks, metals in water were below those values established by the Brazilian law, except for Fe and Al. Contamination by ashes from the power station was verified in the sediments. A cumulative effect of deposition in "marginal sediments" of Jacuí River was found, since values of extractable metals from sediments surpassed those found in ashes.

Based on the exposition we suggest that the final disposal of power station residues should be conducted under adequate criteria and conditions, so that they do not cause more severe environmental problems.

A systematic study is recommended to obtain more technical subsidies with relation to residues from power stations. This will make possible the creation of norms that technically define the specific use of ashes.

## ACKNOWLEDGEMENTS

We thank Fundação Estadual de Proteção Ambiental (FEPAM), former Secretaria da Saúde e do Meio Ambiente - DMA, for the cooperation and assistance during the performance of this work.

## REFERENCES

1. F.R. Aquino Neto, *Química Nova*, 18(6), 597-602 (1995).
2. H. D. Fiedler, A. F. Martins and J. A. Solari, *Ciência Hoje*, 12(68), 39-45(1990).
3. H.D. Fiedler, "Caracterização do carvão em Candiota e implicações ambientais do seu processamento." Dissertação de Mestrado, Engenharia de Materiais, Universidade Federal de Rio Grande do Sul, Porto Alegre, 1987, 156 pp.
4. D.A. Pintaúde, J.C.D. Sanchez and A.J.P. Gomes, *Anais do XXXII Congresso Brasileiro de Geologia*, Sociedade Brasileira de Geologia, Salvador, 1982, pp. 1170-82.
5. J.C. D. Sanchez, E.C. Teixeira and I.D. Fernandes. *Proceedings of the Fourth Internat.Symposium on Environmental Issues and Waste Management in Energy and Mineral Production*, Cagliari, Italy, 1996, pp 1169-1176.
6. J.C.D Sanchez, E.C. Teixeira, I.D Fernandes, M.H.D. Pestana and R.P. Machado, *Geochim.Brasil.*, 8(1),41-50(1994).
7. E.C. Teixeira, J. Samama, and A. Brun, *Environmental Technology*,13, 1187-1192 (1992).
8. L.E.Eary, D.Rai, S.V. Mattigot and C.C. Ainsworth, *J.Environ. Qual.* 19, 202-214 (1990).

H.D. Fiedler, M. Carneiro & E.C. Teixeira

9. R.W Roy; R.G. Thiery; R.M. Schuller; J.J. Suloway, *Environ. Geology Notes*, 96, 69 (1981).
10. E.C. Teixeira, R.B. Binotto, J.C.D. Sanchez, I.D. Fernandes, A. Jablonski, A.J.C. Simch da Silva and G. Rossi. Proceedings of the Fourth Internat. Symposium on Environmental Issues and Waste Management in Energy and Mineral Production, Cagliari, Italy, 1996, pp. 231-238.
11. International Standard Organization, "Norm for Hard Coal Sampling", Geneve, Switzerland, 1988, pp. 90.
12. Standard Methods. Standard Methods for the Examination of Water and Wastewater. A.D. Eaton; L.S. Clesceri and A.E. Greenberg, Editors, 16th edition, Washington DC, 1985, xii, 1268p.
13. C Bernades Junior, e R Zaniolo Jr., Teste de Lixiviação - CETESB, São Paulo. Anais do XI Congresso Nacional de Engenharia Sanitária e Ambiental - Fortaleza, 1981.
14. L.F.D.A.Cybis "Lixiviação Microbiológica Aplicada ao Controle de Poluição na Mineração de Carvão", Dissertação de Mestrado, Instituto de Pesquisas Hidráulicas, Universidade Federal de Rio Grande do Sul, Porto Alegre, 1987, 146 pp.
15. Ph. Quevauviller, G. Rauret, H. Muntau, A.M. Ure, R. Rubio, J.F López-Sanchez, H.D Fiedler and B. Griepink, *Fresenius J. Anal Chem.* 349, 808-814 (1994).
16. H.D.Fiedler, J.F. López-Sánchez, R. Rubio, G. Rauret, Ph. Quevauviller, A.M Ure and H. Muntau, *Analyst*, 119, 1109-1114 (1994).
17. X. Querol, R.Juan, A. Lopez-Soler, J.L.Fernandez-Turiel and C.R.Ruiz, *Fuel*, 75 (7), 821-838 (1996).
18. T.Y.J Chu, R.J. Ruane and P.A. Krenkel, *J. Water Pollution Control Federation*, 50, 2494-2504 (1978).
19. T.L Theis. and L. Wirth, *Environ.Sci. Technol.*, 11(12), 1096-1100 (1977).

**X-RAY STUDIES ON  $Tl_2HgI_4$ ,  $PbHgI_4$ ,  $CdHgI_4$  AND  $Au_2HgI_4$   
INORGANIC COMBINATIONS**

**Tudor ROSU\*, Lidia PARUTA\*\*, Mirela CALINESCU\*, Anca EMANDI\***

\* Faculty of Chemistry - University Bucharest, 70609 Bucharest, Romania

\*\* Institute of Physical Chemistry of Romanian Academy, Spl. Independentei 202,  
77208 Bucharest, Romania

**ABSTRACT**

The parameters of the crystalline elementary cells were calculated starting from the diffraction X-ray spectra obtained on microcrystalline powders of compounds with thermochromic and semiconductor properties. The respective cell/units belong to the tetragonal system and have the following values:  $a=6.450$  Å,  $c=3.14$  Å for the  $Tl_2HgI_4$  compound;  $a=6.875$  Å,  $c=13.110$  Å for the  $PbHgI_4$  compound;  $a=6.40$  Å,  $c=13.12$  Å for the  $Au_2HgI_4$  compound. The wet synthesis method is described for the  $CdHgI_4$  compounds.

**RESUMO**

Os parâmetros das células unitárias cristalinas foram calculados a partir de espectra de difração de raios-x obtidos de pós microcristalinos dos compostos que exibem propriedades termocrômicas e semicondutoras. As respectivas células unitárias pertencem ao grupo tetragonal e tem os seguintes valores:  $a=6.450$  Å,  $c=3.14$  Å para  $Tl_2HgI_4$ ;  $a=6.875$  Å,  $c=13.11$  Å para o composto  $PbHgI_4$ ;  $a=6.40$  Å,  $c=13.12$  Å para o composto  $Au_2HgI_4$ . A síntese via úmida dos compostos do grupo  $CdHgI_4$  é descrita.

**KEYWORDS:** X-Ray diffraction, tetraiodomercurates, thermochromic properties, semiconductor properties, cell parameters.

## INTRODUCTION

Barlot and all<sup>1</sup> supplied (1921) the first information regarding to the physico-chemical properties of the  $Tl_2HgI_4$  compound, specifying that these properties are much different to that of the  $Ag_2HgI_4$  and  $Cu_2HgI_4$  compounds. No details regarding this compound were known since 1973, when Halmos and al<sup>2</sup> had synthesised and studied the  $Tl_2HgI_4$  and  $PbHgI_4$  compounds. They expressed the electrical conductivity versus the temperature and the differential thermal analysis, with no details regarding the type and the parameters of the crystalline lattice. It was 1975 when Joy<sup>3</sup> performed the X-ray diffraction spectra on the  $Tl_2HgI_4$  compound, without establishing its structure. Ammlung and all contributors<sup>4</sup> in 1979, measured the electrical conductivity of the  $Tl_2HgI_4$  compound, at 250°C, a much lower temperature than the corresponding ones for the  $M_2HgI_4$  homologues ( $M^+ = Ag^+, Cu^+$ ), as a result of the decreased mobility of the  $Tl^+$  ion, compared with  $Ag^+$  and  $Cu^+$  ions. The dependence of the Raman spectra for the  $Tl_2HgI_4$  and  $PbHgI_4$  compounds on pressure, was studied in 1983 by Adams and all<sup>5</sup>, obtaining information about the existence of the phase transitions for these compounds, under the pressure effect. The thermoanalytic behaviour of the  $Tl_2HgI_4$  and  $PbHgI_4$  compounds was studied in 1986 by Negoiu and all<sup>6</sup>, in order to clear up the thermocronic transitions temperatures. Two compounds were also added to the  $M_xHgI_4$  complex combination class, ( $M^+ = Ag^+, Cu^+, Tl^+, Pb^{2+}$ ), namely  $CdHgI_4$  and  $Au_2HgI_4$ . These last compounds haven't been described in the speciality literature and data confirming the formation of the respective compound or other information referring to its physico-chemical properties are not known yet.

The aim of this paper is to establish and finalise the crystalline structure of the mentioned combinations. In order to provide a comparison basis, the authors considered necessary to synthesise the  $Cu_2HgI_4$  and  $Ag_2HgI_4$  compounds and to study the X-ray diffraction spectra on the powders of these compounds. The diffractometric data, compared to the one existing in the literature, is represented in table 3 and 4.

## EXPERIMENTAL PART

The  $Tl_2HgI_4$  and  $PbHgI_4$  combinations have been obtained through the wet synthesis described by Well and all<sup>7</sup>, otherwise applied by Adams too, in 1983. This method isn't much different to the one used for obtaining the  $Ag_2HgI_4$ .

The same technique has been generally applied for the  $CdHgI_4$  and  $Au_2HgI_4$  compounds. A  $CdI_2$  (0,5 M) and a  $AuCl$  (0,5 M) solution respectively were added to a  $K_2HgI_4$  (4 M) solution, until the stoichiometric ratio is reached. The solution obtained by this method were slowly heated at 75 - 80°C. Carmin-red, respectively redish-golden precipitates were formed, containing crystals with metallic-reflexion. The precipitates were then washed with water in order to remove the possible soluble impurities, were dried under vacuum on phosphorus pentoxide for 60 h, at the room temperature, and then kept in containers, until being used for investigation.

The compounds obtained by this method have been characterised by elementary analysis, as follows:

\* Mercury was determined through atomic absorption spectrophotometry method, described by El-Awady and all<sup>11</sup> and completed by Luca and all<sup>12</sup>.

Thus, the  $CdHgI_4$  and  $Au_2HgI_4$  combinations were decomposed by the wet way, into an aq.  $HNO_3$  solution (1 N), through slowly heating. Then, the mercury was brought back by the elementary state using  $Sn^{2+}$  chloride and drowe through the cell of an atomic absorbtion spectrophotometer. The absorbtion of the radiation was determined at  $\lambda = 253.7$  nm.

The standard Hg (II) solution with a 1000  $\mu g/ml$  concentration, was obtained by dissolving the necessary pure mercuric chloride quantity into distilled water. The mercury quantity within the complex samples (table 1 and 2) was calculated using the calibration curve.

\* Cadmium was determined according with the method described by Fries and Getrost<sup>13</sup>, using diphenilthyocarbazone, the solution to be analysed being brought to pH = 7-8. At pH = 7-8 the cadmium ions form, in the presence of the diphenilthyocarbazone a macromolecular complex, which exhibits a maximum absorbtion of the light radiation at  $\lambda = 520$  nm.

The standard Cd (II) solution, with 1000  $\mu g/ml$  concentration was obtained by diluting the necessary quantity of pure  $CdI_2$  into the distilled water. The calibration curve Abs ( $\lambda = 520$  nm) versus the standard Cd (II) concentration initially traced and the  $Cd^{2+}$  quantity within the samples taken in work was calculated by extrapolating the calibration curve.

\* Gold was determined to the method described by Fries and Getros<sup>14</sup> using tetraethylrodamine, the analysed solution being brought to a pH = 5. In the presence of the B rhodamine, the gold ions form a macromolecular complex which is extracted in diisopropylic ether. The formed complex exhibits a maximum absorbtion of the light radiation at  $\lambda = 565$  nm.

The standard Au (I) solution with a 100  $\mu g/10$  ml concentration was obtained by diluting the necessary pure  $AuCl$  quantity in distilled water. The  $Au^+$  ions were complexed at once with B rhodamine, and the form compound was separated in diisopropylic ether. The calibration curve Abs ( $\lambda = 565$  nm) versus the standard Au (I)

concentration was then traced. The  $\text{Au}^+$  quantity was calculated by extrapolating this curve and using the samples taken in work.

\* Jodine was determined by difference, accordingly to the quantities of samples taken in work.

Tables 1 and 2 contain results obtained using five different complex of the  $\text{CdHgI}_4$  and  $\text{Au}_2\text{HgI}_4$  compounds.

All the obtained results confirm the formation of the  $\text{CdHgI}_4$  and  $\text{Au}_2\text{HgI}_4$  inorganic combinations.

The  $\text{Tl}_2\text{HgI}_4$ ,  $\text{PbHgI}_4$ ,  $\text{CdHgI}_4$  and  $\text{Au}_2\text{HgI}_4$  compounds obtained through this method are microcrystalline powders, in the following colours: yellow, orange, carmine-red and respectively, redish-golden.

The complex were dry ground to a mean size particles (aprox. 15  $\mu$ ) in order to perform X-ray diffraction studies. Determinations were performed at room temperature.

The diffraction spectra were obtained between 15 and 35° Bragg using a TUR-M-62 HZG apparatus equiped with 3 diffractometer. The  $\text{CuK}\alpha$  radiation ( $\lambda = 1.54051$  A) was used, the radiation was filtered through a Ni sheet; the rate of the counter was 0.5 /min.

## RESULTS AND DISCUSSION

Tables 3 - 8 contain the "d" lines positions expressed in A and the relative intensities  $I/I_1$  of these lines, beside the same properties experimental obtained from diffraction spectra of the respective complex combinations.

This thing was carried out because it is not known quite if the conditions of the used preparation methods lead either to pure equilibrium compounds or to mixtures of non-equilibrium compounds and reactants.

Anyway, for the indexation, the diffraction lines of the reactants were as much as possible not taken in consideration.

In order to index the diffraction spectra on powders, the recurrent formulae given within the international crystallography tables of the cubic, tetragonal and rhombic systems were used. This thing was performed because the preliminary microscopic studies have shown that the crystalline shape of this compounds can be defined within one of this systems.

It has been proven that all the four compounds:  $\text{Tl}_2\text{HgI}_4$ ,  $\text{PbHgI}_4$ ,  $\text{CdHgI}_4$  and  $\text{Au}_2\text{HgI}_4$ , beside the  $\text{Ag}_2\text{HgI}_4$  and  $\text{Cu}_2\text{HgI}_4$  compounds belong to the tetragonal system, having the "d" parameter values and the hkl index shown in tables 3-8.

Tables 3 - 8.

Table 9 exhibits the crystalline elementary cells parameters of the  $\text{M}_x\text{HgI}_4$  synthesised complex combinations, compared to the existent literature data. These parameters were calculated using the diffraction patterns obtained on the microcrystalline powders of the compounds. At the room temperature, a single tetragonal structural phase (named  $\beta$  phase) exists for the up to date known  $\text{M}_x\text{HgI}_4$  substances class ( $\text{M} = \text{Ag}, \text{Cu}, \text{Tl}, \text{Pb}, \text{Cd}, \text{Au}$ ).

Table 9.

As observed in table 9, the crystalline elementary cells parameters of the  $\text{Ag}_2\text{HgI}_4$  and  $\text{Cu}_2\text{HgI}_4$  compounds are likewise those presented within the literature<sup>4</sup>.



Table 1. Some Properties of the  $\text{CdHgI}_4$  Compound.

Table 1

No.	$\text{CdHgI}_4$ g/50ml	$\text{Cd}^{2+}$ , g/50ml		$\text{Hg}^{2+}$ , g/50ml		I, g/50ml	
		theoretical	exp.	theoretical	exp.	theoretical	exp.
1.	0.11095	0.0150	0.0148	0.0270	0.0258	0.0675	0.0689
2.	0.1460	0.0200	0.0199	0.0357	0.0350	0.0903	0.0911
3.	0.1826	0.0250	0.0250	0.0446	0.0452	0.1130	0.1124
4.	0.2191	0.0300	0.0301	0.0535	0.0543	0.1356	0.1347
5.	0.2556	0.0350	0.0340	0.0625	0.0630	0.1681	0.1586

Table 2. Some Properties of the  $\text{Au}_2\text{HgI}_4$  Compound.

Table 2

No.	$\text{Au}_2\text{HgI}_4$ g/50ml	$\text{Au}^+$ , g/50ml		$\text{Hg}^{2+}$ , g/50ml		I, g/50ml	
		theoretical	exp.	theoretical	exp.	theoretical	exp.
1.	0.0140	0.0050	0.0048	0.0025	0.0028	0.0065	0.0064
2.	0.0210	0.0075	0.0078	0.0038	0.0041	0.0097	0.0091
3.	0.0285	0.0100	0.0098	0.0052	0.0055	0.0133	0.0132
4.	0.0350	0.0125	0.0122	0.0064	0.0060	0.0161	0.0168
5.	0.0420	0.0150	0.0147	0.0076	0.0071	0.0194	0.0202

Table 3. X-Ray diffraction spectrum on  $\text{Ag}_2\text{HgI}_4$  powder, compared to literature data

$\gamma - \text{AgI}^*$			$\text{Ag}_2\text{HgI}_4$ [16]			$\beta - \text{Ag}_2\text{HgI}_4$ [17]			$\text{Ag}_2\text{HgI}_4$ [19]			$\text{Ag}_2\text{HgI}_4^{**}$			
d, Å	I/I <sub>1</sub>	hkl	d, Å	I/I <sub>1</sub>	hkl	d, Å	I/I <sub>1</sub>	hkl	d, Å	I/I <sub>1</sub>	hkl	d <sub>exp</sub> , Å	I/I <sub>1</sub>	hkl	d <sub>theoretical</sub> , Å
			6.27	2	200	-	-	-	6.33	Fs	100	6.2668	14	002	6.2668
			5.64	3	210	5.47	25	101	5.69	Fs	101	5.6253	19	101	5.6364
			4.47	3	220	4.42	25	110	4.49	Fs	110	4.4622	16	110	4.4622
3.75	100	111	-	-	-	-	-	-	-	-	-	3.7384	19	-	-
			3.65	100	222	3.65	90	112	3.61	I	112	3.6390	100	112	3.6349
			3.50	2	320	3.50	25	103	3.58	Fs	103	3.4941	16	103	3.4836
			-	-	-	3.14	20	004,200	-	-	-	-	-	-	-
			2.82	3	420	2.83	45	202	2.84	S	210	2.8184	16	202	2.8182
			2.76	4	421	2.80	55	211	2.77	Fs	211	2.7525	15	211	2.7532
			2.57	2	422	2.57	45	114	-	-	-	2.5728	14	212	2.5733
			2.48	1	510	-	-	-	-	-	-	-	-	-	-
			2.34	2	F.II	2.34	40	105,213	2.36	Fs	213	2.3433	14	213	2.3386
2.30	60	220	-	-	-	-	-	-	-	-	-	2.2905	16	-	-
			2.23	50	440	2.228	100	204,220	2.24	X	220	2.2317	49	220	2.2311
			2.10	2	600,442	2.109	40	006,222	2.11	Fs	222	2.1040	16	222,300	2.1035
			2.08	2	610	-	-	-	2.08	Fs	301	-	-	006,214	2.0889
1.96	30	311	1.90	30	622	1.90	100	116,312	1.91	X	312	1.9239	28	312	1.9015
			1.88	1	630,543	-	-	-	-	-	-	1.9034	28	116	1.8919

\* - J.C.P.D.S. 9-399; \*\* - this paper

Table 4

Table 4. X-Ray diffraction spectrum on  $\text{Cu}_2\text{HgI}_4$  powder, compared to literature data

$\text{HgI}_2^*$			$\beta\text{-Cu}_2\text{HgI}_4$ [17]			$\beta\text{-Cu}_2\text{HgI}_4^{**}$		
d, Å	$I/I_1$	hkl	d, Å	$I/I_1$	hkl	$d_{\text{exp}}, \text{Å}$	$I/I_1$	$d_{\text{theoretical}}, \text{Å}$
6.22	55	002	-	-	-	6.2056	12	-
-	-	-	5.42	25	101	5.4399	14	5.4399
4.12	70	101	-	-	-	4.1106	16	-
3.58	100	102	-	-	-	3.5699	31	-
-	-	-	3.52	100	112	3.5172	100	3.5116
-	-	-	3.43	25	103	3.3857	14	3.3744
3.11	3	004	-	-	-	-	-	-
3.09	2	110	-	-	-	-	-	-
-	-	-	3.05	15	200;004	-	-	3.0407
3.01	40	103	-	-	-	3.0034	14	-
2.768	30	112	2.72	10	202	2.7592	10	2.7207
-	-	-	-	-	-	-	-	2.7199
-	-	-	2.67	30	211	2.6542	12	2.6542
2.534	7	104	2.52	10	114	-	-	-
-	-	-	2.27	35	105	2.2618	10	2.2595
-	-	-	-	-	-	-	-	2.2589
2.192	60	114	-	-	-	-	-	-
2.186	55	200	-	-	-	2.1881	12	-
2.163	15	105	2.15	100	220;204	2.1562	24	2.1501
-	-	-	-	-	-	-	-	2.1506
-	-	-	-	-	-	2.1454	20	2.1180
-	-	-	-	-	-	-	-	2.1173
2.074	15	006	2.04	10	226;006	2.0651	8	2.0272
-	-	-	-	-	-	-	-	-

\* J.C.P.D.S. 21-1157

\*\* This paper

**Table 5. X-Ray diffraction spectrum on PbHgI<sub>4</sub> powder**

HgI <sub>2</sub> <sup>*</sup>			PbI <sub>2</sub> <sup>**</sup>			PbHgI <sub>4</sub> <sup>***</sup> powder			
d, Å	I/I <sub>1</sub>	hkl	d, Å	I/I <sub>1</sub>	hkl	d <sub>exp</sub> , Å	I/I <sub>1</sub>	hkl	d <sub>theoretical</sub> , Å
			6.98	25	001	6.964	100	-	-
			-	-	-	6.553	10	002	6.552
6.22	55	002	-	-	-	6.188	30	-	-
			-	-	-	-	-	111	4.558
			-	-	-	4.2913	10	003	4.370
4.12	70	101	-	-	-	4.1106	9	-	-
			3.9456	16	100	4.022	8	112	3.905
3.58	100	102	-	-	-	3.5728	13	-	-
			3.489	4	002	3.4767	10	-	-
			3.435	100	101	3.4340	7	-	-
			-	-	-	3.3330	15	201	3.325
			-	-	-	3.2804	13	004	3.278
3.01	40	103	-	-	-	2.994	9	-	-
2.768	30	112	-	-	-	2.7658	14	-	-
			-	-	-	2.6992	10	203	2.703
			-	-	-	2.6345	8	005	2.622
			2.614	55	102	2.6062	10	-	-
			-	-	-	2.4012	7	221	2.390
			2.327	6	003	2.3251	17	-	-
			2.278	65	110	-	-	-	-
2.192	60	114	-	-	-	-	-	-	-
2.186	55	200	-	-	-	2.1821	9	-	-
2.163	15	105	2.166	14	111	2.1580	7	-	-
			-	-	-	2.1415	9	311	2.145
2.074	15	006	-	-	-	2.0705	12	-	-
1.874	15	6	2.0052	16	103	-	-	-	-
1.865	15	212	1.7496	6	004	1.7433	15	-	-
1.654	3	214	-	-	-	1.6856	7	-	-

\* - J.C.P.D.S. 21-1157; \*\* - J.C.P.D.S. 7-235; \*\*\* - this paper

Table 6. X - Ray diffraction spectrum on  $\text{Ti}_2\text{HgI}_4$  powder

d, Å	$\text{HgI}_2^*$		$d_{\text{exp}}, \text{Å}$	$\text{Ti}_2\text{HgI}_4$ - powder **		$d_{\text{theoretical}}, \text{Å}$
	$hkl$	$I/I_1$		$hkl$	$I/I_1$	
-	-	-	6.5823	19	002	6.5700
6.22	55	002	6.2056	133	-	-
-	-	-	4.6091	15	102	4.6027
-	-	-	4.1990	15	111	4.3087
4.12	70	101	4.1068	28	-	-
3.58	100	102	3.5643	41	103	3.6235
-	-	-	3.3309	20	004	3.2850
3.11	3	004	3.1120	100	201	3.1320
3.09	2	110	-	-	-	-
3.010	40	103	3.0114	26	-	-
-	-	-	2.9838	61	104	2.9300
-	-	-	2.9227	15	202	2.9000
2.768	30	112	2.7625	19	211	2.9174
2.634	-	-	2.6110	13	203	2.5970
-	7	104	2.5100	13	-	-
-	-	-	2.4870	13	105	2.4370
-	-	-	2.3563	19	213	2.4090
-	-	-	2.3120	22	204	2.3013
-	-	-	2.2727	17	115	2.2770
-	-	-	2.2222	17	221	2.2468
2.192	60	114	2.1912	24	006	2.1900
2.186	55	200	-	-	-	-
2.163	15	105	2.1591	17	300, 222	2.1218
-	-	-	2.1100	17	301	2.1218
2.074	15	006	2.0750	39	106	2.0737
-	-	-	1.9993	13	311	2.0155
-	-	-	1.9233	13	303	1.9300

\* J.C.P.D.S. 21-1157; \*\* This paper.

Table 7. X - Ray diffraction spectrum on  $CdHgI_4$  powder

$HgI_2^*$			$CdHgI_4$ - powder**			
d, A	$I/I_1$	hkl	$d_{exp}$ , A	$I/I_1$	hkl	$d_{theoretical}$ , A
6.220	55	002	6.2317	83	002	6.220
4.120	70	101	4.1106	76	101	4.122
3.580	100	102	3.5756	100	102	3.575
3.110	3	004	3.1120	21	004	3.110
3.090	2	110	-	-	-	-
3.010	40	103	3.0014	48	103	3.008
2.768	30	112	2.7625	41	112	2.767
2.534	7	104	2.5265	24	104	2.534
2.192	60	114	2.1902	55	114	2.192
2.186	55	200	2.1871	59	200	2.185
2.163	15	105	2.1581	28	105	2.162
2.074	15	006	2.0695	31	006	2.070
2.062	7	202	-	-	002	2.0612
1.931	9	211	1.9285	28	211	1.930
1.874	15	106	1.8732	31	106	1.873
1.865	15	212	1.8609	31	212	1.874

\* I.C.P.D.S. 21-1157

\*\* This paper



Table 8. X - Ray diffraction spectrum on  $\text{Au}_2\text{HgI}_4$  powder

d, Å	$\text{HgI}_2^*$		$d_{\text{exp}}, \text{Å}$	$\text{Au}_2\text{HgI}_4$ - powder**		
	I/I <sub>1</sub>	hkl		I/I <sub>1</sub>	hkl	$d_{\text{theoretical}}, \text{Å}$
6.220	55	002	6.5620	74	002	6.5622
4.120	70	101	4.0865	67	101	4.0987
3.580	100	102	3.5443	12	102	3.6035
3.110	3	004	3.1019	39	004	3.1315
3.090	2	110	-	-	-	-
3.010	40	103	3.0001	32	103	3.0080
2.768	30	112	2.7425	100	112	2.7430
2.534	7	104	2.5011	15	104	2.5240
2.192	60	114	2.1712	46	114	2.1725
2.186	55	200	2.1670	50	200	2.1682
2.163	15	105	2.1592	19	105	2.1588
2.074	15	006	2.0650	22	006	2.0683
2.062	6	202	-	-	202	2.0568
1.931	9	211	-	-	211	1.9460
1.874	15	106	1.8232	22	211	1.8252
1.865	15	212	1.8110	22	211	1.8110

\* J.C.P.D.S. 21-1157

\*\* This paper

Table 9. The parameters of the "a" and "c" crystalline lattice (Å), expressed for the  $M_xHgI_4$  studied compounds

Compound	$r_{M^{n+}}$ , Å	Lattice parameters		References
		a, Å	c, Å	
$Ag_2HgI_4$	1.26	6.353	6.340	15
		12.62	12.62	16
		6.31	12.63	17
		6.322	12.605	18
		6.33	12.66	19
$Cu_2HgI_4$	0.96	6.3105	12.5336	**
		6.09	12.23	17
		6.0814	12.1683	**
$Tl_2HgI_4$	1.40	6.450	13.140	**
$PbHgI_4$	1.20	6.875	13.110	**
$CdHgI_4$	0.97	4.3693	12.4399	**
$Au_2HgI_4$	1.37	6.4010	13.1250	**

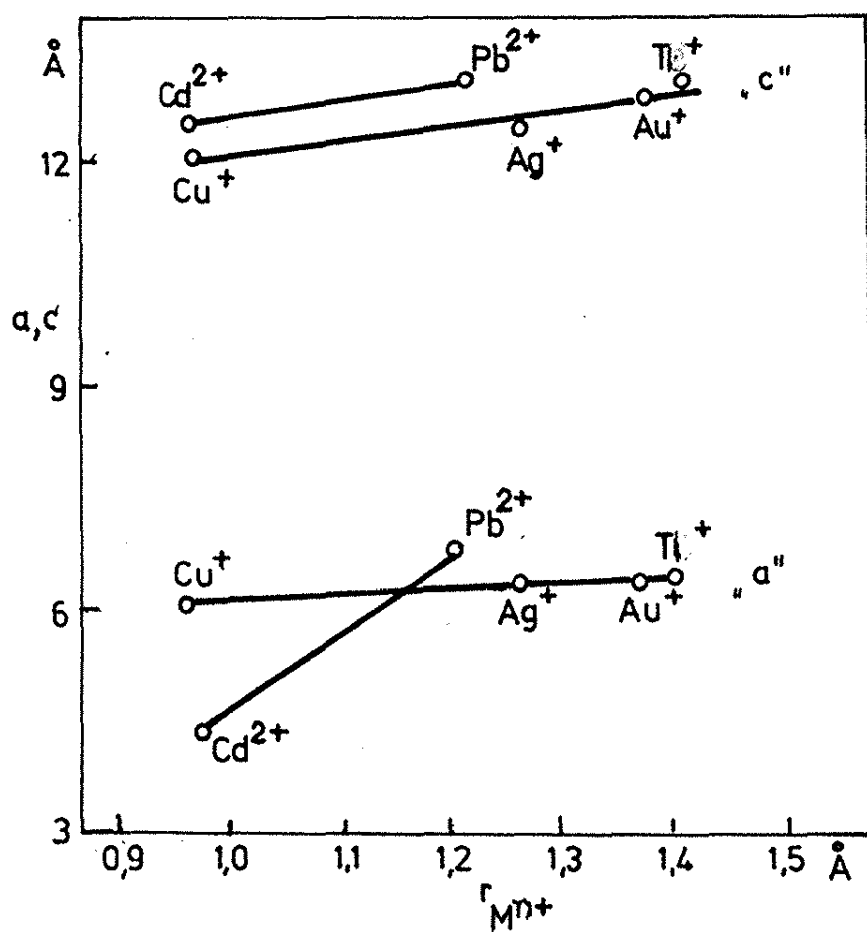


Fig.1. Relationships between the ionic rays and the tetragonal elementary cells parameters, within the  $M_xHgI_4$  system

It is also observed that the elementary cell parameter increases with the increasing of the metallic radius ion, without the alteration of the crystallisation system.

For the  $\text{M}_2\text{HgI}_4$  compounds, the increasing of the reticulate parameter with the metallic radius ion ( $\text{M}^+$ ) is more emphasised on the "c" direction than on the "a" direction and for the  $\text{MHgI}_4$  compounds, with metallic bivalent ions ( $\text{M}^{2+}$ ), the increasing is more emphasised on the "a" direction than on the "c" direction. These relationships are presented in figure 1.

This fact would prove that, at least for the presented cases, the ellipsoidal deformation of the metallic ion is possible in the presence of the  $\text{HgI}_4^{2-}$  anion field.

Considering the monovalent ions cases, the ellipsoidal has the large axis on the "a" direction and in the bivalent ions cases, the ellipsoidal has the large axis on the "c" direction. The spherical symmetry of the  $\text{M}^{n+}$  ions gets an ellipsoidal shape under the influence of the crystalline field. The  $d_{z^2}$  orbital is extended either on the "c" or on the "a" direction, same way with the increasing of the cellular unit parameter in "c" or "a" direction<sup>4</sup>.

## CONCLUSIONS

The inorganic  $\text{CdHgI}_4$  and  $\text{Au}_2\text{HgI}_4$  combinations were synthesized.

The reticulate parameters and the crystalline systems of the  $\text{Tl}_2\text{HgI}_4$ ,  $\text{PbHgI}_4$ ,  $\text{CdHgI}_4$  and  $\text{Au}_2\text{HgI}_4$  not known until now, were determined.

## REFERENCES

1. J. Barlot and J.C. Penet, *Acad. Sa.*, 173, 232, (1921).
2. Z. Halmos and W.W. Wendlandt, *Thermochimica Acta*, 7, 113, (1973).
3. G.C. Joy, *Ph. D. Thesis, Northwestern University, Illinois, USA*, (1975).
4. R.L. Ammlung, R.P. Scaringe, J.A. Ibers, D.F. Shriver and D.H. Whitmore, *J. Chem. Solid State Chem.*, 29, 401, (1979).
5. D.M. Adams and P.D. Hatton, *Raman Spectroscopy*, 14, (3), 154, (1983).
6. D. Negoiu, T. Rosu and D. Todor, *Rev. Chimie (Bucuresti)*, 33, (8), 723, (1987).
7. R. Weil and A.W. Lawson, *J. Chem. Phys.*, 41, 832, (1964).
8. S. Miyake, S. Hoshino and T. Takenaka, *J. Phys. Soc. Japan*, 7, 19, (1952).
9. T. J. Neubert and G.M. Nichols, *J. Am. Chem. Soc.*, 80, 2619, (1958).
10. C.E. Olson and P.M. Harris, *Air Force Report AFOSR T.N.-59-756*.
11. A.A. El-Awady, R.B. Miller and M. Carter, *J. Analyt. Chem.*, 48, 110, (1976).
12. C. Luca, F. Danet and C. Radu, *Rev. Chimie (Bucuresti)*, 36, 856, (1958).
13. J. Fries and H. Cetrost, *Organic Reagents For Trace Analysis*, 78, (1977).
14. J. Fries and H. Cetrost, *Organic Reagents For Trace Analysis*, 175, (1977).
15. J.A.A. Ketelaar, *Krist*, 80, 190, (1931).
16. L.K. Frevel and P.P. North, *J. Appl. Phys.*, 21, 1038, (1950).
17. H. Hahn, G. Frank and W. Klinger, *J. Anorg. Chem.*, 279, 27, (1955).
18. K. W. Browall and J. S. Kasper, *J. Solid State*, 10, 20, (1974).
19. J.W. Brightwell, C.N. Buckley, R.C. Hollyoak and B.J. Ray, *Materials Science Letters*, 3, 443, (1984).

**SOLID SUBSTRATE FERMENTATION OF CACTUS PULP BY  
ASPERGILLUS NIGER**

Arnaldo D. S. Júnior ; Rosangela B. Garcia; Dina G. Rodrigues and Jorge Nozaki\*

(\*) Departamento de Química, Universidade Estadual de Maringá

87020-900 Maringá, Paraná, Brazil. Fax:044-263-5116

E-mail: jnozaki@cybertelecom.com.br

**ABSTRACT:** A new method of culture is described to study the growth of *Aspergillus niger* on cactus pulp in the solid state. After extraction of viscous polyelectrolytes, employed in water treatment, the pulp of *Cereus peruvianus* was used as substrate for solid -state fermentation by a wild strain of *A. niger*. The good conditions for *A. niger* growth were 60% moisture, initial pH 3.0, 35°C, a nitrogen source made of 11% ammonium and 2% urea (on a nitrogen basis), 5% potassium phosphate, and 3.2 g spores/100 g substrate. Related to the dry pulp, maximum fungal growth was observed after 120 hours of fermentation with 14% of protein production.

**Keywords:** solid-state fermentation, protein, *Aspergillus*, agricultural wastes, cactus

**RESUMO.** Investigou-se um novo método de cultura para o crescimento do *Aspergillus niger* sobre a polpa do cactus no estado sólido. Após a extração do polieletrólito natural, uma substância viscosa utilizada em tratamento de águas, a polpa do cactus *Cereus peruvianus* foi utilizada como substrato na fermentação sólida por cepas naturais de *A.niger*. As condições ótimas para o crescimento do *A. niger* foram: umidade de 60%, pH inicial 3,0, 35°C, fontes de nitrogênio constituído de 11% de amônia e 2% de urea (baseados no nitrogênio), 5% de fosfato de potássio, e 3,2 g de esporos por 100 g/substrato. Em relação à polpa seca, o crescimento máximo do fungo foi observado após 120 horas de fermentação com produção de 14% de proteína.

(\*) To whom correspondence should be addressed

## INTRODUCTION

Protein production by solid substrate fermentation (SSF) using renewable sources received worldwide attention. This is an important way, in developed countries, of dietary changes for the partial substitution of animal protein with plant protein<sup>1</sup>.

Fermentation with *Aspergillus niger*, a filamentous fungi, have been studied for citric acid<sup>2</sup>, xylanolytic enzyme<sup>3</sup>, pectolytic enzyme<sup>4</sup>,  $\beta$ -glucosidase<sup>5</sup>, alpha and gluco-amylase<sup>6</sup>, and nucleic acid-related substances production<sup>7</sup>. The study of fungal growth in SSF shows advantages over submerged cultures because liquid media are far from the natural environment of fungi<sup>8</sup>.

*Cereus peruvianus*, a kind of cactus native in South America, is used as animal feed, despite its very low protein content, and is also used in the production of natural polyelectrolytes. The polyelectrolytes are used in water treatment as an auxiliary of flocculation and sedimentation<sup>9</sup>. Water, starch, cellulose, chlorophyll, and hemicellulose are the main constituents of cactus, with small amounts of pectin, and lignin<sup>10</sup>. After extraction of polyelectrolytes (soluble carbohydrates) there is the production of large amount of solid wastes constituted basically of fibers, starch, cellulose, and hemicellulose. It is the purpose of this research to use of cactus pulp, after extraction of natural polyelectrolytes, as animal and human feed. Wild strains of *A. niger* were used throughout this work, because of its high amylolytic and cellulolytic activities, for converting cactus pulp directly to feedable microbial protein by solid-state fermentation.

## EXPERIMENTAL PROCEDURE

### Organism

Wild strains of *Aspergillus niger* were isolated from decomposed wood pulps at different locations, and screened on agar plates containing 100g of dried cactus pulp, 10g (NH<sub>4</sub>)SO<sub>4</sub>, 5 g K<sub>2</sub>HPO<sub>4</sub>, 1.5 g MgSO<sub>4</sub>·7 H<sub>2</sub>O, pH 3.6, for 5 days. Cactus pulp was used as the only carbon source, and those black colonies that grew well under such environment, were isolated and retained for second screening. Those isolated organisms from the previous screening were cultured in flasks at 35°C, after autoclaving (110°C for 20 min.), at pH 3.0, containing 10 g of D-glucose and the same medium as the first screening.

### Pulp preparation

After removing the external chlorophyll, the cactus was cut in small pieces ( 10 x 30 mm ). Approximately 132 g of cactus pieces and 750 mL of tap water were transferred to 2 liters flask with shaking for 30 min. The extraction of liquid and viscous natural polyelectrolytes ( soluble sugars ) was performed by maceration. The polyelectrolytes was kept at 4°C until use in water treatment. The solid waste was dried, exposing directly to the sun for 6 hours, before using as substrate for SSF.

### Solid-state fermentation

Five gram of  $\text{KH}_2\text{PO}_4$  ( Merck -Germany),  $(\text{NH}_4)_2\text{SO}_4$  ( Merck ) ( 11.5 g ), and urea ( 33.7 g ) were added to a ( 30 x 30 cm ) tray containing 100 g of dried cactus pulp. After adjusting the moisture to 60 - 65 % with tap water and pH 3.0 with diluted solution of sulfuric acid , 0.5 g of inoculum was transferred to its surface. Three more trays were prepared in the same way and put inside of the greenhouse at 35°C. The first tray was on the bottom surface , and the vertical distance among the first , second , third , and fourth trays were 15 cm respectively. The aeration was performed with an air compressor using silicone tube ( 60 cm lenght and 5 mm i.d ) from the top of the greenhouse.

### Analytical methods

#### Protein and sugar determinations

Fermented mold was soaked with 100 mL of phosphate buffer ( pH 6.9 ) and stirred for 30 min at 60°C. The extract was collected by filtration. The extraction process was repeated five times , all the extractants were transferred to flask, and the final volume was made up to 100 mL with distilled water. The method of Lowry et al was employed for protein determination<sup>11</sup> using bovine serum albumin as standard. Reducing sugars was determined using dinitrosalicylic acid (DNS ) method<sup>12</sup> , and starch was measured by polarimetric method.

#### Sample preparation and starch determination by polarimetric method

Crushed sample ( 2.5 g ) and 50 mL of 0.14 mol.L<sup>-1</sup> HCl ( Merck-Germany ) were transferred to a 100 mL volumetric flask in a thermostatic bath with shaking for 15 minutes. After cooling, clarifier solutions constituted by 10 mL of 1 mol.L<sup>-1</sup> zinc acetate dihydrate ( Aldrich-USA ) and 10 mL of 0.25 mol.L<sup>-1</sup> potassium ferrocyanide trihydrate (

Aldrich ) were transferred to the flask, and the final volume was made up to 100 mL with distilled water. After one or two filtrations this solution was clear enough for polarimetric measurements. The sample solution was transferred to a 20 cm length polarimetric cell and the concentration was determined using the following relationship:

$$[\alpha]_{D(20)} = \frac{\text{observed rotation, degree} \times 100}{\text{optical path length (dm)} \times \text{concentration (g / 100 mL)}}$$

$$\text{and } C = 100 \times \alpha / L \times \alpha_{D20}$$

D = line of sodium (  $\lambda = 589.3 \text{ nm}$  ), L = optical path length ( dm )

C = concentration ( g / 100 mL ) ,  $\alpha$  = observed rotation ( degree )

The specific factor used for starch  $[\alpha]_{D20}$  was 84.8 ( 20°C ).

## RESULTS AND DISCUSSION

Table 1 shows the average composition of cactus *Cereus peruvianus*. The composition of cellulose, hemicellulose, chlorophyll, and lignin are variable and depends on cactus age, soil, time of collecting, etc. Table 2 shows the protein contents of cactus pulp, after extraction of natural polyelectrolytes, but before the solid-state fermentation.

Figure 1 shows the influence of moisture on mycelial growth and protein production by *Aspergillus niger* with optimal moisture observed at 60%. Higher moisture may increase the viscosity, decreasing the porosity and oxygen diffusion. The pH also play an important role in solid fermentation. The average pH should be low enough, otherwise the system will have problems with bacterial contamination. Starting with pH 3.0, after 140 hours of fermentation the pH increased to 6.0 ( Figure 4 ), even keeping the moisture approximately at 60%. The increase of pH was due to the urea hydrolysis, and it should be controlled during the experiment. Starch consumption was not very related to the protein production, as shown in figure 2, because the substrate used was constituted mainly by cellulose and hemicellulose. This was a clear indication that *Aspergillus niger* was able to produce not only amylolytic, but also hemicellulolytic and cellulolytic enzymes. On the other hand, the glucose consumption was closely related to the protein production as shown in Figure 3.



Table 1. Average composition % (m/m)\* of cactus pulp<sup>10</sup>

Moisture	75-80
Sugar	12
Pectin	1
Protein	< 1

(\*) Cactus *Cereus peruvianus*Table 2. Protein content % (m/m) in cactus pulp ( *Cereus peruvianus* )

Cactus pulp (powder )	% protein (*)
after extraction of chlorophyll (* *)	0.85
without extraction of chlorophyll (* *)	1.58
Protein determination by Lowry method	0.80

(\*) Average of six determinations. Standard deviation of  $\pm 0,05\%$ .

(\* \*) Chlorophyll extracted using acetone and protein determination by Kjeldhal method .

Figure 1. Influence of moisture on mycelial growth of *Aspergillus niger*

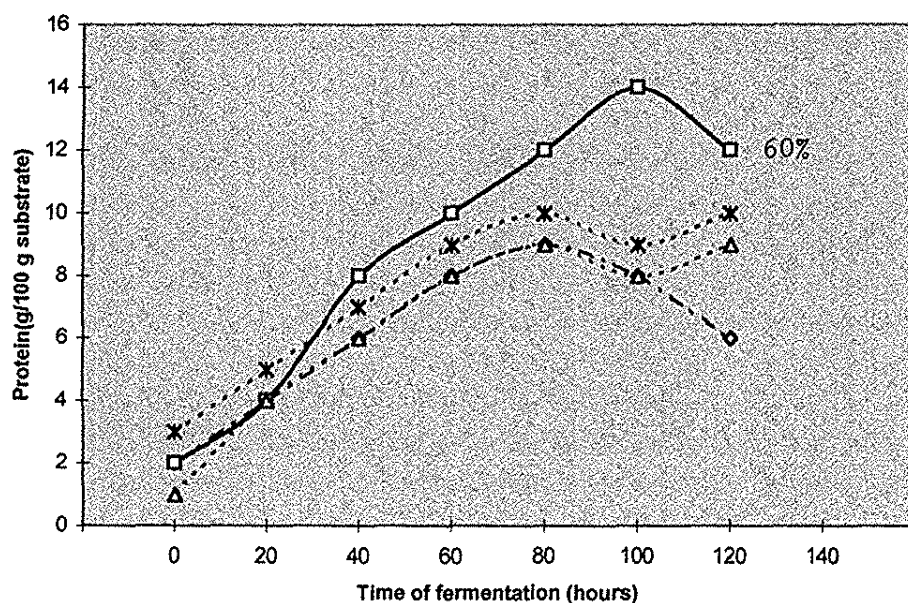


Figure 2. Starch consumption during fermentation

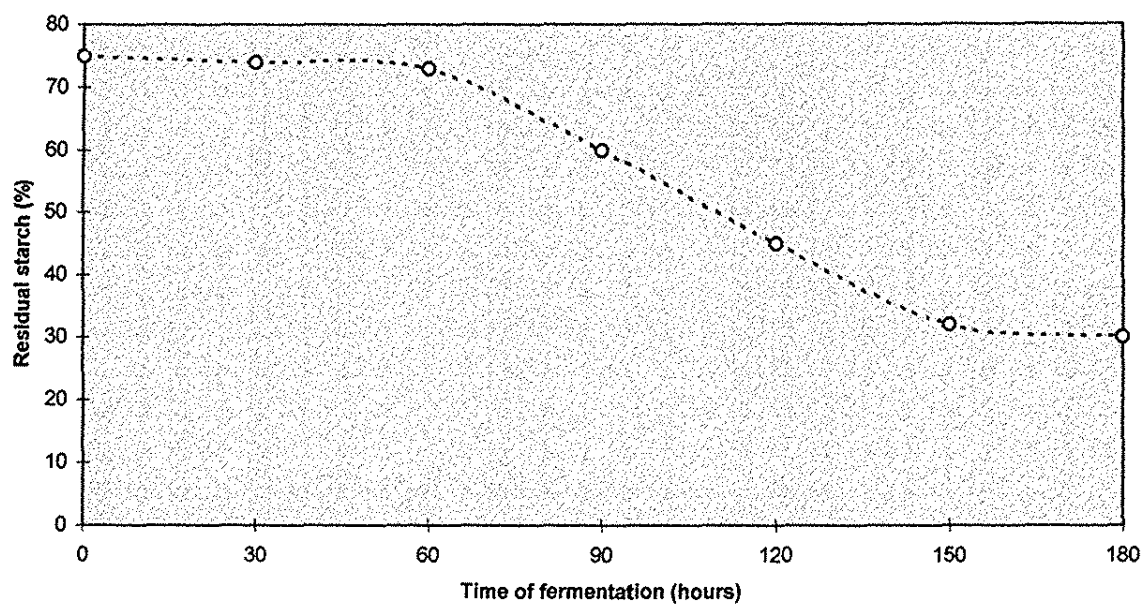


Figure 3. Glucose consumption and protein production during fermentation

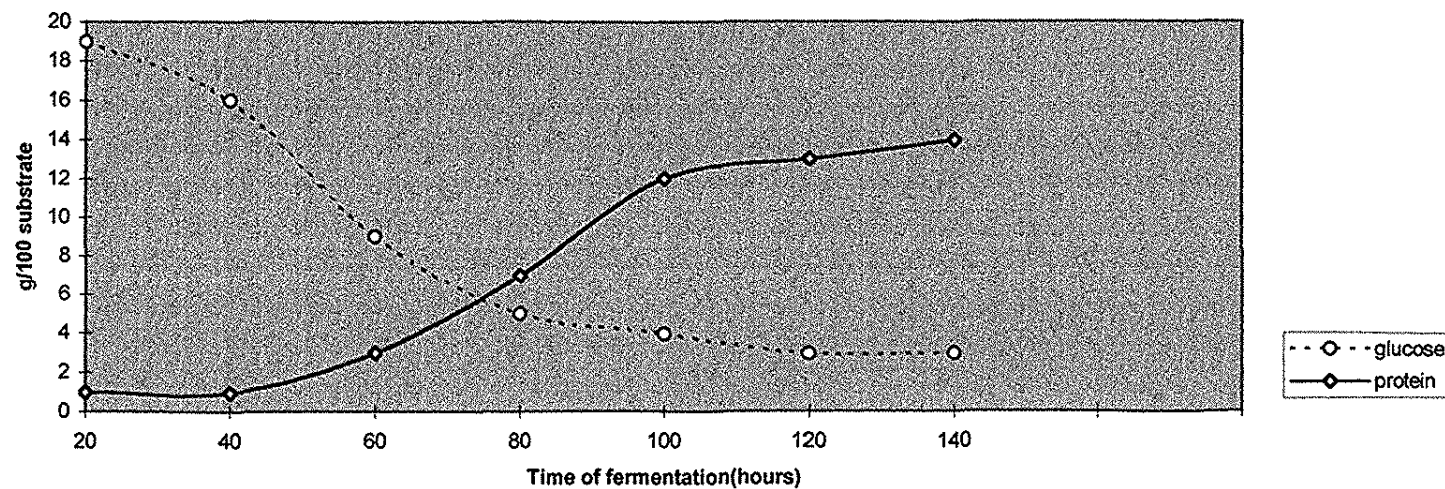
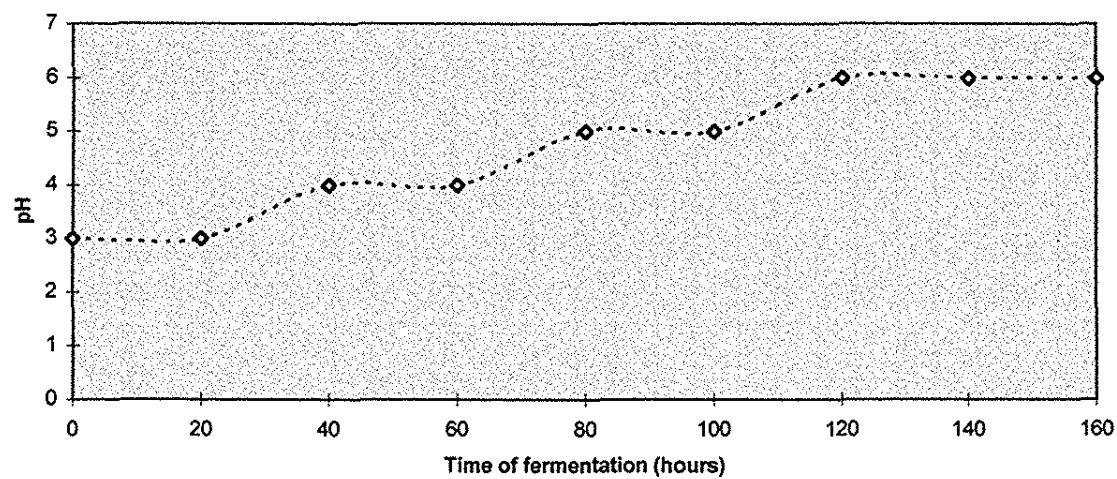


Figure 4. pH variation during fermentation



**Conclusion**

High efficiency of protein production, reduced energy requirement, low wastewater output, nonaseptic conditions, and low capital investment were the advantages of SSF with wild strain of *Aspergillus niger* using cactus pulp as substrate. High viscosity, due to the presence of natural polyelectrolytes, was a drawback for oxygen diffusion. The difficulty of oxygen diffusion was the main limitation of the process.

**Acknowledgements**

The authors would like to thank FNMA/MMA, CAPES, and CNPq (Brazil) for financial support.

**REFERENCES**

1. Jwanny, E. W., Rashad, M.M., and Abdu, H.M., **Applied Biochemistry and Biotechnology**, 50, 71-78, (1995).
2. Matthey, M, **Crit. Rev. Biotechnol.** 12, 87-132, (1992).
3. Ferreira, M.C., Dias, A., Máximo, C., Morgado, M.J., Martins, G.S., and Duarte, J.C. **Applied Biochemistry and Biotechnology**, 44, 231-242, (1994).
4. Antier, P., Minjares, A., Roussos, S., Raimbault, M., and Gonzalez, G.V, **Enzyme Microb. Technol.**, 15, 254-260, (1993).
5. Fadda, M.B., Curreli, N., Pompei, R., Rescigno, A., Rinaldi, A., and Sanjust, E, **Applied Biochemistry and Biotechnology**, 44, 263-270, (1994).
6. Cadmus, M. C., Jayko, L.G., Hensley, D. F., Gasdorf, H., and Smiley, K.L, **Cereal Chemistry**, 43, 658-669, (1966).
7. Carvalho, A., Faria, C.R., e Molinari, R, **Eclética Química**, 3, 55-67, (1978).
8. Raimbault, M., and Alazard, D, **European J. Appl. Microbiol. Biotechnol.**, 9, 199-209, (1980).
9. Messerschmidt, I., Rodrigues, D. G., and Nozaki, J, **Arquivos de Biologia e Tecnologia**, 36 (4), 51-56, (1993).
10. La Mar, V. and Healy, K, **Rev. Pure App. Chem.**, 13, 112-132, (1963).
11. Lowry, O. H., Rosebrough, N. J., Farr, A. L. and Randall, R. J, **J. Biol. Chem.**, 193, 265-275, (1951).
12. Wood, T. M. and Bhat K. M, **Methods in Enzymology**, 160, 87-116, (1988).

**SOME NEW N-BENZOYL-N'-SUBSTITUTED PHENYL THIOUREA  
COMPLEXES OF COPPER(II)**

Tudor ROSU\*, Viorel CÂRCU\*, Maria NEGOIU\*, Ovidiu MAIOR\*\* and Niculina BADICU\*

\*Dept. of Inorganic Chemistry, Faculty of Chemistry, University of Bucharest, 23 Dumbrava Rosie st.,  
Bucharest, Romania

\*\*Dept. of Organic Chemistry, Faculty of Chemistry, University of Bucharest, Romania

**ABSTRACT**

The new N-benzoyl-N'-substituted phenyl thiourea ligands have been used to prepare copper(II) complexes  $[\text{Cu}(\text{L})_2\text{Cl}_2]$ . The novel complexes were characterized by ESR, IR, NIR, electronic spectroscopy and conductivity measurements. Tentative geometry of the complexes involves four-coordinate environments (tetrahedral distorted  $\text{D}_{2d}$ ) for the copper ion and a monodentate behaviour for ligands. In all these complexes N,N'-substituted thiourea is sulphur-bonded to the copper ion.

**RESUMO**

Os novos ligantes de N-benzoila-N'-substituidos por feniltio-urea foram usados para preparar complexos os complexos  $\text{Cu}(\text{L})_2\text{Cl}_2$ . Os novos complexos foram caracterizados usando métodos de RSE, infravermelho, infra-vermelho próximo, espectroscopia eletrônica e medidas de condutividade. A geometria proposta tentativamente para os complexos envolve ambientes tetra-coordenados ( $\text{D}_{2d}$ , tetraédrico distorcido) para o íon de cobre e comportamento monodentado para os ligantes. Em todos os complexos a N,N'-tio-urêia substituída está ligada ao íon de cobre através do átomo de enxofre.

**KEYWORDS :** thiourea, copper(II), complexes, ESR spectra.

## INTRODUCTION

A numerous series of thiourea and some N or N,N'-substituted thioureas complex with transition metals are reported in literature<sup>1-4</sup>, and the N-benzoyl-N'-substituted thiocarbamides have received very little attention<sup>5,6</sup>. These compounds are used successfully as extractive reagents<sup>7,8</sup>. The coordination behaviour of these derivatives of thiourea is very interesting due to three donor sites for the coordination: the sulfur atom of the C=S group, the oxygen atom of the C=O group and the nitrogen atoms of the NHR groups. We therefore prepared some new N-benzoyl-N'-phenyl substituted thioureas complexes with copper(II) in order to study the coordination and stereochemistry via the synthesis ways. The structure of the formed Cu(II) complexes was established via physicochemical studies including IR, NIR, UV-VIS, ESR spectral and conductance measurements.

## EXPERIMENTAL PART

Reagents of the best chemical grade were used.

The ligands N-benzoyl-N'-phenyl substituted thioureas were prepared according to the procedure described elsewhere<sup>9</sup>. The copper(II) complexes of the ligands L<sub>1</sub>-L<sub>7</sub> (fig. 1), may be prepared by addition of an methanolic solution containing 2mM of copper(II) chloride to an methanolic suspension containing 4mM of the ligand. In each case the copper(II) complex is formed as a yellow-orange solid. The complexes are stable under atmospheric conditions and are soluble in chloroform, DMF and partially in acetone. If an aqueous solution of the sodium salt of the L<sub>1</sub> ligand was added to an aqueous solution of copper(II) chloride a [CuL<sub>1</sub>H<sub>2</sub>O] complex type<sup>10</sup> is formed.

*Physical measurements*

Elemental analysis were been performed with a Carlo Erba L1108 model automatic analyzer (C, N), with AAS-1N Carl Zeiss Jena spectrometer (Cu) and Mettler Toledo 355 Ion Analyzer (Cl). The electronic spectra of all compounds were obtained, in solution (chloroform), with a SHIMADZU UV 160A spectrophotometer. The IR spectra were run with a FT-IR BIO RAD FTS spectrophotometer in the 4000-500 cm<sup>-1</sup> and with a SPECORD M80 Carl Zeiss Jena spectrophotometer in the 500-250 cm<sup>-1</sup>, in KBr pellets and NIR spectra with NIR Systems spectrophotometer. The ESR spectra of copper(II) complexes were measured on polycrystalline powders with VARIAN E-9. Conductivities were measured at room temperature in dimethylformamide (DMF) with a HACH TDS-meter.

## RESULTS AND DISCUSSION

Colours, analytical data and conductivity values for the complexes are given in Table 1. As outlined by the analytical data in Table 1, the composition of the compounds may be represented as [Cu(L)<sub>2</sub>Cl<sub>2</sub>]. The molar conductivities in DMF shows that these complexes are non-electrolytes.

*Structure*

The structure of the ligands can be represented in a variety of ways, two containing the tioketo group(I, II) and the other two in the thiol forms (III, IV) (fig. 1).

Table 1. Analytical data, colours and molar conductivity for the  $[\text{Cu}(\text{L})_2\text{Cl}_2]$  complexes.

Compound	Colour	C		N		Cl		Cu		$\Lambda_M$
		exp.	calc.	exp.	calc.	exp.	calc.	exp.	calc.	
$[\text{Cu}(\text{L}_1)_2\text{Cl}_2]$	yellow pale	53.94	54.66	7.20	7.97	9.80	10.08	8.84	9.04	39.5
$[\text{Cu}(\text{L}_2)_2\text{Cl}_2]$	yellow	53.29	54.66	7.35	7.97	9.70	10.08	8.87	9.04	44.8
$[\text{Cu}(\text{L}_3)_2\text{Cl}_2]$	yellow canar	53.90	54.66	7.13	7.97	9.15	10.08	8.90	9.04	43.3
$[\text{Cu}(\text{L}_4)_2\text{Cl}_2]$	yellow canar	53.85	54.66	7.17	7.97	9.72	10.08	8.78	9.04	42.4
$[\text{Cu}(\text{L}_5)_2\text{Cl}_2]$	yellow cream	55.22	55.85	6.98	7.66	9.53	9.70	8.20	8.69	28.9
$[\text{Cu}(\text{L}_6)_2\text{Cl}_2]$	orange	44.80	45.20	9.91	10.54	8.20	8.90	7.53	7.97	43.3
$[\text{Cu}(\text{L}_7)_2\text{Cl}_2]$	yellow pale	50.12	50.96	7.05	7.92	9.32	10.03	8.75	8.99	26.0

\*The conductivity values is given in  $\text{ohm}^{-1}\cdot\text{cm}^2\cdot\text{mol}^{-1}$ .Table 2. IR bands ( $\text{cm}^{-1}$ ) of N-benzoyl-N'-substituted phenyl thioureas.

Compound	$\nu(\text{C}=\text{O})$	$\nu_{\text{asym}}(\text{N}-\text{C}-\text{N})$	$\nu_{\text{sym}}(\text{N}-\text{C}-\text{N})$	$\nu(\text{C}-\text{S})$	$\nu(\text{C}-\text{NO}_2)$	$\nu(\text{C}-\text{O}-\text{CH}_3)$
$\text{L}_1$	1670	1530, 1506	1330	731	-	-
$\text{L}_2$	1670	1531, 1523	1335	730	-	-
$\text{L}_3$	1668	1553, 1528	1350	725	-	-
$\text{L}_4$	1670	1561, 1528	1350	710	-	-
$\text{L}_5$	1668	1527, 1504	1330	720	-	-
$\text{L}_6$	1672	1523, -	1314	720	1345	1268
$\text{L}_7$	1668	1536, 1510	1340	736	-	1270

Table 3. IR bands ( $\text{cm}^{-1}$ ) of N-benzoyl-N'-substituted phenyl thioureas copper(II) complexes.

Compound	$\nu(\text{C}=\text{O})$	$\nu_{\text{asym}}(\text{N}-\text{C}-\text{N})$	$\nu_{\text{sym}}(\text{N}-\text{C}-\text{N})$	$\nu(\text{C}-\text{S})$	$\nu(\text{C}-\text{NO}_2)$	$\nu(\text{C}-\text{O}-\text{CH}_3)$
$[\text{Cu}(\text{L}_1)_2\text{Cl}_2]$	1670	1533	1330	685	-	-
$[\text{Cu}(\text{L}_2)_2\text{Cl}_2]$	1674	1534	1333	685	-	-
$[\text{Cu}(\text{L}_3)_2\text{Cl}_2]$	1671	1553	1322	685	-	-
$[\text{Cu}(\text{L}_4)_2\text{Cl}_2]$	1670	1528	1320	668	-	-
$[\text{Cu}(\text{L}_5)_2\text{Cl}_2]$	1666	1533	1323	686	-	-
$[\text{Cu}(\text{L}_6)_2\text{Cl}_2]$	1681	1525	1306	684	1353	1276
$[\text{Cu}(\text{L}_7)_2\text{Cl}_2]$	1670	1513	1353	680	-	1270

Table 4. Electronic spectra (recorded in chloroform) of  $\text{L}_1$ - $\text{L}_7$  ligands and their copper(II) complexes ( $\text{cm}^{-1}$ ).

Ligands		Complexes	
$\text{L}_1$	39200, 36650	$[\text{Cu}(\text{L}_1)_2\text{Cl}_2]$	39400, 33000, 7680
$\text{L}_2$	39850, 37300	$[\text{Cu}(\text{L}_2)_2\text{Cl}_2]$	39200, 37000, 6800
$\text{L}_3$	39200, 36300	$[\text{Cu}(\text{L}_3)_2\text{Cl}_2]$	39500, 31250, 8050
$\text{L}_4$	39500, 36300	$[\text{Cu}(\text{L}_4)_2\text{Cl}_2]$	39100, 32250, 8010
$\text{L}_5$	39700, 35850	$[\text{Cu}(\text{L}_5)_2\text{Cl}_2]$	38600, 35700, 7300
$\text{L}_6$	37600, 27000	$[\text{Cu}(\text{L}_6)_2\text{Cl}_2]$	38800, 27000, 7520
$\text{L}_7$	39500, 36500	$[\text{Cu}(\text{L}_7)_2\text{Cl}_2]$	39200, 35700, 7280

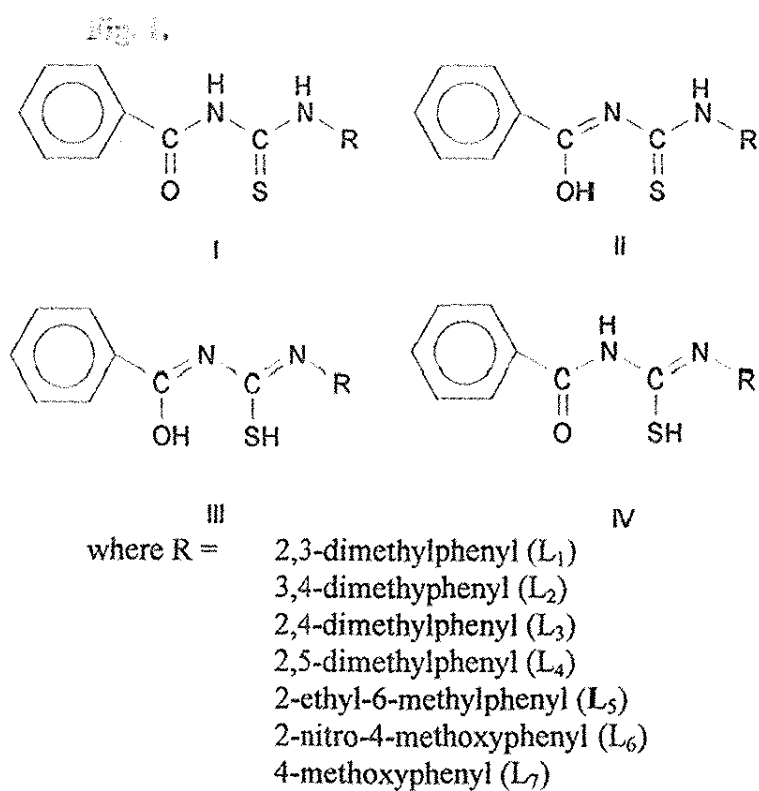


Fig. 1. Structure of the Ligands Used.



The main IR bands of the ligands  $L_1$ - $L_7$  and their copper complexes are listed in Tables 2 and 3.

The IR spectra of the ligands is highly complex and shows a larger number of bands. We have not attempted to make a complete analysis of the spectra; however attention has been focused on a limited number of bands which provide considerable structural significance in order to suggest the most probable manner of coordination of the ligand with copper(II) ion. It has been stated the thione group ( $C=S$ ) is relatively unstable in the monomeric form and tends to a stable  $C-S$  single bond by enethiolization, if there is at least one hydrogen atom adjacent to the  $C=S$  bond. The IR spectra of  $L_1$ - $L_7$  do not display any vibrational ( $S-H$ ) bond near  $2500\text{ cm}^{-1}$  indicating that, at least, in the solid state they remain in the thione form. The carbonyl stretching band appears  $\sim 1670\text{ cm}^{-1}$ . The position of this band is not changed in the IR spectra of the complexes suggesting that  $C=O$  group is not involving in coordination to the copper ion. The characteristic absorption region of ( $C=S$ ) stretching are reported in the free thiocarbamide at  $730, 1080, 1120$  and  $1400\text{ cm}^{-1}$ . A relatively sharp band of medium intensity appears in the spectra of ligands at  $710\text{-}730\text{ cm}^{-1}$  which most probably arises due to  $C=S$  stretching vibrations. In the metal complexes this band disappears and another band of same intensity appears in the range  $670\text{-}685\text{ cm}^{-1}$ . This observation indicates the shift of ligand  $\nu(C-S)$  vibration towards a lower frequency region and further attribute the coordination of  $C=S$  group with the copper(II) ion.

In the region  $1500\text{-}1560\text{ cm}^{-1}$  there are two strong bands. These twin bands can be attributed to  $\nu_{\text{asym}}(N-C-N)$  stretching vibrations. In all the complexes spectra one of these twin bands disappears suggesting also the participation of  $C=S$  group in coordination. In the far infrared, several new bands are observed in the spectra of the complexes, typical of the  $M-S$  ( $300\text{-}320\text{ cm}^{-1}$ ) vibrations<sup>11,12</sup>.

The electronic spectroscopy data for ligands and their copper complexes, in solution (chloroform), are quoted in Table 4.

Table 4

All these derivatives of thiourea have a strong band due to a  $n \rightarrow \pi^*$  transition at ca  $39500\text{ cm}^{-1}$  and a second  $\pi \rightarrow \pi^*$  at ca  $36500\text{ cm}^{-1}$  (except for  $L_6$  at  $27000\text{ cm}^{-1}$ ). Both of these are found in the electronic spectra of complexes. All the electronic spectra of copper(II) complexes exhibits an absorption in the  $7000\text{-}8000\text{ cm}^{-1}$  region which it may be assigned to a  ${}^2B_2 \rightarrow {}^2E$  transition<sup>13</sup>, comparable to those reported for four-coordinate complexes, distorted tetrahedral environment ( $D_{2d}$ ).

Figures 2,3

The ESR spectrum obtained on polycrystalline powder at room temperature of  $[Cu(L_1)_2Cl_2]$  is shown in Fig. 2. For the  $[CuL_1H_2O]$  complex the ESR spectrum is shown in Fig. 3. The ESR spectrum of  $[Cu(L_1)_2Cl_2]$  complex quite different from those of the  $[CuL_1H_2O]$  which posses an octahedral tetragonal distorted geometry<sup>10,14</sup>, this compound being prepared in different conditions (alkaline medium).

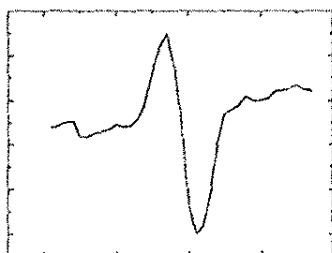


Fig. 2. The ESR spectrum of  $[\text{Cu}(\text{L}_1)_2\text{Cl}_2]$  complex ( $g = 2.2228$ ,  $\Delta H = 111.25\text{G}$ )

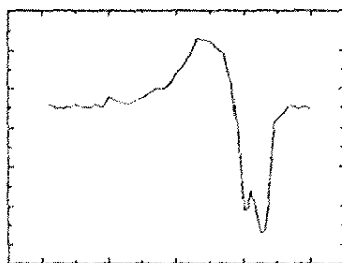


Fig. 3. The ESR spectrum of the  $[\text{CuL}_1\text{H}_2\text{O}]$  complex ( $g_{\parallel} = 1.9667$ ,  $g_{\perp} = 2.1410$  and  $\Delta H = 111\text{G}$ )

## REFERENCES

1. D. Venkappayya, D.H. Brown, *J. Inorg. Nucl. Chem.*, 36, 1023, (1974).
2. G. Marcotrigiano, G. Peyronel, R. Battistuzzi, *J. Inorg. Nucl. Chem.*, 37, 1675, (1975).
3. M.M. Shoukry, A.E.S. Mahgoub, M.H. Eluagdi, *J. Inorg. Nucl. Chem.*, 42, 1171, (1980).
4. M.M. Shoukry, K. Azik, E.M. Shoukry, S. Haurdallah, *Transition Met. Chem.*, 14(2), 115, (1989).
5. K.C. Satpathy, H.P. Mishra, T.D. Mahana, *J. Indian Chem. Soc.*, 56(3), 248, (1979).
6. K.C. Satpathy, H.P. Mishra, G.C. Pradhan, *J. Indian Chem. Soc.*, 58(9), 844, (1981).
7. E. Uhlemann, H. Bukowsky, *Z. Anorg. allg. Chem.*, 470, 177, (1980).
8. D.M. Ambore, A.P. Joshi, *J. Indian Chem. Soc.*, 68(3), 175, (1991).
9. O. Maior, M. Badica, manuscript in preparation.
10. K.C. Satpathy, H.J.P. Mishra, A.K. Panda, A.K. Satpathy, *J. Indian Chem. Soc.*, 56(8), 761, (1979).
11. K. Nakamoto, *Infrared Spectra of Inorganic and Coordination Compounds*, J. Wiley & Sons, Inc., New York, (1986).
12. J. Granifo, H. Rocha, *J. Coord. Chem.*, 34, 23, (1995).
13. A.B.P. Lever, *Inorganic Electronic Spectroscopy*, Elsevier, Amsterdam, 554, (1984).
14. B.J. Hathaway, D.L. Billing, *Coord. Chem. Rev.*, 5(2), 143, (1970).

**THE PÉRCIO DE MORAES BRANCO COLLECTION OF RARE MINERALS  
OF THE UNIVERSIDADE LUTERANA DO BRASIL (ULBRA).\*\***

**\*Paulo César Pereira das Neves - [neves@mozart.ulbra.tche.br](mailto:neves@mozart.ulbra.tche.br)  
Universidade Luterana do Brasil - ULBRA  
Centros de Ciências Naturais e Exatas e de Tecnologia - Museu de Ciências  
Laboratório de Mineralogia - Cursos de Química e Engenharia Civil  
Rua Miguel Tostes, 101 - Bairro São Luís - Fax (051)-477-1313  
CEP 92420-280, Canoas, RS, Brasil.**

**Pércio de Moraes Branco - [pmbranco@portoweb.com.br](mailto:pmbranco@portoweb.com.br)  
Companhia de Pesquisas de Recursos Minerais - CPRM  
Rua Banco da Província, 105 - Bairro Santa Teresa  
CEP 90840-030, Porto Alegre, RS, Brasil.**

**Paulo Anselmo Mاتيoli - [matioli@if.ufrgs.br](mailto:matioli@if.ufrgs.br)  
Museu de Ciências e Tecnologia/MCPUCRS  
Pontifícia Universidade Católica do Rio Grande do Sul. CEP 90619-900, Porto  
Alegre, RS, Brasil.**

**ABSTRACT**

*The Mineral Collection of the Lutheran University of Brazil is one of the most valuable mineral collections of the South American Continent and consists of approximately 500 catalogued minerals of which about 200 can be classified as rare or very rare. The majority of them are present in paragenesis with other minerals in the form of euhedric, subhedric and anhedral crystals. The minerals come from different mineralogic provinces including Denmark, United States of America, Canada, Italy, Romania, Russia, Sweden, Brazil, Mexico, Chile, Slovenia, Germany, Algeria, England and others. The Collection is organized in mineralogical classes with the exception of meteorites, organic compounds and mineraloids and is found on permanent display and open to visitors in the Laboratory of Mineralogy, Building I, Central Campus of ULBRA in Canoas, RS, Brazil.*

**Keywords:** *Rare Minerals, Mineralogic Provinces, Mineralogical Classes, Meteorites.*

**\* Author to whom correspondence should be addressed.**

**\*\*This paper is dedicated to the 10<sup>th</sup> anniversary (1988-1998) of the Chemistry Course at ULBRA.**

## RESUMO

*A coleção de minerais da Universidade Luterana do Brasil, constitui-se numa das mais valiosas coleções mineralógicas do Brasil, com aproximadamente 500 espécies catalogadas das quais, aproximadamente, 200 podem ser enquadradas como raras a muito raras. Grande parte das mesmas apresenta-se em paragênese com outros minerais, havendo cristais euédricos, subédricos e anédricos. Os minerais provêm de diversas províncias mineralógicas, como Dinamarca, Rússia, Estados Unidos da América, Canadá, Itália, Romênia, Brasil, México, Suécia, Chile, Argentina, Alemanha, Argélia e Inglaterra, entre outras. A Coleção encontra-se sistematizada em classes mineralógicas, com exceção dos meteoritos e mineralóides, estando em exposição permanente na sala 127 - Prédio I (Laboratório de Mineralogia) da ULBRA, Campus de Canoas.*

## INTRODUCTION

The purpose of this paper is to stimulate the collection of minerals and present reasons that we consider of importance in this activity. In addition, this paper aims to present a partial list of rare minerals present in the Pécio de Moraes Branco Collection of the Lutheran University of Brazil - ULBRA.

The ULBRA Mineral Collection was acquired from the collector Pécio de Moraes Branco in October 1996 thanks to the good will and sensibility of Dr. Ruben Eugen Becker, Magnificent Rector of the Lutheran University of Brazil. This acquisition permitted the permanence in Rio Grande do Sul of one of Brazil's major mineralogic collections. This collection was later enriched with samples already existing in the University and through exchange with Paulo Anselmo Matioli, who is one of largest private collectors of the country.

Before the public exposition, the Collection passed through revision and sistematic organization under the supervision of Professor Paulo César Pereira das Neves with help of geologists Paulo Anselmo Matioli, Milena Matioli and Kátia Beppler. The organization was done using the systematics of Klein and Hurbult Jr<sup>1</sup>. The chemical compositions were compiled from the work of Fleischer and Mandarino<sup>2</sup>. Other references used in the classification included the works of Branco<sup>3</sup>, Milovsky and Kononov<sup>4</sup> and of Klockmann and Rhämdor<sup>5</sup>.

The Collection was formally inaugurated on August 13, 1997 is located in Room 127, Building I, Main Campus of ULBRA in Canoas and is an integral part of the Department of Chemistry (Science Museum). It is open to public visitation and was visited by about 2,000 persons since its inauguration.

## MINERALS AND MINERAL COLLECTORS

Collecting things is part of human nature. Many of us have a tendency that begins in childhood to collect objects of different kinds in an orderly or disordely manner. As children we collect figurines, decals, coins, stamps, etc. As adults we

tend to prefer more valuable objects such as watches, clocks and works of art. We may even continue to collect coins and stamps, only that with a different vision and disposition paying more attention to the monetary value and not only for the pleasure of having a large quantity of the things that we like.

Collecting minerals is then no strange custom. On the contrary, it is a very common one in places like the United States of America and Italy, for example. On the other hand, in Brazil in spite of the great diversity and abundance of mineral treasure and specially of precious stones and gems there are only a few collectors.

Until a few years ago (the end of the 1980's) there were relatively few mineral collectors. Only recently, especially due to the large demand for minerals for energization, cure and other esoteric purposes there has been a large interest in mineral collection among the general public and at the present time it is not difficult to encounter people that collect minerals. This increasing interest in mineral collection is now also present among Brazilian children. Its reasons, however, are not easy to judge.

#### REASONS FOR COLLECTING MINERALS

Being able to collect so many other different things why would a person choose to collect minerals? A good reason may be their beauty, especially of those minerals that are well crystallized. But this reason is too obvious, for every collector seeks and searches for objects that are pleasant to the eye. A more specific reason is the possibility to obtain pieces for the collection without need to purchase them or make exchange. Collections, as a whole, grow and are expanded through exchange and purchase from other collectors. Minerals, however, are much more accessible since they occur freely in nature. This is particularly true for collectors that work in the mineral field such as geologists and mining engineers.

Another characteristic of mineral collection is its universality. Collections of stamps, coins, works of art are usually related to a particular country or region of the Earth. It is true, they may have a certain international flavor and outlook, but they are not naturally international like minerals. Besides, what other kind of collection can count with samples that originate far from the Earth, like meteorites, tectites or rock samples from the Moon? What is the age of a document, work of art or coin, measured in centuries or millenia when compared to the age of minerals and rocks that span millions of years?

Another characteristic of minerals is that they are substances produced without human participation, and as such they are not subject to personal evaluation as far as the ability of who made them and the artistic disposition or taste of who produced them. The minerals, beautiful or not, are as they are because Mother Nature made them so, not because of the more or less able hands that molded them. Besides, characteristics that may be classified as defects, are very often details that make the sample very rare, if not unique.

For geologists and other geoscientists the collection of minerals is the best way to recognize them. The constant handling, the comparative examination of individual samples of the same type or species coming from different regions and

the observation of peculiarities help the collector to develop an acute perception of the characteristics of the material that is being collected. This type of perception cannot be obtained even by reading and studying the best manuals and treatises of mineralogy.

Although there exist a large number of minerals that are easily damaged because of their softness, sensibility to light, humidity and other factors, as a whole, minerals have a very high physical resistance and endurance, much superior to living beings, and also greater than that of objects such as paintings, stamps and photographs. This is another good reason to collect minerals.

### HOW TO COLLECT MINERALS

The first big decision faced upon beginning the collection of minerals is as to what type of material one should collect. Systematic collections include all type of minerals and diversity is the main objective and the aspect of major value. Systematic collections are usually the best option for beginners. With the passing of time collectors may decide to specialize, collecting only a specific group of minerals. A collection limited to a few types of minerals is indicated when there are limitations of space or of financial resources. For a systematic collection to be important it needs to grow and this requires space. On the other hand, a specific collection may rival with that of good museums. A good example of this is given by Jules Sauer, one of the greatest jewellers from Brazil. Although he has the means to acquire a wide variety of minerals from all over the world, he collects only tourmalines.

Another important factor intimately related to the space available is the size of the samples present in the collection. Obviously, if the space is restricted a large number of samples of big dimension can not be accommodated and the choice is the one of "cabinet", "thumb nails" or "micromount" collections, as American geologists call them. The samples present in a collection, however can not be so small that their identification is made difficult. Samples of common minerals that require the reading of the tag in order to be identified are too small. The distinctive characteristics should be easily recognizable.

A collection increases not only through exchange of minerals but also through exchange of information among collectors. At times, an experienced mineralogist with a solid background in geology can have difficulty in identifying a sample that another person with less formal training identifies with ease. The same may be true in regards to the origin of the mineral. An experienced collector may identify the unknown origin of a mineral on the basis of a few typical physical characteristics. This exchange is more fruitful when done through societies of mineralogists and collectors. In such a case, the information reaches a larger public and the scientific value of the information is formally recognized and better employed.

Another good source of information are museums. Collectors should appreciate the beauty of the samples on display, learn about their composition and origin and propose exchange of materials and information. A true and conscient

collector respects his fellow collectors. When taking samples from a prospection site, he never takes more than the necessary and does not do any damage to the samples he does not take. Other scientists and collectors that may visit the same site and deserve the opportunity to find what they are searching for. There may be some exceptions: in quarries where all the rocks removed are used for gravel, a true collector not only may but he must collect everything within his reach and donate the samples that he does not need to museums and schools or exchange them with other collectors.

On an identification tag that accompanies a mineral on exposition the following information is considered essential: name of the mineralogic species, chemical composition, crystal system and origin. The written information should be presented in a manner that is in visual harmony with the mineral on display and special care should be given to the size of the tag.

### REASONS FOR COLLECTING MINERALS

According to Frederick H. Pough, one of North American's greatest mineralogists, only Mineralogy among the basic sciences is an educational past-time for it combines Chemistry, Physics and Mathematics.

### RARE MINERALS IN THE MINERAL COLLECTION OF THE LUTHERAN UNIVERSITY OF BRAZIL - ULBRA

Below we present a list of the rare samples present in the mineral collection of the Lutheran University of Brazil. The samples are listed with the respective mineralogic classes. Rare species were considered all those that are not listed as common in the Mineral Tables by Dietrich<sup>6</sup>.

#### a) ORGANIC COMPOUNDS

\* Idrialite -  $C_{22}H_{14}$  - Orthorrombic System - Idrija, Slovenia.

\* Mellite -  $Al_2[C_6(COO_6)].18H_2O$  - Tetragonal System - Tartabanya, Hungary.

#### b) NATIVE ELEMENTS

\* Antimony - Sb - Trigonal System - Arsenic Group - Lake George Mine, New Brunswick, Canada.

\* Arsenic - As - Cubic System - Kuse Mine, Sarawak, North Bau, Borneo, Indonesia.

\* Bismuth - Bi - Trigonal System - Arsenic Group - Pietra Majori, Sarrabus, Sardinia, Italy.

\* Cohenite -  $(Fe,Ni,Co)_3C$  - Orthorrombic System - Nandan Meteorite, Nandan, Lihu, People's Republic of China.



- \* Iron terrestrial - Fe - Cubic System (body-centered), alpha-iron - Tajymir, Russia.
- \* Iron-nickel meteoric - (Fe-Ni) - Cubic System - Bendengó Meteorite - Bendengó River, Monte Santo, Bahia, Brazil.
- \* Kamacite - (Fe,Ni) - alpha-Nickel-iron - Cubic System (body-centered) - Nandan Meteorite, Nandan, Lihu, People's Republic of China.
- \* Osbornite - TiN - Cubic System - Vaca Muerta Meteorite, Taltal, Atacama, Chile.
- \* Palladium - Pd - Cubic System - Gongo Soco, Caeté, Minas Gerais, Brazil.
- \* Platinum - Pt - Cubic System - Gongo Soco, Caeté, Minas Gerais, Brazil.
- \* Schreibersite - (Rhabdite) - (Fe,Ni)<sub>3</sub>P - Tetragonal System - Vaca Muerta Meteorite, Taltal, Atacama, Chile.
- \* Taenite - (Ni,Fe) -  $\gamma$ -Nickel-iron - Cubic System (face-centered) - Nandan Meteorite, Nandan, Lihu, People's Republic of China.

### c) SULFIDES and SULFOSALTS

Due to chemical affinity the sulfide and sulfosalts classes also includes tellurides, arsenides, sulfoarsenides and antimonides (Klein & Hurlburt Jr<sup>1</sup>).

- \* Apuanite -  $\text{Fe}^{2+}\text{Fe}_4^{3+}\text{Sb}_4^{3+}\text{O}_{12}\text{S}$  - Tetragonal System - Mina Bucca Della Vena, Santa Zzema, Lucca, Toscana, Italy.
- \* Boulangerite -  $\text{Pb}_5\text{Sb}_4\text{S}_{11}$  - Monoclinic System - Cleaveland Mine, Stevens County, Washington, USA.
- \* Calaverite -  $\text{AuTe}_2$  - Monoclinic System - Strong Mine, Colo County, Colorado, USA.
- \* Cubanite (variety Chalmersite) -  $\text{CuFe}_2\text{S}_3$  - Orthorrombic System - Mina do Morro Velho, Nova Lima, Minas Gerais, Brazil.
- \* Digenite -  $\text{Cu}_9\text{S}_5$  - Cubic System - Mina Capoeira, Parelhas, Rio Grande do Norte, Brazil.
- \* Geocronite -  $\text{Pb}_{14}(\text{Sb,As})_6\text{S}_{23}$  - Monoclinic System - Falün, Sweden.
- \* Löllingite -  $\text{FeAs}_2$  - Orthorrombic System - Löllingite Group - Lavra do João, Conselheiro Pena, Minas Gerais, Brazil.
- \* Metacinnabar -  $\text{HgS}$  - Sphalerite Group - Cubic System - Idrija, Slovenia.
- \* Pentlandite -  $(\text{Fe,Ni})_9\text{S}_8$  - Cubic System - Pentlandite Group - Nickel Mine, Sudbury, Ontario, Canada.
- \* Polydymite -  $\text{NiNi}_2\text{S}_4$  - Cubic System - Linnaeite Group - Nickel Mine, Sudbury, Ontario, Canada.
- \* Rayite -  $(\text{Ag,Tl})_2\text{Pb}_8\text{Sb}_8\text{S}_{21}$  - Monoclinic System - Herja Mine, Baia Sprie, Maramures, Romania.
- \* Semseyite -  $\text{Pb}_9\text{Sb}_8\text{S}_{21}$  - Monoclinic System - Herja Mine, Baia Sprie, Maramures, Romania.
- \* Skutterudite -  $\text{CoAs}_{2.3}$  - Cubic System - Bou Azzer, Anti Atlas, Morocco.
- \* Sudburyite -  $(\text{Pd,Ni})\text{Sb}$  - Hexagonal System - Nickeline Group - Nickel Mine, Sudbury, Ontario, Canada.

- \* Tochilinite -  $6\text{Fe}_{0.9}\text{S}_5(\text{Mg},\text{Fe}^{2+})(\text{OH})_2$  - Monoclinic or Triclinic Systems - Ottawa, Canada.
- \* Troilite -  $\text{FeS}$  - Hexagonal System - Nandan Meteorite, Nandan, Lihu, People's Republic of China.
- \* Valleriite -  $4(\text{Fe},\text{Cu})\text{S}_3(\text{Mg},\text{Al})(\text{OH})_2$  - Hexagonal System - Mina El Teniente, Rancagua, Chile.
- \* Versiliaite -  $\text{Fe}_4^{2+}\text{Fe}_8^{3+}\text{Sb}_{12}^{3+}\text{O}_{32}\text{S}_2$  - Orthorhombic System - Mina Bucca Della Vena, Santa Zzema, Lucca, Toscana, Italy.

#### e) OXIDES and HYDROXIDES

- \* Akaganeite - *beta*- $\text{Fe}^{3+}(\text{O},\text{OH},\text{Cl})$  - Monoclinic System (Pseudo Tetragonal) - Nandan Meteorite, Nandan, Lihu, People's Republic of China.
- \* Bindheimite -  $\text{Pb}_2\text{Sb}_2\text{O}_6(\text{O},\text{OH})$  - Cubic System - Stibconite Group - Pereta Mine, Grosseto, Toscana, Italy.
- \* Cervantite -  $\text{Sb}^{3+}\text{Sb}^{5+}\text{O}_4$  - Orthorhombic System - Pereta Mine, Grosseto, Toscana, Italy.
- \* Chalcophanite -  $(\text{Zn},\text{Fe}^{2+},\text{Mn}^{2+})\text{Mn}_4^{3+}\text{O}_7\cdot 3\text{H}_2\text{O}$  - Trigonal System - Tamara, Tunisia.
- \* Emmonsite -  $\text{Fe}_2^{3+}\text{Te}_3^{4+}\text{O}_9\cdot 2\text{H}_2\text{O}$  - Triclinic System - Coral Zone, Louisville, Jefferson County, Kentucky, USA.
- \* Feroxyhyte - *delta*- $\text{Fe}^{3+}\text{O}(\text{OH})$  - Hexagonal System - Nandan Meteorite, Nandan, Lihu, People's Republic of China.
- \* Hercynite -  $\text{Fe}^{2+}\text{Al}_2\text{O}_4$  - Cubic System - Spinel Group - San Vito, Monte Somma, Vesuvio, Napoli, Italy.
- \* Hollandite -  $\text{Ba}(\text{Mn}^{4+},\text{Mn}^{2+})_8\text{O}_{16}$  - Monoclinic (Pseudo Tetragonal) System - Cryptomelane Group - Hurdal, Norway.
- \* Maghemite -  $\gamma\text{-Fe}_2\text{O}_3$  - Nandan Meteorite, Nandan, Lihu, People's Republic of China.
- \* Minium -  $\text{Pb}_2^{2+}\text{Pb}^{4+}\text{O}_4$  - Tetragonal System - Mine Kurfürst Ernest, Bonkhausen, Sauerland, Germany.
- \* Ramsdellite -  $\text{Mn}^{4+}\text{O}_2$  - Orthorhombic System - Mistake Mine, Yavapai County, Arizona, USA.
- \* Senarmontite -  $\text{Sb}_2\text{O}_3$  - Cubic System - Hamitate, Djebel, Constantine, Algeria.
- \* Simpsonite (Calogerasite) -  $\text{Al}_4(\text{Ta},\text{Nb})_3(\text{O},\text{OH},\text{F})_{14}$  - Trigonal System - Alto do Giz, Equador, Rio Grande do Norte, Brazil.
- \* Tripuhyte -  $\text{Fe}^{2+}\text{Sb}_2^{5+}\text{O}_6$  - Tetragonal System - Ferrotapiolite Group - Pereta Mine, Grosseto, Toscana, Italy.
- \* Uranmicrolite - (Djalmaite)  $(\text{U},\text{Ca},\text{Ce})_2(\text{Ta},\text{Nb})_2\text{O}_6(\text{OH},\text{F})$  - Cubic System - Pyrochlore Group - São João Del Rei, Minas Gerais, Brazil.
- \* Valentinite -  $\text{Sb}_2\text{O}_3$  - Orthorhombic System - Sidi Adris, Algeria.
- \* Varlamoffite (a variety of Cassiterite) -  $(\text{Sn},\text{Fe})(\text{O},\text{OH})_2$  - Tetragonal System - Cligga Mine, Cornwall, England.
- \* Wodginite -  $\text{Mn}^{2+}(\text{Sn}^{4+},\text{Ta})\text{Ta}_2\text{O}_8$  - Monoclinic System - Bernic Lake, Manitoba, Canada.

## g) HALIDES

- \* Boleite -  $\text{Pb}_{26}\text{Ag}_{10}\text{Cu}_{24}^{2+}\text{Cl}_{62}(\text{OH})_{48} \cdot 3\text{H}_2\text{O}$  - Cubic System - Mina de Plúton, Santa Rosalia, Boleo, Baja California, Mexico.
- \* Chlorargyrite (Cerargyrite) -  $\text{AgCl}$  - Cubic System - Silver Reef Ledge, Utah, USA.
- \* Cryolite -  $\text{Na}_3\text{AlF}_6$  - Monoclinic System - Ivigtut, Greenland, Denmark.
- \* Diaboleite -  $\text{Pb}_2\text{Cu}^{2+}\text{Cl}_2(\text{OH})_4$  - Tetragonal System - Mina de Plúton, Santa Rosalia, Boleo, Baja California, Mexico.
- \* Eriochalcite -  $\text{Cu}^{2+}\text{Cl}_2 \cdot 2\text{H}_2\text{O}$  - Orthorrombic System - Mina La Farola, Copiapó, Atacama, Chile.
- \* Gearksutite -  $\text{CaAl}(\text{OH})\text{F}_4 \cdot \text{H}_2\text{O}$  - Monoclinic System - Mina Mato Preto, Cerro Azul, Paraná, Brazil.
- \* Kainite -  $\text{MgSO}_4 \cdot \text{KCl} \cdot 3\text{H}_2\text{O}$  - Monoclinic System - Bochnia, Cracow, Poland.
- \* Lawrencite -  $(\text{Fe}^{2+}, \text{Ni})\text{Cl}_2$  - Trigonal System - Nandan Meteorite, Nandan, Lihu, People's Republic of China.
- \* Nantokite -  $\text{CuCl}$  - Cubic System - Mina La Farola, Copiapó, Atacama, Chile.
- \* Onoratoite -  $\text{Sb}_8\text{O}_{11}\text{Cl}_2$  - Monoclinic System - Pereta Mine, Grosseto, Toscana, Italy.
- \* Sal ammoniac -  $\text{NH}_4\text{Cl}$  - Cubic System - Fichteberg, Saxonia, Germany.
- \* Sellaite -  $\text{MgF}_2$  - Tetragonal System - Serra das Éguas, Brumado, Bahia, Brazil.
- \* Weberite -  $\text{Na}_2\text{MgAlF}_7$  - Orthorrombic System - Ivigtut, Greenland, Denmark.

## h) CARBONATES

- \* Artinite -  $\text{Mg}_2(\text{CO}_3)(\text{OH})_2 \cdot 3\text{H}_2\text{O}$  - Monoclinic System - Clear Creek, San Benito County, California, USA.
- \* Burbankite -  $(\text{Na}, \text{Ca})_3(\text{Sr}, \text{Ba}, \text{Ce})_3(\text{CO}_3)_5$  - Hexagonal System - Pedreira da Prefeitura, Poços de Caldas, Minas Gerais, Brazil.
- \* Burkeite -  $\text{Na}_6(\text{CO}_3)(\text{SO}_4)_2$  - Orthorrombic System - Searles Lake, San Benito County, California, USA.
- \* Canavesite -  $\text{Mg}_2(\text{CO}_3)(\text{HBO}_3) \cdot 5\text{H}_2\text{O}$  - Monoclinic System - Pereta Mine, Grosseto, Toscana, Italy.
- \* Dawsonite -  $\text{NaAl}(\text{CO}_3)(\text{OH})_2$  - Orthorrombic System - Monte Ammiata, Toscana, Italy.
- \* Dypingite -  $\text{Mg}_5(\text{CO}_3)_4(\text{OH})_2 \cdot 5\text{H}_2\text{O}$  - Monoclinic System (?) - Rapid Creek, Yukon, Canada.
- \* Hydrotalcite -  $\text{Mg}_6\text{Al}_2(\text{CO}_3)(\text{OH})_{16} \cdot 4\text{H}_2\text{O}$  - Trigonal System - Hydrotalcite Group - Dypingdal, Snarum, Buskerud, Norway.
- \* Ikaite -  $\text{CaCO}_3 \cdot 6\text{H}_2\text{O}$  - Monoclinic System - Ika, Ivigtut, Greenland, Denmark.
- \* Manasseite -  $\text{Mg}_6\text{Al}_2(\text{CO}_3)(\text{OH})_{16} \cdot 4\text{H}_2\text{O}$  - Hexagonal System - Manasseite Group - Dypingdal, Snarum, Buskerud, Norway.
- \* Nullaginite -  $\text{Ni}_2(\text{CO}_3)(\text{OH})_2$  - Monoclinic System - Rosasite Group - Cottonwood Mine, Bolivia Ghost Town, Churchill County, Nevada, USA.

- \* **Schröckingerite** -  $\text{NaCa}_3(\text{UO}_2)(\text{CO}_3)_3(\text{SO}_4)\text{F} \cdot 10\text{H}_2\text{O}$  - Triclinic System - Huemul Mine, Malargüe, Mendoza, Argentina.
- \* **Stichtite** -  $\text{Mg}_6\text{Cr}_2(\text{CO}_3)(\text{OH})_{16} \cdot 4\text{H}_2\text{O}$  - Orthorrombic System - Hydrotalcite Group - Stichtit Hill, Dundas, Tasmania, Australia; Campo Formoso, Bahia, Brazil.
- \* **Uranocalcarite** -  $\text{Ca}(\text{UO}_2)_3(\text{CO}_3)(\text{OH})_6 \cdot 3\text{H}_2\text{O}$  - Orthorrombic System - Huemul Mine, Malargüe, Mendoza, Argentina.
- \* **Weloganite** -  $\text{Sr}_3\text{Na}_2\text{Zr}(\text{CO}_3)_6 \cdot 3\text{H}_2\text{O}$  - Triclinic System (Pseudo Trigonal) - Francon Quarry, Montreal Island, Quebec, Canada.

#### i) NITRATES

- \* **Nitratine** - (Soda Niter)  $\text{NaNO}_3$  - Trigonal System - Oficina Maria Elena, Salitreras, Atacama, Chile.
- \* **Nitro** -  $\text{KNO}_3$  - Orthorrombic System - Morro do Chapéu, Irecê, Bahia, Brazil.

#### j) IODATES

- \* **Bellingerite** -  $\text{Cu}_2^{2+}(\text{IO}_3)_6 \cdot 2\text{H}_2\text{O}$  - Triclinic System - Oficina Maria Elena, Salitreras, Atacama, Chile.
- \* **Brüggénite** -  $\text{Ca}(\text{IO}_3)_2 \cdot \text{H}_2\text{O}$  - Monoclinic System - Oficina Maria Elena, Salitreras, Atacama, Chile.

#### k) BORATES

- \* **Boracite** -  $\text{Mg}_3\text{B}_7\text{O}_{13}\text{Cl}$  Orthorrombic System (Pseudo Cubic) - Stassfurt Mine, Stassfurt, Germany.
- \* **Kurnakovite** -  $\text{MgB}_3\text{O}_3(\text{OH})_5 \cdot 5\text{H}_2\text{O}$  - Orthorrombic System - Kern County, Boron, California, USA.
- \* **Ludwigite** -  $\text{Mg}_2\text{Fe}^{3+}\text{BO}_5$  - Orthorrombic System - Ludwigite Group - Corcolle, Roma, Italy.
- \* **Meyerhofferite** -  $\text{Ca}_2\text{B}_6\text{O}_6(\text{OH})_{10} \cdot 2\text{H}_2\text{O}$  - Triclinic System - Mt. Blanco DC., Kern County, California, USA.
- \* **Szaibelyite** -  $\text{MgBO}_2(\text{OH})$  - Monoclinic System - Herja Mine, Baia Sprie, Maramures, Romania.
- \* **Vonsenite** -  $\text{Fe}_2^{2+}\text{Fe}^{3+}\text{BO}_5$  - Orthorrombic System - Ludwigite Group - Corcolle, Roma, Italy.

#### l) PHOSPHATES

- \* **Anapaite** -  $\text{Ca}_2\text{Fe}^{2+}(\text{PO}_4)_2 \cdot 4\text{H}_2\text{O}$  - Triclinic System - Kerch, Crimea, Ukraine.
- \* **Arrojadite** -  $\text{KNa}_4\text{CaMn}_4^{2+}\text{Fe}_{10}^{2+}\text{Al}(\text{PO}_4)_{12}(\text{OH},\text{F})_2$  - Monoclinic System - Rapid Creek, Yukon, Canada.
- \* **Augelite** -  $\text{Al}_2(\text{PO}_4)(\text{OH})_3$  - Monoclinic System - Asbestos, Quebec, Canada.

- \* Carbonate-hydroxylapatite - (Dahllite)  $\text{Ca}_5(\text{PO}_4, \text{CO}_3)_3(\text{OH})$  - Hexagonal System - Apatite Group - Carnaúba dos Dantas, Rio Grande do Norte, Brazil.
- \* Chalcociderite -  $\text{Cu}^{2+}\text{Fe}_6^{3+}(\text{PO}_4)_4(\text{OH})_8 \cdot 4\text{H}_2\text{O}$  - Triclinic System - Turquoise Group Somerset, England.
- \* Cornetite -  $\text{Cu}_3^{2+}(\text{PO}_4)(\text{OH})_3$  - Orthorrombic System - Star Mine, Lubumbashi, Democratic Republic of Congo.
- \* Eosphorite -  $\text{Mn}^{2+}\text{Al}(\text{PO}_4)(\text{OH})_2 \cdot \text{H}_2\text{O}$  - Monoclinic System - Lavra da Ilha, Itinga, Minas Gerais, Brazil.
- \* Ernstite -  $(\text{Mn}^{2+}_{1-x}, \text{Fe}^{3+}_x)\text{Al}(\text{PO}_4)(\text{OH})_{2-x}\text{O}_x$  - Monoclinic System - Lavra da Ilha, Itinga, Minas Gerais, Brazil.
- \* Frondelite -  $\text{Mn}^{2+}\text{Fe}_4^{3+}(\text{PO}_4)_3(\text{OH})_5$  - Orthorrombic System - Lavra do João, Conselheiro Pena, Minas Gerais, Brazil.
- \* Goyazite -  $\text{SrAl}_3(\text{PO}_4)_2(\text{OH})_5 \cdot \text{H}_2\text{O}$  - Trigonal System - Crandallite Group - Rapid Creek, Yukon, Canada.
- \* Hinsdalite -  $(\text{Pb}, \text{Sr})\text{Al}_3(\text{PO}_4)(\text{SO}_4)(\text{OH})_6$  - Trigonal System - Beudantite Group - Mina Los Bolones, Combarbala, IV Region, Chile.
- \* Hentschelite -  $\text{Cu}^{2+}\text{Fe}_2^{3+}(\text{PO}_4)_2(\text{OH})_2$  - Monoclinic System - Lazulite Group - Rajo de Vicuña, Andacollo, Chile.
- \* Hureaulite -  $\text{Mn}_5^{2+}(\text{PO}_4)_2[\text{PO}_3(\text{OH})]_2 \cdot 4\text{H}_2\text{O}$  - Monoclinic System - Lavra do João, Conselheiro Pena, Minas Gerais, Brazil.
- \* Hydroxylherderite -  $\text{CaBe}(\text{PO}_4)(\text{OH})$  - Monoclinic System - Benett Quarry, Buckfield, Maine, USA.
- \* Ludjibaite -  $\text{Cu}_5^{2+}(\text{PO}_4)_2(\text{OH})_4$  - Triclinic System - Star Mine, Lubumbashi, Democratic Republic of Congo.
- \* Ningyoite -  $(\text{U}, \text{Ca}, \text{Ce})_2(\text{PO}_4)_2 \cdot 1-2\text{H}_2\text{O}$  - Orthorrombic System (Pseudo Hexagonal) - Rhabdophane Group - Ningyo-Toge Mine, Tottori, Japan.
- \* Pseudomalachite -  $\text{Cu}_5^{2+}(\text{PO}_4)_2(\text{OH})_4$  - Monoclinic System - Rajo de Vicuña, Andacollo, Chile.
- \* Rhabdophane-(Ce) -  $(\text{Ce}, \text{La})\text{PO}_4 \cdot \text{H}_2\text{O}$  - Hexagonal System - Rhabdophane Group - Ningyo-Toge Mine, Tottori, Japan.
- \* Rockbridgeite -  $(\text{Fe}^{2+}, \text{Mn}^{2+})\text{Fe}_4^{3+}(\text{PO}_4)_3(\text{OH})_5$  - Orthorrombic System - Lavra do João, Conselheiro Pena, Minas Gerais, Brazil.
- \* Roscherite -  $\text{Ca}(\text{Mn}^{2+}, \text{Fe}^{2+})_2\text{Be}_3(\text{PO}_4)_3(\text{OH})_3 \cdot 2\text{H}_2\text{O}$  - Monoclinic and Triclinic Systems - Lavra da Ilha, Itinga, Minas Gerais, Brazil.
- \* Scholzite -  $\text{CaZn}_2(\text{PO}_4)_2 \cdot 2\text{H}_2\text{O}$  - Orthorrombic System - Reaphook Hill, Queensland, Australia.
- \* Scorzalite -  $(\text{Fe}^{+2}, \text{Mg})\text{Al}_2(\text{PO}_4)_2(\text{OH})_2$  - Monoclinic System - Lazulite Group - Carnaúba dos Dantas, Rio Grande do Norte, Brazil.
- \* Souzalite -  $(\text{Mg}, \text{Fe}^{2+})_3(\text{Al}, \text{Fe}^{3+})_4(\text{PO}_4)_4(\text{OH})_6 \cdot 2\text{H}_2\text{O}$  - Monoclinic System - Rapid Creek, Yukon, Canada.
- \* Wardite -  $\text{NaAl}_3(\text{PO}_4)_2(\text{OH})_4 \cdot 2\text{H}_2\text{O}$  - Tetragonal System - Rapid Creek, Yukon, Canada.
- \* Whiteite-(CaFeMg) -  $\text{Ca}(\text{Fe}^{2+}, \text{Mn}^{2+})\text{Mg}_2\text{Al}_2(\text{PO}_4)_4(\text{OH})_2 \cdot 8\text{H}_2\text{O}$  - Monoclinic System - Whiteite Group - Rapid Creek, Yukon, Canada.

\* Zanzazziite -  $\text{Ca}_2(\text{Mg}, \text{Fe}^{2+})(\text{Mg}, \text{Fe}^{2+}, \text{Al})_4\text{Be}_4(\text{PO}_4)_6(\text{OH})_4 \cdot 6\text{H}_2\text{O}$  - Monoclinic System - Lavra da Ilha, Itinga, Minas Gerais, Brazil.

#### m) ARSENATES AND VANADATES

\* Bayldonite -  $\text{PbCu}_3(\text{AsO}_4)_2(\text{OH})_2 \cdot \text{H}_2\text{O}$  - Monoclinic System - Wheal Carpenter, Saint Hilary, Cornwall, England.

\* Carnotite -  $\text{K}_2(\text{UO}_2)_2\text{V}_2\text{O}_8 \cdot 3\text{H}_2\text{O}$  - Monoclinic System - Huemul Mine, Malargüe, Mendoza, Argentina.

\* Ceruleite -  $\text{Cu}_2\text{Al}_7(\text{AsO}_4)_4(\text{OH})_{13} \cdot 12\text{H}_2\text{O}$  - Triclinic System - Mina Los Bolones, Combarbala, IV Region, Chile.

\* Cornwallite -  $\text{Cu}_5^{2+}(\text{AsO}_4)_2(\text{OH})_4 \cdot \text{H}_2\text{O}$  - Monoclinic System - Wheal Jewell, Saint Day, Cornwall, England.

\* Descloizite -  $\text{PbZn}(\text{VO}_4)(\text{OH})$  - Orthorhombic System - Descloizite Group - Itacarambi, Minas Gerais, Brazil.

\* Erythrite -  $\text{Co}_3(\text{AsO}_4)_2 \cdot 8\text{H}_2\text{O}$  - Monoclinic System - Vivianite Group - Modum, Norway; Bou Azzer, Anti Atlas, Morocco.

\* Hidalgoite -  $\text{PbAl}_3(\text{AsO}_4)(\text{SO}_4)(\text{OH})_6$  - Trigonal System - Beudantite Group - Mina Los Bolones, Combarbala, IV Region, Chile.

\* Huemulite -  $\text{Na}_4\text{MgV}_{10}^{5+}\text{O}_{28} \cdot 24\text{H}_2\text{O}$  - Triclinic System - Huemul Mine, Malargüe, Mendoza, Argentina.

\* Kemmlitzite -  $(\text{Sr}, \text{Ce})\text{Al}_3(\text{AsO}_4)(\text{SO}_4)(\text{OH})_6$  - Trigonal System - Beudantite Group - Mina Los Bolones, Combarbala, IV Region, Chile.

\* Metaschoderite -  $\text{Al}_2(\text{PO}_4)(\text{VO}_4) \cdot 6\text{H}_2\text{O}$  - Monoclinic System - Van Nav San Clain, Fish Creek Range, Eureka County, Nevada, USA.

\* Metatyuyamunite -  $\text{Ca}(\text{UO}_2)_2\text{V}_2^{5+}\text{O}_8 \cdot 3\text{H}_2\text{O}$  - Orthorhombic System - Huemul Mine, Malargüe, Mendoza, Argentina.

\* Mottramite -  $\text{PbCu}^{2+}(\text{VO}_4)(\text{OH})$  - Orthorhombic System - Descloizite Group - Barranca del Cobre, Chihuahua, Mexico.

\* Olivenite -  $\text{Cu}_2^{2+}(\text{AsO}_4)(\text{OH})$  - Orthorhombic System - Clara Mine, Wolfach, Schwarzwald, Germany.

\* Parnauite -  $\text{Cu}_9^{2+}(\text{AsO}_4)_2(\text{SO}_4)(\text{OH})_{10} \cdot 7\text{H}_2\text{O}$  - Orthorhombic System - Majuba Hill, Pershing County, Nevada, USA.

\* Pharmacosiderite -  $\text{KFe}^{3+}(\text{AsO}_4)_3(\text{OH})_4 \cdot 6\text{H}_2\text{O}$  - Cubic System - Wheal Garland, Cornwall, England.

\* Roselite -  $\text{Ca}_2(\text{Co}^{2+}, \text{Mg})(\text{AsO}_4)_2 \cdot 2\text{H}_2\text{O}$  - Monoclinic System - Roselite Group - Bou Azzer, Anti Atlas, Morocco.

\* Saneroite -  $\text{Na}_2(\text{Mn}^{2+}, \text{Mn}^{3+})_{10}\text{Si}_{11}\text{VO}_{34}(\text{OH})_4$  - Triclinic System - Mina Gambatesa, Genova, Liguria, Italy.

\* Schlossmacherite -  $(\text{H}_3\text{O}, \text{Ca})\text{Al}_3(\text{AsO}_4, \text{SO}_4)_2(\text{OH})_6$  - Trigonal System - Beudantite Group - Mina Los Bolones, Combarbala, IV Region, Chile.

\* Stibivanite -  $\text{Sb}_2^{3+}\text{V}^{4+}\text{O}_5$  - Monoclinic System - Mina Bucca Della Vena, Santa Zzema, Lucca, Toscana, Italy.

\* Tyuyamunite -  $\text{Ca}(\text{UO}_2)_2\text{V}_2\text{O}_8 \cdot 5\text{H}_2\text{O}$  - Orthorhombic System - Huemul Mine, Malargüe, Mendoza, Argentina.

## n) SULFATES, CROMATES AND MOLIBDATES

- \* **Arthurite** -  $\text{Cu}^{2+}\text{Fe}_2^{3+}(\text{AsO}_4\text{PO}_4\text{SO}_4)_2(\text{O},\text{OH})_2\cdot 4\text{H}_2\text{O}$  - Monoclinic System - Arthurite Group - Mina La Farola, Copiapó, Atacama, Chile; Hingston Down Mine, Cornwall, England.
- \* **Campigliaite** -  $\text{Cu}_4^{2+}\text{Mn}^{2+}(\text{SO}_4)_2(\text{OH})_6\cdot 4\text{H}_2\text{O}$  - Monoclinic System - Mina El Teniente, Rancagua, Chile.
- \* **Connellite** -  $\text{Cu}_{19}^{2+}\text{Cl}_4(\text{SO}_4)(\text{OH})_{32}\cdot 3\text{H}_2\text{O}$  - Hexagonal System - Saint Just, Cornwall, England.
- \* **Epsomite** -  $\text{MgSO}_4\cdot 7\text{H}_2\text{O}$  - Orthorhombic System - Cueva de los Gitanos, Cataluña, Spain.
- \* **Kleibergite** -  $\text{Sb}_4^{3+}\text{O}_4(\text{OH})_2(\text{SO}_4)$  - Orthorhombic System - Pereta Mine, Grosseto, Toscana, Italy.
- \* **Misenite** -  $\text{K}_2\text{SO}_4\cdot 10\text{H}_2\text{O}$  (?) - Monoclinic System - Stassfurt Salt Mine, Sachsen, Germany.
- \* **Peretaite** -  $\text{CaSb}_4^{3+}\text{O}_4(\text{OH})_2(\text{SO}_4)_2\cdot 2\text{H}_2\text{O}$  - Monoclinic System - Pereta Mine, Grosseto, Toscana, Italy.
- \* **Pickeringite** -  $\text{MgAl}_2(\text{SO}_4)_4\cdot 22\text{H}_2\text{O}$  - Monoclinic System - Halotrichite Group - Libros, Terrel, Spain.
- \* **Picromerite** -  $\text{K}_2\text{Mg}(\text{SO}_4)_2\cdot 6\text{H}_2\text{O}$  - Monoclinic System - Picromerite Group - Rössleben, Germany.
- \* **Polyhalite** -  $\text{K}_2\text{Ca}_2\text{Mg}(\text{SO}_4)_4\cdot 2\text{H}_2\text{O}$  - Triclinic System - Bochnia, Cracow, Poland.
- \* **Ponsjakite** -  $\text{Cu}_4^{2+}(\text{SO}_4)(\text{OH})_6\cdot \text{H}_2\text{O}$  Monoclinic System - Mina El Teniente, Rancagua, Chile.
- \* **Retgersite** -  $\text{NiSO}_4\cdot 6\text{H}_2\text{O}$  - Tetragonal System - Cottonwood Mine, Bolivia Ghost Town, Churchill County, Nevada, USA.
- \* **Schulenbergite** -  $(\text{Cu}^{2+},\text{Zn})_7(\text{SO}_4\text{CO}_3)_2(\text{OH})_{10}\cdot 3\text{H}_2\text{O}$  - Trigonal System - Wheal Unity, Cornwall, England.
- \* **Serpierite** -  $\text{Ca}(\text{Cu}^{2+},\text{Zn})_4(\text{SO}_4)_2(\text{OH})_6\cdot 3\text{H}_2\text{O}$  - Monoclinic System - Grube, Friedrichsegen, Lahn, Denmark.
- \* **Tamarugite** -  $\text{NaAl}(\text{SO}_4)_2\cdot 6\text{H}_2\text{O}$  - Monoclinic System - Mina Le Cetine, Siena, Toscana, Italy.
- \* **Wroewolfeite** -  $\text{Cu}_4^{2+}(\text{SO}_4)(\text{OH})_6\cdot 3\text{H}_2\text{O}$  - Monoclinic System - Nantycragal Mine, Cardigan Shire, Wales.

## o) SILICATES

- \* **Afghanite** -  $(\text{Na},\text{Ca},\text{K})_8(\text{Si},\text{Al})_{12}\text{O}_{24}(\text{SO}_4\text{Cl},\text{CO}_3)_3\cdot \text{H}_2\text{O}$  - Hexagonal System - Cancrinite Group - Pitigliano, Grosseto, Toscana, Italy.
- \* **Babingtonite** -  $\text{Ca}_2(\text{Fe}^{2+},\text{Mn})\text{Fe}^{3+}\text{Si}_5\text{O}_{14}(\text{OH})$  - Triclinic System - Maramello, Genova, Liguria, Italy.
- \* **Balangerite** -  $(\text{Mg},\text{Fe}^{3+},\text{Fe}^{2+},\text{Mn}^{2+})_{42}\text{Si}_{16}\text{O}_{54}(\text{OH})_{40}$  - Orthorhombic System - Balangero, Val di Lanzo, Piemonte, Italy.
- \* **Benitoite** -  $\text{BaTiSi}_3\text{O}_9$  - Hexagonal System - Big Creek, Fresno, California, USA.

- \* Buergerite -  $\text{NaFe}^{3+}\text{Al}_6(\text{BO}_3)_3\text{Si}_6\text{O}_{21}\text{F}$  - Trigonal System - Tourmaline Group - Lavra do Escondido, Governador Valadares, Minas Gerais, Brazil.
- \* Caporcianite (a variety of Laumontite) -  $\text{CaAl}_2\text{Si}_4\text{O}_{12}\cdot 4\text{H}_2\text{O}$  - Monoclinic System - Zeolite Group - Montecatini, Val di Celina, Toscana, Italy.
- \* Carpholite -  $\text{Mn}^{2+}\text{Al}_2\text{Si}_2\text{O}_6(\text{OH})_4$  - Orthorhombic System - Krasno, Czech Republic.
- \* Chapmanite -  $\text{Sb}^{+3}\text{Fe}_2^{3+}(\text{SiO}_4)_2(\text{OH})$  - Monoclinic System - Mina Tafone, Grosseto, Toscana, Italy.
- \* Charoite -  $\text{K}(\text{Ca},\text{Na})_2\text{Si}_4\text{O}_{10}(\text{OH},\text{F})\cdot \text{H}_2\text{O}$  (?) - Monoclinic System - Chare, Kola, Russia.
- \* Clintonite -  $\text{Ca}(\text{Mg},\text{Al})_3(\text{Al}_3\text{Si})\text{O}_{10}(\text{OH})_2$  - Monoclinic System - Mica Group - Lago Della Vacca, Adamello, Lombardia, Italy.
- \* Cowlesite  $\text{CaAl}_2\text{Si}_3\text{O}_{10}\cdot 6\text{H}_2\text{O}$  - Orthorhombic System - Zeolite Group - Antrim, Northern Ireland.
- \* Creaseyite -  $\text{Pb}_2\text{Cu}_2^{2+}\text{Fe}_2^{3+}\text{Si}_5\text{O}_{17}\cdot 6\text{H}_2\text{O}$  - Orthorhombic System - Mammoth Saint Anthony Mine, Tiger, Pima County, Arizona, USA.
- \* Cuspidine -  $\text{Ca}_4\text{Si}_2\text{O}_7(\text{F},\text{OH})_2$  - Monoclinic System - Pitigliano, Grosseto, Toscana, Italy; Magliano Romano, Roma, Italy.
- \* Davyne -  $(\text{Na},\text{Ca},\text{K})_8\text{Al}_6\text{Si}_6\text{O}_{24}(\text{Cl},\text{SO}_4,\text{CO}_3)_{2-3}$  - Hexagonal System - Cancrinite Group - Cava di Pollena, Monte Somma, Vesuvio, Italy.
- \* Deerite -  $(\text{Fe}^{2+},\text{Mn}^{2+})_6(\text{Fe}^{3+},\text{Al})_3\text{Si}_6\text{O}_{20}(\text{OH})_5$  - Monoclinic System (Pseudo Orthorhombic)- Longvalle Quarry, Fresno County, California, USA.
- \* Epistilbite -  $\text{CaAl}_2\text{Si}_6\text{O}_{16}\cdot 5\text{H}_2\text{O}$  - Monoclinic System - Zeolite Group - Osilo, Sardinia, Italy.
- \* Ferrierite -  $(\text{Na},\text{K})_2\text{Mg}(\text{Si},\text{Al})_{18}\text{O}_{36}(\text{OH})\cdot 9\text{H}_2\text{O}$  - Orthorhombic and Monoclinic Systems - Zeolite Group - Monastire, Sardinia, Italy.
- \* Fluorrichterite -  $\text{Na}_2\text{Ca}(\text{Mg},\text{Fe}^{2+})_5\text{Si}_8\text{O}_{22}(\text{F},\text{OH})_2$  - Monoclinic System - Amphibole Group - Wilbforce, Ontario, Canada.
- \* Fraipontite -  $(\text{Zn},\text{Al})_3(\text{Si},\text{Al})_2\text{O}_5(\text{OH})_4$  - Monoclinic System - Kaolinite-Serpentine Group - Silver Hill Mine, Gleeson, Arizona, USA.
- \* Franzinite -  $(\text{Na},\text{Ca})_7(\text{Si},\text{Al})_{12}\text{O}_{24}(\text{SO}_4,\text{CO}_3,\text{OH},\text{Cl})_3\cdot \text{H}_2\text{O}$  - Hexagonal System - Cancrinite Group - Magliano Romano, Roma, Italy.
- \* Fresnoite -  $\text{Ba}_2\text{TiSi}_2\text{O}_8$  - Tetragonal System - Big Creek, Fresno, California, USA.
- \* Ganophyllite -  $(\text{K},\text{Na})_2(\text{Mn},\text{Al},\text{Mg})_8(\text{Si},\text{Al})_{12}\text{O}_{29}(\text{OH})_{7-8}\cdot 9\text{H}_2\text{O}$  - Monoclinic System - Mina Gambatesa, Genoa, Liguria, Italy.
- \* Gillepsite -  $\text{BaFe}^{2+}\text{Si}_4\text{O}_{10}$  - Tetragonal System - Big Creek, Fresno, California, USA.
- \* Gismondine -  $\text{Ca}_2\text{Al}_4\text{Si}_4\text{O}_{16}\cdot 9\text{H}_2\text{O}$  - Monoclinic System - Zeolite Group - Capo Pula, Sardinia, Italy.
- \* Gmelinite -  $(\text{Na}_2\text{Ca})\text{Al}_2\text{Si}_4\text{O}_{12}\cdot 6\text{H}_2\text{O}$  - Hexagonal System - Zeolite Group - Glenarm, Antrim, Northern Ireland.
- \* Gyrolite -  $\text{NaCa}_{16}(\text{Si}_{23}\text{Al})\text{O}_{60}(\text{OH})_5\cdot 15\text{H}_2\text{O}$  - Triclinic System (Pseudo Hexagonal) - Poona, Maharas, India.
- \* Hyalite (a variety of opal) -  $\text{SiO}_2\cdot n\text{H}_2\text{O}$  - Amorphous - Valec, Slovenia.



- \* Kaersutite -  $\text{NaCa}_2(\text{Mg}, \text{Fe}^{2+})_4\text{Ti}(\text{Si}_6\text{Al}_2)\text{O}_{22}(\text{OH})_2$  - Monoclinic System - Amphibole Group - Mont Saint Hilaire, Quebec, Canada.
- \* Kaliophilite -  $\text{KAlSiO}_4$  - Hexagonal System - Orvello, Roma, Lazio, Italy.
- \* Kalsilite -  $\text{KAlSiO}_4$  - Hexagonal System - Orvello, Roma, Lazio, Italy.
- \* Kinoite -  $\text{Ca}_2\text{Cu}_2^{2+}\text{Si}_3\text{O}_8(\text{OH})_4$  - Monoclinic System - Christmas Mine, Gila County, Arizona, USA.
- \* Krauskopfite -  $\text{BaSi}_2\text{O}_4(\text{OH})_2 \cdot 2\text{H}_2\text{O}$  - Monoclinic System - Big Creek, Fresno, California, USA.
- \* Latiumite -  $(\text{Ca}, \text{K})_8(\text{Al}, \text{Mg}, \text{Fe})(\text{Si}, \text{Al})_{10}\text{O}_{25}(\text{SO}_4)$  - Monoclinic System - Latiume, Roma, Lazio, Italy; Magliano Romano, Roma, Lazio, Italy.
- \* Liottite -  $(\text{Ca}, \text{Na}, \text{K})_8(\text{Si}, \text{Al})_{12}\text{O}_{24}[(\text{SO}_4), (\text{CO}_3), \text{Cl}, \text{OH}]_4 \cdot \text{H}_2\text{O}$  - Hexagonal System - Cancrinite Group - Pitigliano, Grosseto, Toscana, Italy.
- \* Macdonaldite -  $\text{BaCa}_4\text{Si}_{16}\text{O}_{36}(\text{OH})_2 \cdot 10\text{H}_2\text{O}$  - Orthorhombic System - Big Creek, Fresno, California, USA; Rush Creek, Fresno, California, USA.
- \* Magnesioferrikatophorite -  $\text{Na}_2\text{Ca}(\text{Mg}, \text{Fe}^{2+})_4\text{Al}(\text{Si}_7\text{Al})\text{O}_{22}(\text{OH})$  - Monoclinic System - Amphibole Group - Kipawa, Quebec, Canada.
- \* Manganophyllite (Manganian biotite) -  $\text{K}(\text{Mg}, \text{Fe}^{2+})_3(\text{Al}, \text{Fe}^{3+})\text{Si}_3\text{O}_{10}(\text{OH}, \text{F})_2$  (a Mn-rich variety of biotite) - Monoclinic System - Mica Group - Langban Mine, Filipstad, Sweden.
- \* Marialite -  $3\text{NaAlSi}_3\text{O}_8 \cdot \text{NaCl}$  - Tetragonal System - Scapolite Group - Cava di Pollena, Monte Somma, Vesuvio, Italy.
- \* Mattheddeleite -  $\text{Pb}_{20}(\text{SiO}_4)_7(\text{SO}_4)_4\text{Cl}_4$  - Hexagonal System - Monte Arci, Sardinia, Italy.
- \* Meionite -  $3\text{CaAl}_2\text{Si}_2\text{O}_8 \cdot \text{CaCO}_3$  - Tetragonal System - Scapolite Group - Cava di Polleno, Monte Somma, Vesuvio, Italy.
- \* Melanophlogite -  $\text{SiO}_2$  with organic compounds - Cubic or Tetragonal Systems (Pseudo Cubic)- Il Fortullino, Livorno, Italy.
- \* Melilite -  $(\text{Ca}, \text{Na})_2(\text{Al}, \text{Mg})(\text{Si}, \text{Al})_2\text{O}_7$  - Tetragonal System - Melilite Group - Laghetto, Roma, Lazio, Italy; Orvello, Roma, Lazio, Italy.
- \* Merwinite -  $\text{Ca}_3\text{Mg}(\text{SiO}_4)_2$  - Monoclinic System - Crestmore Quarry, Mendocino County, California, USA.
- \* Milarite -  $\text{KCa}_2\text{AlBe}_2\text{Si}_{12}\text{O}_{30} \cdot 0.5\text{H}_2\text{O}$  - Hexagonal System - Osumilite Group - Pegmatito de Jaraguau, Timóteo, Minas Gerais, Brazil.
- \* Muirite -  $\text{Ba}_{10}\text{Ca}_2\text{Mn}^{2+}\text{TiSi}_{10}\text{O}_{30}(\text{OH}, \text{Cl}, \text{F})_{10}$  - Tetragonal System - Big Creek, Fresno, California, USA.
- \* Mullite -  $\text{Al}_6\text{Si}_2\text{O}_{13}$  - Orthorhombic System - Mina do Leão I, Minas do Leão, Rio Grande do Sul, Brazil.
- \* Narsarsukite -  $\text{Na}_2(\text{Ti}, \text{Fe}^{3+})\text{Si}_4(\text{O}, \text{F})_{11}$  - Tetragonal System - Mont Saint Hilaire, Quebec, Canada.
- \* Naujakasite -  $\text{Na}_6(\text{Fe}^{2+}, \text{Mn}^{2+})\text{Al}_4\text{Si}_8\text{O}_{26}$  - Monoclinic System - Naujakasik, Kvanefjeld Tunnel, Illimaussaq Complex, Greenland, Denmark.
- \* Norbergite -  $\text{Mg}_3(\text{SiO}_4)(\text{F}, \text{OH})_2$  - Orthorhombic System - Humite Group - Pargas, Finland.
- \* Okenite -  $\text{Ca}_{10}\text{Si}_{18}\text{O}_{46} \cdot 18\text{H}_2\text{O}$  - Triclinic System - Poona, Maharashtra, India.

- \* Osumilite -  $(K,Na)(Fe^{2+},Mg)_2(Al,Fe^{3+})_3(Si,Al)_{12}O_{30}$  - Hexagonal System - Osumilite Group - Monte Arci, Sardinia, Italy.
- \* Pargasite -  $NaCa_2(Mg,Fe^{2+})_4Al(Si_6Al_2)O_{22}(OH)_2$  - Monoclinic System - Amphibole Group - Pargas Valley, Finland.
- \* Piemontite (Piedmontite) -  $Ca_2(Al,Mn^{3+},Fe^{3+})_3(SiO_4)_3(OH)$  - Monoclinic System - Epidote Group - Prabhora Mine, St. Marcel, Val D'aosta, Piemonte, Italy.
- \* Pitiglianoite -  $K_2Na_6Si_6Al_6O_{24}(SO_4).2H_2O$  - Hexagonal System - Cancrinite Group, Pitigliano, Grosseto, Toscana, Italy.
- \* Polyolithionite -  $KLi_2AlSi_4O_{10}(F,OH)_2$  - Monoclinic System - Mica Group - Varutrark, Sweden.
- \* Pumpellyite- $(Fe^{2+})$  -  $Ca_2Fe^{2+}Al_2(SiO_4)(Si_2O_7)(OH)_2.H_2O$  - Monoclinic System - Pumpellyite Group - Campegli, Genova, Italy.
- \* Pyroxmangite -  $Mn^{2+}SiO_3$  - Triclinic System - Maramello, Genoa, Liguria, Italy.
- \* Rectorite - a clay mineral, Monoclinic System, 1:1 regular interstratification of a dioctahedral Mica and a dioctahedral Smectite - Solmestai Quarry, Djibouti, Somalia.
- \* Sanbornite -  $BaSi_2O_5$  - Orthorhombic System - Big Creek, Fresno, California, USA.
- \* Sarcolite -  $NaCa_6Al_4Si_6O_{24}F$  - (?) System - Cava Novella, Monte Somma, Vesuvio, Napoli, Italy.
- \* Serandite -  $Na(Mn^{2+},Ca)_2Si_3O_8(OH)$  - Triclinic System - Mont Saint Hilaire, Quebec, Canada.
- \* Spurrte -  $Ca_5(SiO_4)_2(CO_3)$  - Monoclinic System - Crestmore Quarry, Mendocino County, California.
- \* Stellerite -  $CaAl_2Si_7O_{18}.7H_2O$  - Orthorhombic System - Zeolite Group - Alghero, Bosa Route, Sardinia, Italy.
- \* Sugilite -  $KNa_2(Fe^{2+},Mn^{2+},Al)_2Li_3Si_{12}O_{30}$  - Hexagonal System - Osumilite Group - Wessels Mine, Kuruman, Cape Province, South Africa.
- \* Taramellite -  $Ba_4(Fe^{3+},Ti,Fe^{2+},Mg)_4(B_2Si_8O_{27})O_2Cl_x$  - Orthorhombic System - Big Creek, Fresno, California, USA; Rush Creek, Fresno, California, USA.
- \* Tinzenite -  $(Ca,Mn^{2+}Fe^{2+})_3Al_2BSi_4O_{15}(OH)$  - Triclinic System - Axinite Group - Mina Gambatesa, Genova, Liguria, Italy.
- \* Traskite -  $Ba_9Fe_2^{2+}Ti_2(SiO_3)_{12}(OH,Cl,F)_6.6H_2O$  - Hexagonal System - Rush Creek, Fresno, California, USA.
- \* Tundrite-(Ce) -  $Na_3(Ce,La)_4(Ti,Nb)_2(SiO_4)_2(CO_3)_3O_4(OH).2H_2O$  - Triclinic System - Chare, Kola, Russia.
- \* Tuscanite -  $K(Ca,Na)_6(Si,Al)_{10}O_{22}[SO_4,CO_3,(OH)_2].H_2O$  - Monoclinic System - Magliano Romano, Roma, Italy.
- \* Verplanckite -  $Ba_2(Mn^{2+},Fe^{2+},Ti)Si_2O_6(O,OH,Cl,F)_2.3H_2O$  - Hexagonal System - Big Creek, Fresno, California, USA.
- \* Walstromite -  $BaCa_2Si_3O_9$  - Triclinic System - Big Creek, Fresno, California, USA.
- \* Wöhlerite -  $NaCa_2(Zr,Nb)Si_2O_7(O,OH,F)_2$  - Monoclinic System - Saga II, Tvedal, Norway.

## REFERENCES

1. C. Klein and C. S. Hurlbult Jr., *Manual of Mineralogy*. 21<sup>st</sup> ed., after J. Dana (1848), John Wiley & Sons, New York, 1993, 683p.
  2. M. Fleischer and J. Mandarino, *Glossary of Minerals Species*. 7<sup>th</sup> ed., The Mineralogical Record Inc., Tucson, Arizona, 1995. 280 p.
  3. A.V. Milovsky and O. V. Kononov. *Mineralogy*. 2<sup>nd</sup> ed., Mir Publishers, Moscow, 1985, 320 p.
  4. P. de M. Branco. *Dicionário de Mineralogia*. 3<sup>a</sup> ed., Sagra, Porto Alegre, 1987, 362 p.
  5. F. Klockmann and P. Rämndhor. *Tratado de Mineralogía*. Gustavo Gili, Barcelona, 1961, 847 p.
- R. V. Dietrich. *Mineral Tables*, McGraw-Hill, New York, 1968.

## ACKNOWLEDGEMENTS

We hereby acknowledge the special assistance received from Dr. Ruben Eugen Becker, Magnificent Rector of ULBRA, Engineer Leandro Becker, Pro-Rector of ULBRA and Professors Aldoir Rigoni, Sirlei Dias Gomes, Elenita Ribas Gonçalves, Volnei Falkenbach, Tânia Prochnow and Nélson Cauduro. Their efforts were fundamental in obtaining a space and home for the Mineral Collection that is worthy of the Lutheran University of Brazil.

**TRANSITION METAL COMPLEXES OF THE FORMYL-VANILLINE  
DERIVATIVES LIGAND FAMILY**

Tudor ROSU\*, Angela KRIZA\*, Viorel CARCU\*, Anca NICOLAE\*\*

\*Dept. of Inorganic Chemistry, Faculty of Chemistry, University of Bucharest, 23 Dumbra  
Rosie st., Bucharest, Romania

\*\*Dept. of Organic Chemistry, Faculty of Chemistry, University of Bucharest, Romania

**ABSTRACT**

Divalent 3d metal complexes with formyl-vanilline derivatives, of the type  $ML_2$  or  $ML_2X_2$  ( $M = Cu(II), Co(II)$ ;  $X = Cl$ ), were synthesized by reaction of the corresponding metal(II) chlorides with 1-[3'-formyl-4'-methoxy-6'-hydroxybenzilydene]-2-phenazino/hydrazine, (FBFH), 1-benzilydene-2-phenazino/hydrazine, (BFH), and 3'-formyl-5',6'-dihydroxybenzilydene-2-nitro-4-methylaniline, (FBAH). The novel complexes were characterized by ESR, IR, electronic spectroscopy, molar electric conductivity measurements and magnetic studies. These compounds appear to be hexacoordinated.

**RESUMO**

Complexos divalentes de metais 3d com derivados de formilvanilina foram sintetizados através da reação do cloreto de metal(II) correspondente com 1-(3'-formil-4'-metoxi-6'-hidroxibenzilideno)-2-fenazinoilhidrazina, (FBFH), 1-benzilideno-2-fenazinoilhidrazina, (BFH), e 3'-formil-5',6'-dihidroxibenzilideno-2-nitro-1-metil-anilina, (FBAH). Os complexos tem a estrutura geral  $ML_2$  ou  $ML_2X_2$  ( $M=Cu(II), Co(II)$ ;  $X=Cl$ ). Os novos complexos foram caracterizados usando técnicas de RSE, infravermelho, condutibilidade molar elétrica e estudos magnéticos. Estes complexos parecem ser hexacoordenados.

**KEYWORDS :** phenazino/hydrazine, copper(II), cobalt(II), hydroxybenzilydene, IR spectra

## INTRODUCTION

In coordinative chemistry an important part in the coordination process is played by the ligands characterized by the presence of several donor groups. Thus the derivatives resulting from 3-formyl-5,6-dihydroxybenzilidene or 2-formyl-4-methoxy-benzilidene with phenazinoilhydrazine can favour the coordination of the metal ions by several chromophore groups. In 1979, Mihaceva L.H. and co-workers<sup>1</sup> synthesized and characterized by means of X-Ray spectrum studies the Co(II) and Cu(II) complexes with ligands, derived from the amide of the nicotinic acid. The structural data point to an octahedral geometry of the metal ions and their coordination with the amide nitrogen atom.

Hughes M.N. and co-workers<sup>2</sup>, Nonoyama M. and co-workers<sup>3</sup> have shown that in the Co(II) and Cu(II) complexes with amides derivated from hydrazine, the metal ion has an octahedral geometry. Thus, the occurrence of the absorption band fairly intensive at  $1530\text{ cm}^{-1}$  can be assigned to the vibration frequency of the amide group,  $\nu_{>\text{C}=\text{O}}$ , and the sharp bands specific to the complexes that occur at  $1595\text{ cm}^{-1}$  and  $1630\text{ cm}^{-1}$  are characteristic of the  $\nu_{>\text{C}=\text{N}}$  groups.

## EXPERIMENTAL PART

The work has aimed at the synthesis and the solid-phase characterization of the Co(II) and Cu(II) complexes with 1-[3'-formyl-4'-methoxy-6'-hydroxybenzilidene]-2-phenazinoilhydrazine, (FBFH), 1-benzilydene-2-phenazinoilhydrazine, (FBH), and 3'-formyl-5',6'-dihydroxybenzilidene-2-nitro-4-methylaniline, (FBAH).

In order to obtain the Co(II) and Cu(II) complexes with the above-mentioned ligands the methanol solutions of  $\text{CuCl}_2 \cdot 2\text{H}_2\text{O}$  and  $\text{CoCl}_2 \cdot 6\text{H}_2\text{O}$  have been prepared the methanol solutions of the above-mentioned ligands have been prepared separately. The thus prepared solutions have been mixed so that the combination ratio M:L should be around 1:2 ( $\text{Cu(II):FBFH} = 1:2$ ;  $\text{Cu(II):FBH} = 1:2$ ;  $\text{Co(II):FBFH} = 1:2$ ;  $\text{Co(II):FBH} = 1:2$  and  $\text{Cu(II):FBAH} = 1:2$ ). After some 45 minutes refluxing the solutions were cooled to get a differently coloured precipitates. After filtering, methanol washing and drying, the precipitates were subject to elementary analysis, thus determining C%, N%, O%, Cl% and M(II)%, respectively (Carlo Erba LA 1108 analyser and AAS 1N Carl Zeiss Jena atomic absorption spectrophotometer). To characterize the prepared complexes the IR spectra in the KBr pellet for the  $4000\text{--}200\text{ cm}^{-1}$  (Specord M-80 Carl Zeiss Jena), the electronic spectra in diffuse reflectance by using MgO as a dilution matrix (VSU-2P Carl Zeiss Jena spectrophotometer), the electronic spectra in solution (Shimadzu 310 PS spectrophotometer), the ESR spectra (Varian E-9 spectrophotometer at room temperature on powder); conductivity measurements using dimethylformamide as a solvent (HACH TDS-meter conductometer) have been performed. The magnetic measurements have been performed by the Faraday method at room temperature, using  $\text{Hg}[\text{Co}(\text{SCN})_4]$  as a blank test.

## RESULTS AND DISCUSSION

The synthesized complexes occur under the form of microcrystalline, differently coloured, water insoluble, sparingly soluble in tetrahydrofuran and soluble in dimethylformamide powders. The elementary analysis led to the results presented in Table 1.

Table 1

As one can easily conclude from the above presented data, the combination ratio M:L for all the prepared complexes is 1:2.

With a view of determining the coordination pattern of the ligands with the metal ions Cu(II) and Co(II) the IR spectra for the 4000-200  $\text{cm}^{-1}$  range have been determined. From the data presented in Tables 2-4 it has been ascertained that the absorption bands specific to the vibration frequencies of the groups non-involved in the formation of the chemical bonds with the metal ions, Cu(II) and Co(II), remain unchanged. In Table 2 the IR spectra for the Cu(II) and Co(II) complexes with the FBFH ligand are presented.

Table 2

The absorption band from 1670  $\text{cm}^{-1}$  with an increased intensity in the ligand spectrum specific to the stretching vibration frequency  $\nu_{\text{C=O}}$  (amide I) shifts towards smaller wave numbers and it splits into absorption bands of average intensity: 1652  $\text{cm}^{-1}$ , 1638  $\text{cm}^{-1}$  for the complex of the Cu(II) ion and 1660  $\text{cm}^{-1}$ , 1643  $\text{cm}^{-1}$  respectively, for the complex of the Co(II) ion. This behaviour can be assigned to the formation of the chemical bond of the ligand with the metal ion M(II) via the  $>\text{C=O}$  group. Likewise, the 1620  $\text{cm}^{-1}$  absorption band specific to the frequency of the  $\nu_{\text{C=N}}$  valency vibration (the chemical bond  $>\text{C=N}$  was formed as a result of the condensation of formyl-vanillin with phenazinoilhydrazine) shifts with about 20  $\text{cm}^{-1}$  towards smaller wave numbers, to 1603  $\text{cm}^{-1}$  for the Cu(II) complex and 1605  $\text{cm}^{-1}$  respectively for the Co(II) complex, confirming the coordination of nitrogen atom to the respective metal ions. The 1160  $\text{cm}^{-1}$  absorption band, very strong and sharp, specific to the frequency of  $\nu_{\text{Ar-OH}}$  valency vibration shifts towards wave numbers that are about 15  $\text{cm}^{-1}$  smaller and it diminishes its intensity. In the IR spectrum of the two complexes this band lies at 1145  $\text{cm}^{-1}$  for the Cu(II) complex and at 1148  $\text{cm}^{-1}$  for the Co(II) one, respectively.

Similarly, in the IR spectra of the two complexes there occur absorption bands of low intensity located at 505, 475, 329  $\text{cm}^{-1}$  and at 520, 393, 308  $\text{cm}^{-1}$  respectively, that are assigned to the vibration frequencies  $\nu_{\text{M-O}}$  and  $\nu_{\text{M-N}}$ ,  $\delta_{\text{N-M-N}}$ , respectively. This order of the frequencies of the vibrations  $\nu_{\text{M-O}}$ ,  $\nu_{\text{M-N}}$ , respectively corresponds to the values presented by Nonoyama<sup>3</sup>, Anagnostopoulos<sup>4</sup>, Nakamoto<sup>5</sup>. The IR spectra for the Cu(II) and Co(II) complexes with the BFH ligand are presented in Table 3.

Table 3

As in the previous case it has been ascertained that the absorption band from 1680  $\text{cm}^{-1}$  in the ligand spectrum, specific to the vibration frequency  $\nu_{\text{C=O}}$  (amide I) shifts, within the spectrum of the complexes, towards smaller wave numbers and splits in to two bands pointing to a coordination of the oxygen atom from the  $>\text{C=O}$  group to the corresponding metal ions. Similarly, the absorption band from 1625  $\text{cm}^{-1}$  typical of the  $\nu_{\text{C=N}}$  stretching vibration frequency shifts within the spectrum of the complexes towards wave numbers that are about 20  $\text{cm}^{-1}$  smaller. This behaviour points out the coordination of the nitrogen atom with the Cu(II) and Co(II) metal ions.

Table 1. Elementary chemical analysis for the prepared complexes

Compound	C %		N %		O %		Cl %		M %	
	calc.	exp.	calc.	exp.	calc.	exp.	calc.	exp.	calc.	exp.
Cu(FBFH) <sub>2</sub>	61.28	60.74	13.15	12.33	14.85	14.07	-	-	7.37	6.85
Cu(FBAHCl) <sub>2</sub>	61.26	60.89	14.29	13.98	3.82	3.17	8.93	8.21	8.10	7.83
Co(BFH) <sub>2</sub>	61.61	60.32	13.06	12.62	14.93	15.35	-	-	6.88	6.11
Co(BFHCl) <sub>2</sub>	61.53	60.81	14.35	13.82	3.85	3.20	9.10	8.69	7.57	7.18
Cu(BFAHCl) <sub>2</sub>	48.97	48.17	7.62	7.11	21.76	20.92	9.65	8.87	8.70	8.25

Table 2. IR bands of the MC<sub>44</sub>N<sub>8</sub>O<sub>8</sub>H<sub>30</sub> complexes and the C<sub>22</sub>N<sub>4</sub>O<sub>4</sub>H<sub>16</sub> ligand (cm<sup>-1</sup>)

C <sub>22</sub> N <sub>4</sub> O <sub>4</sub> H <sub>16</sub>	CuC <sub>44</sub> N <sub>8</sub> O <sub>8</sub> H <sub>30</sub>	CoC <sub>44</sub> N <sub>8</sub> O <sub>8</sub> H <sub>30</sub>	Assignment
3018 (m)	3018 (m)	3018 (m)	ν <sub>CH</sub> (Ar)
1460 (m)	1460 (m)	1462 (m)	ν <sub>C=C</sub> (Ar)
2850 (m)	2850 (m)	2852 (m)	ν (-OCH <sub>3</sub> )
1282 (s)	1280 (s)	1282 (s)	
1070 (s)	1070 (s)	1069 (s)	
2720 (m)	2718 (m)	2722 (m)	ν <sub>Ar-CHO</sub>
1695 (s)	1693 (s)	1697 (s)	
1620 (s)	1603 (m)	1605 (m)	ν <sub>C=N</sub>
1670 (s)	1652 (m)	1660 (m)	ν <sub>C=O</sub>
	1638 (m)	1643 (w)	amida I
1580 (s)	1580 (s)	1579 (s)	ν <sub>C-N</sub>
			amida II
1044 (m)	1056 (m)	1054 (m)	ν <sub>N-N</sub>
1160 (s)	1145 (m)	1148 (m)	ν <sub>Ar-OH</sub>
	505 (m)	520 (m)	ν <sub>M-O</sub>
	475 (w)	393 (w)	ν <sub>M-N</sub>
	329 (w)	308 (w)	δ <sub>N-M-N</sub>

s - strong; m - medium; w - weak

Table 3. IR bands of the  $\text{MC}_{40}\text{N}_8\text{O}_2\text{H}_{28}\text{Cl}_2$  complex and the  $\text{C}_{20}\text{N}_4\text{OH}_{14}$  ligand ( $\text{cm}^{-1}$ )

$\text{C}_{20}\text{N}_4\text{OH}_{14}$	$\text{CuC}_{40}\text{N}_8\text{O}_2\text{H}_{28}\text{Cl}_2$	$\text{CoC}_{40}\text{N}_8\text{O}_2\text{H}_{28}\text{Cl}_2$	Assignment
3010 (m)	3010 (m)	3012 (m)	$\nu_{\text{CH}}$ (Ar)
1880 (w)	1888 (w)	1892 (w)	$\delta_{\text{CH}}$ (Ar)
1450 (m)	1450 (m)	1452 (m)	$\nu_{\text{C}=\text{C}}$ (Ar)
1625 (s)	1608 (m)	1605 (m)	$\nu_{\text{C}=\text{N}}$
1680 (s)	1662 (m) 1647 (w)	1668 (m) 1651 (w)	$\nu_{\text{C}=\text{O}}$ (amida I)
1595 (s)	1592 (s)	1596 (s)	$\nu_{\text{C}-\text{N}}$ (amida II)
1037 (m)	1051 (m)	1050 (m)	$\nu_{\text{N}-\text{N}}$
	512 (w) 493 (w) 309 (w) 276 (w)	535 (w) 415 (w) 328 (w) 294 (w)	$\nu_{\text{M}-\text{O}}$ $\nu_{\text{M}-\text{N}}$ $\delta_{\text{N}-\text{M}-\text{N}}$ $\nu_{\text{M}-\text{Cl}}$

s- strong; m - medium; w - weak

Table 4. Ir bands of the  $\text{CuC}_{30}\text{N}_4\text{O}_{10}\text{H}_{24}\text{Cl}_2$  complex of the  $\text{C}_{15}\text{N}_2\text{O}_5\text{H}_{12}$  ligand ( $\text{cm}^{-1}$ )

$\text{C}_{15}\text{N}_2\text{O}_5\text{H}_{12}$	$\text{CuC}_{30}\text{N}_4\text{O}_{10}\text{H}_{24}\text{Cl}_2$	Assignment
2962 (s)	2962 (s)	$\nu$ ( $\text{CH}_3$ ) as
2870 (m)	2870 (m)	$\nu$ ( $\text{CH}_3$ ) sim
1035 (m)	1038 (m)	$\nu_{\text{CH}}$ (Ar)
1490 (s)	1492 (s)	$\nu_{\text{C}=\text{C}}$ (Ar)
1560 (s)	1562 (s)	$\nu$ ( $\text{NO}_2$ ) as
1370 (s)	1370 (s)	$\nu$ ( $\text{NO}_2$ ) sim
875 (m)	878 (m)	$\nu_{\text{C}-\text{N}}$
2720 (m)	2718 (m)	$\nu_{\text{Ar}-\text{CHO}}$
1690 (s)	1690 (s)	
1173 (s)	1170 (w) 1138 (m)	$\nu_{\text{Ar}-\text{OH}}$
1635 (s)	1620 (m)	$\nu_{\text{C}=\text{N}}$
	573 (m) 437 (w) 320 (w) 265 (m)	$\nu_{\text{Cu}-\text{O}}$ $\nu_{\text{Cu}-\text{N}}$ $\delta_{\text{N}-\text{Cu}-\text{N}}$ $\nu_{\text{Cu}-\text{Cl}}$
3402 (m)	3380 (w)	$\nu$ ( $\text{Ar}-\text{NH}_2$ )
810 (s)	758 (m)	

s- strong; m - medium; w - weak



The analysis of the IR spectra for both complexes in the range of the small wave numbers has rendered evident the presence of some new bands of low intensity, ranging between  $270\text{ cm}^{-1}$  and  $540\text{ cm}^{-1}$ . These absorption bands were assigned to the  $\nu_{\text{M-O}}$  and  $\nu_{\text{M-N}}$  vibration frequencies whose values are in accordance with observations made by the Nakamoto<sup>5</sup> for complexes endowed with an octahedral geometry. The absorption bands from  $276\text{ cm}^{-1}$  and  $294\text{ cm}^{-1}$ , respectively, were assigned to the  $\nu_{\text{M-Cl}}$  valency vibration frequencies<sup>6,7</sup>. From the Tables 2 and 3 one can notice that for FBFH and BFH ligands the absorption bands occur at  $1044\text{ cm}^{-1}$  and  $1037\text{ cm}^{-1}$  respectively, typical of the  $\nu_{\text{M-N}}$  stretching vibration frequencies. In the IR spectra of the four complexes of the Cu(II) and Co(II) ions, these bands shift with  $10\text{-}15\text{ cm}^{-1}$  towards bigger wave numbers, confirming in this way the coordination of the  $\text{sp}^2$  hybridized nitrogen atom with the metal ions<sup>8</sup>. In Table 4 the IR absorption bands of the  $\text{CuC}_{30}\text{N}_4\text{O}_{10}\text{H}_{24}\text{Cl}_2$  complex and of FBAH ligand are presented.

Table 4

The vibration frequencies specific to the groups involved in the formation of the chemical bonds with Cu(II) ion ( $\nu_{\text{Ar-OH}} = 1173\text{ cm}^{-1}$ ,  $\nu_{\text{Ar-NH}} = 810\text{ cm}^{-1}$ ) shifted towards smaller wave numbers with in IR spectrum of the complex. The new absorption bands that occurred in the IR spectrum of the complex in the range of the small wave numbers of low intensity at  $573\text{ cm}^{-1}$  and  $320\text{ cm}^{-1}$  are assigned to the vibrations of  $\nu_{\text{Cu-O}}$  and  $\nu_{\text{Cu-N}}$  valency and to the deformation vibration  $\delta_{\text{N-Cu-N}}$ <sup>3,5</sup>. The absorption band from  $265\text{ cm}^{-1}$  was assigned to the frequency of  $\nu_{\text{Cu-Cl}}$  valency vibration frequencies<sup>6,7</sup>.

The bands corresponding to the electronic transitions and assigned to these ones for the prepared complexes and the ligands are presented in Table 5.

Table 5

As it can easily ascertained from the data presented in the table, the absorption bands specific to the chromophore group of the ligands are included in the  $30770\text{-}38815\text{ cm}^{-1}$  range. As for the complexes, the above mentioned absorption bands are found again in the spectrum, but they shifted towards the lower frequencies and there occur further bands due to the d-d transitions. The assignment of the electronic transitions of the Co(II) complexes has been performed by using a splitting diagram in accordance with the data presented by Meredith P.L. and co-workers<sup>9</sup>.

Driessen W.L. and co-workers<sup>10</sup> and for the Cu(II) complexes a splitting diagram for a distorted octahedral geometry was used<sup>11,12</sup>.

The frequencies of the electronic transitions for all the complexes point to a distorted octahedral geometry with a stronger distortion for the  $\text{CuC}_{30}\text{N}_4\text{O}_{10}\text{H}_{24}\text{Cl}_2$  complex. This statement is in accordance with the values of the electron parameters of the ligand field (Table 6) for the Co(II) complexes.

Table 6

The different values of the  $\Delta t$  and  $\Delta s$  splitting parameters of the two complexes of Co(II) point to the presence of the chlorine ions within the coordination area of Co(II). Similarly, the value of the  $\beta$  parameter suggests the fact that the chemical bond in the  $\text{CoC}_{40}\text{N}_8\text{O}_2\text{H}_{22}\text{Cl}_2$  combination has a stronger ionic nature than the  $\text{CoC}_{44}\text{N}_8\text{O}_8\text{H}_{30}$  combination. The values of the experimental magnetic moments (Table 7) both for the Co(II) complexes and for the Cu(II) ones confirm the distorted octahedral geometry<sup>13,14</sup>.

Table 7

Table 5. Electronic spectra and the assignment of the transitions ( $\text{cm}^{-1}$ )

Compound	$\nu, \text{cm}^{-1}$	Assignment
$\text{C}_{22}\text{N}_4\text{O}_4\text{H}_{16}$ $\text{CoC}_{44}\text{N}_8\text{O}_8\text{H}_{30}$	35715	$\pi \rightarrow \pi^*$
	30770	$n \rightarrow \pi^*$
	33200	$\pi \rightarrow \pi^*$
	29020	$n \rightarrow \pi^*$
	21100	$4T_{1g}(4F) \rightarrow 4T_{1g}(4P)$
	16540	$4T_{1g}(4F) \rightarrow 4A_{2g}(4F)$
	9120	$4T_{1g}(4F) \rightarrow 4T_{2g}(4F)$
$\text{CuC}_{44}\text{N}_8\text{O}_8\text{H}_{30}$	34278	$\pi \rightarrow \pi^*$
	29435	$n \rightarrow \pi^*$
	15420	$z^2 \rightarrow x^2-y^2$
	10250	$xz, yz, xy \rightarrow x^2-y^2$
$\text{C}_{20}\text{N}_4\text{OH}_{14}$ $\text{CoC}_{40}\text{N}_8\text{O}_2\text{H}_{22}\text{Cl}_2$	35210	$\pi \rightarrow \pi^*$
	32430	$n \rightarrow \pi^*$
	34015	$\pi \rightarrow \pi^*$
	31210	$n \rightarrow \pi^*$
	22840	$4T_{1g}(4F) \rightarrow 4T_{1g}(4P)$
	17415	$4T_{1g}(4F) \rightarrow 4A_{2g}(4F)$
	9260	$4T_{1g}(4F) \rightarrow 4T_{2g}(4F)$
$\text{CuC}_{40}\text{N}_8\text{O}_2\text{H}_{28}\text{Cl}_2$	33890	$\pi \rightarrow \pi^*$
	31075	$n \rightarrow \pi^*$
	15940	$z^2 \rightarrow x^2-y^2$
	.9850	$xz, yz, xy \rightarrow x^2-y^2$
$\text{C}_{15}\text{N}_2\text{O}_5\text{H}_{12}$ $\text{CuC}_{30}\text{N}_4\text{O}_{10}\text{H}_{24}\text{Cl}_2$	38315	$\pi \rightarrow \pi^*$
	35720	$n \rightarrow \pi^*$
	36500	$\pi \rightarrow \pi^*$
	33720	$n \rightarrow \pi^*$
	16400	$x^2-y^2 \rightarrow xy$
	18250	$z^2 \rightarrow xy$

Table 6. Electronic parameters of the ligand field for the Co(II) complexes ( $\text{cm}^{-1}$ )

Parameters	$\text{CoC}_{44}\text{N}_8\text{O}_8\text{H}_{30}$	$\text{CoC}_{40}\text{N}_8\text{O}_2\text{H}_{22}\text{Cl}_2$
10Dq	7420	8155
B	690	820
$\beta$	0,710	0,844
$\Delta_t$	390	647
$\Delta_g$	652	548

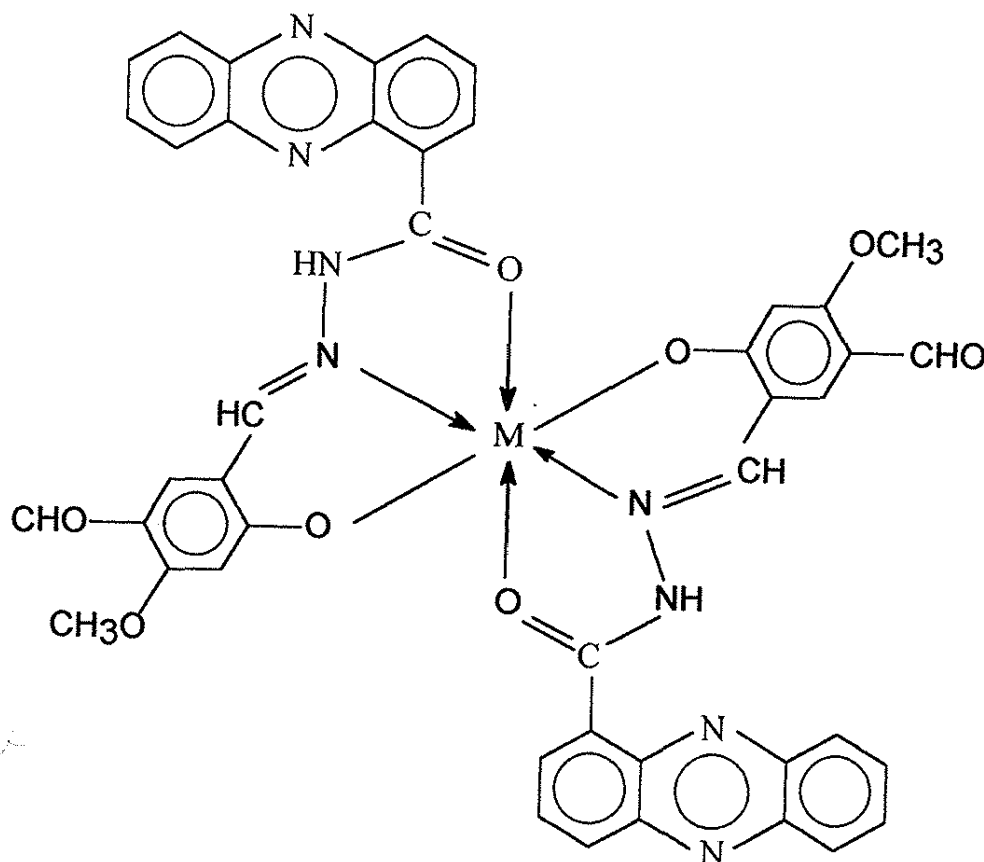
Table 7. The molar electric conductibilities,  $\Lambda_M$  ( $\Omega^{-1}\text{cm}^2\text{mol}^{-1}$ ), and the experimental magnetic moments,  $\mu_{\text{exp}}$  (MB), for the prepared complexes

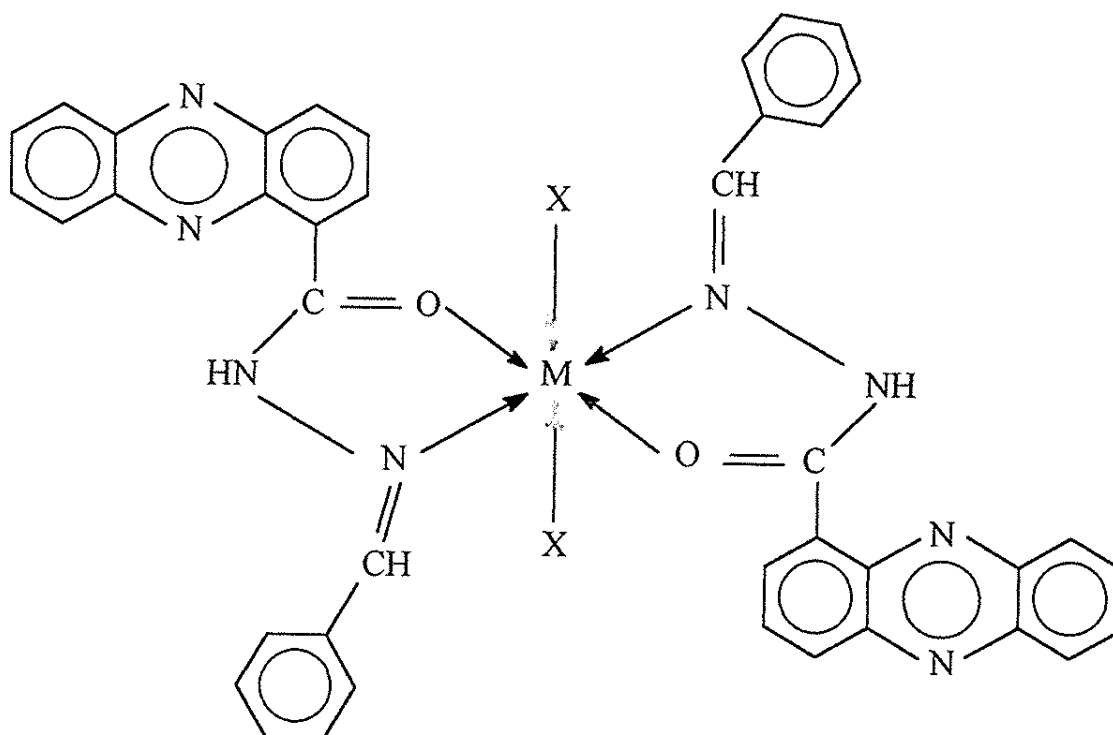
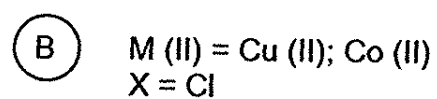
Compound	$\Lambda_M$ ( $\Omega^{-1}\text{cm}^2\text{mol}^{-1}$ )	$\mu_{\text{exp}}$ (MB)
$\text{CoC}_{44}\text{N}_8\text{O}_8\text{H}_{30}$	36	5,17
$\text{CoC}_{40}\text{N}_8\text{O}_2\text{H}_{22}\text{Cl}_2$	24	5,04
$\text{CuC}_{44}\text{N}_8\text{O}_8\text{H}_{30}$	19	1,92
$\text{CuC}_{40}\text{N}_8\text{O}_2\text{H}_{22}\text{Cl}_2$	27	2,10
$\text{CuC}_{30}\text{N}_4\text{O}_{10}\text{H}_{24}\text{Cl}_2$	13	2,05

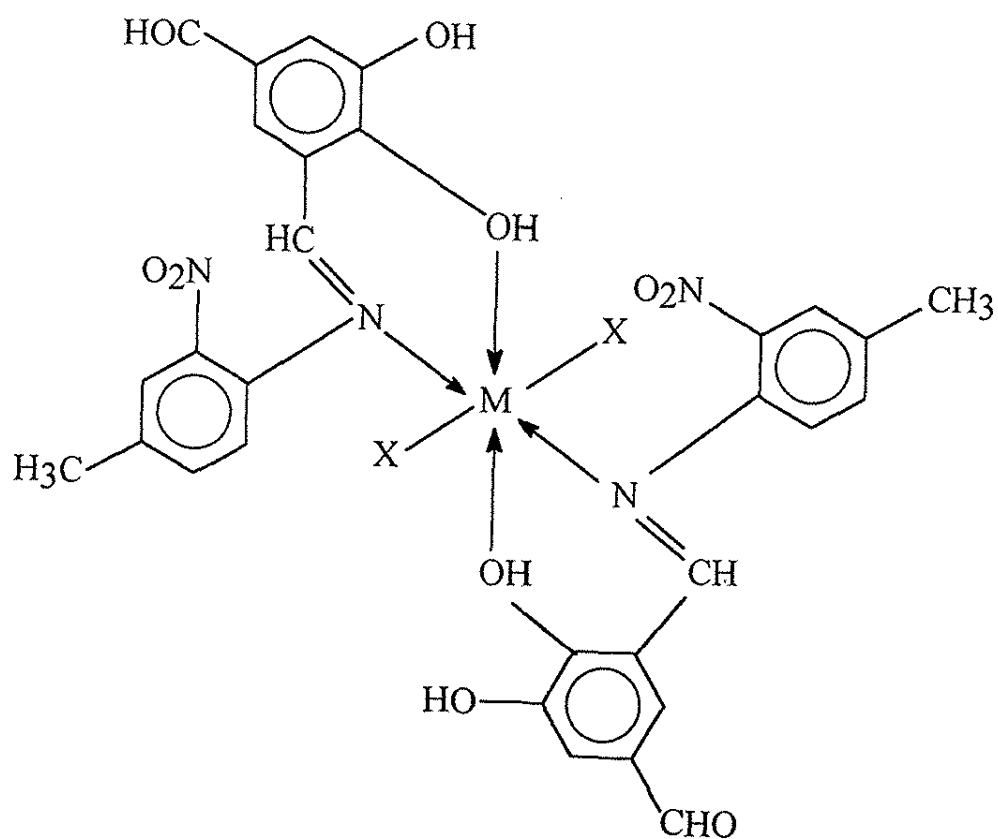
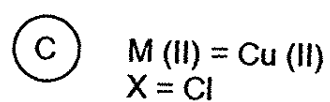
Table 8. The values of the splitting parameter, g, for the Cu(II) complexes

Parameter {g}	$\text{CuC}_{44}\text{N}_8\text{O}_8\text{H}_{30}$	$\text{CuC}_{40}\text{N}_8\text{O}_2\text{H}_{22}\text{Cl}_2$	$\text{CuC}_{30}\text{N}_4\text{O}_{10}\text{H}_{22}\text{Cl}_2$
$g_x$	2,077	2,005	2,015
$g_y$	2,142	2,204	2,198
$g_z$	2,266	2,175	2,112

(A) M (II) = Cu (II); Co (II)







The molar electric conductibilities of the solutions of  $10^{-3}$ M concentration, in DMF, for all the prepared complexes, have values lower than  $65 \Omega^{-1}\text{mol}^{-2}\text{cm}^{-1}$  (Table 7) establishing in this way the non-electrolyte nature of these ones. The values of the tensor  $\{g\}$  obtained from the ESR spectra for the Cu(II) complexes are mentioned in Table 8.

Table 8

The intensity of the bands and the anizotropy of the  $g_x$  and  $g_y$  parameters from the equatorial plane may result from the different interactions with the ligands which cause a rather strong distortion<sup>15</sup>. Correlating the values of the experimental determinations one can hold that all the prepared complexes belong to the distorted octahedral symmetry group (Figures a,b,c).

## CONCLUSIONS

New complexes with derivatives of phenazinoilhydrazine have been synthesised.

Spectral and magnetic estimations on microcrystalline powders of the prepared complexes have been performed;

The Co(II) and Cu(II) complexes belong to the distorted  $O_h$  symmetry group.

## REFERENCES

1. L.H.Mihaceva: *Koord.Khim.*, 5, 12 (1979);
2. M.N.Hughes, K.J.Rutt: *J.Chem.Soc.Dalton Trans.*, 1311 (1973);
3. M.Nonoyama, S.Tomita, K.Yamasaki: *Inorg.Chim.Acta*, 12, 33 (1975);
4. A.Anagnostopoulos: *Inorg.Nucl.Chem.Letters*, 12, 225 (1976)
5. K.Nakamoto: *"Infrared Spectra of Inorganic and Coordination Compounds"*. J.Wiley & Sons, Inc., New York (1986)
6. B.R.Carson, D.L.Gerrard, J.R.Allan: *Thermochim.Acta*, 153, 173 (1989);
7. A.D.Paton, J.R.Allan, K.Turvey: *Thermochim.Acta*, 186, 293 (1991);
8. G.S.Huang, Y.M.Liang: *J.Coord.Chem.*, 26, 237-242 (1992);
9. P.L.Meredith, R.A.Palmer: *Inorg.Chem.*, 10, 1546 (1971)
10. W.L.Driessen, W.L.Groeneveld: *Rev.Trav.Chim.Pays.*, 90, 95 (1971);
11. C.D.Olsen, G.Basu, R.L.Belford: *J.Coord.Chem.*, 1, 17 (1971);
12. A.P.B.Lever: *"Inorganic Electronic Spectroscopy"*, Elsevier (1984);
13. J.S.Ahuja, R.Singh: *Indian J.Chem.*, 12, 107 (1974);
14. D.J.Hodgson: *Progress in Inorganic Chemistry*, 19, 173 (1975);
15. T.D.Smith, J.R.Pilbrow: *Coord.Chem.Rev.*, 13, 173 (1979)

**SORPTION AND SEPARATION OF Cu(II), Co(II) AND Ni(II)  
ON 1(4'-AZOBENZYLCELLULOSE)-2-NAPHTOL**

TINCA ONOFREI, CECILIA ARSENE and CARMEN MITA  
"Al. I. Cuza" University Jassy, Faculty of Chemistry, Bd.Mangeron 71,6600 - Jassy,  
Romania

**ABSTRACT**

*The mechanism of Cu(II), Co(II) and Ni(II) sorption on 1(4'-azobenzylcellulose)-2-naphtol has been investigated along with the possible chromatographic separation of the three elements on this chelating sorbent. The data obtained from the dependence of the distribution coefficients on pH and from isotherms, as well, have evidenced that physical sorption of the three elements is accompanied by chemical sorption, adsorption being predominant for Co(II) and chemisorption for Ni(II) and Cu(II) being much more pronounced for the last element. The modifications in IR and diffuse reflectance spectra lead to the conclusion that chemical sorption involves the formation of chelates. The sorbent may be employed for the separation of Co(II)-Ni(II)-Cu(II) through successive elution with 0.01 N HCl, 0.1 N HCl and 1 N HCl.*

**KEYWORDS**

Sorption, Separation, Copper, Nickel, Cobalt, Chelating cellulose

**RESUMO**

*O mecanismo da sorção de Cu(II), Co(II) e Ni(II) sobre 1(4'-azobenzilcelulose)-2-naftol foi estudado tendo em vista a separação cromatográfica dos tres íons por este sorbente quelante. Os resultados obtidos para a dependência dos coeficientes de distribuição com pH e os isoterms mostraram que a fisissorção dos tres elementos é seguida por quimissorção. O processo de adsorção química predomina para Co(II) e a quimissorção para Ni(II) e Cu(II), sendo mais pronunciada para o Cu(II). As análises de espectros no infravermelho e de reflectância difusa indicam que a sorção química envolve a formação de quelatos. O sorbente pode ser utilizado para a separação de Co(II)-Ni(II)-Cu(II) através de eluições sucessivas com 0,1 e 1 N de HCl.*

## INTRODUCTION

Modified celluloses with analytical functional groups as well as other natural and synthetic chelating polymers, combine the properties of selectivity with those of sorbent, being extremely useful in analytical investigations, for both concentrations and separations of elements<sup>1-3</sup>.

Separation of Cu(II) - Co(II) - Ni(II) has been performed by various researchers on polyamino-carboxylate<sup>4</sup>-and polyiminodiacetate<sup>5</sup> - type chelating resin and on cellulose modified by oxime-compounds<sup>6</sup> and antranilic acid<sup>7</sup>.

The present paper discussed the sorption of Cu(II), Co(II) and Ni(II) on 1(4'-azobenzylcellulose)-2-naphtol as well as the possible chromatographic separation of such elements.

## EXPERIMENTAL

1(4'-azobenzylcellulose)-2-naphtol has been synthesised from PAB-cellulose diazotized and coupled with 2-naphtol in a weakly alkaline medium<sup>8</sup>.

In order to establish the mechanism of Cu(II), Co(II) and Ni(II) sorption on the sorbent considered for the study, the following determinations have been performed:

- a. dependence of the distribution coefficients ( $K_d$ ) on pH, at 25°C;
- b. sorption isotherms at 25°C;
- c. calculation of the apparent free enthalpy;
- d. IR spectra of the sorbent both before and after sorption, between 400-4000 cm<sup>-1</sup>;
- e. diffuse reflectance spectra.

The distribution coefficients have been determined by an equilibrium method involving stirring of  $\approx 0.2$  g sorbent with 25 mL standard solution of copper chloride (5.08 mg Cu(II)/ L), cobalt chloride (5.05 mg Co(II)/ L) and nickel chloride (5.19 mg Ni(II)/ L) with a given pH, at constant temperature (25°C) for one hour. Experimentally, it has been established that the time necessary for attaining the equilibrium is below one hour. The solid phase has been separated through filtration, the equilibrium pH ( $pH_e$ ) being measured in the aqueous phase. The excess of Cu(II), Co(II) and Ni(II) has been determined in a part of filtrate, by flame atomic absorption spectrometry<sup>9</sup>, on a PERKIN-ELMER 3300 spectrophotometer.

For the isotherms, solutions with concentrations ranging between 0.1-1 mmole/L have been employed. The sorption isotherms have been represented in the  $\bar{X}_M = q/q_0 - X_M = c/c_0$  coordinates ( $\bar{X}_M$  - the equivalent fraction of the element in sorbent phase and  $X_M$  - the equivalent fraction of the element in solution),  $q$  and  $c$  having the following significance:  $q$  - amount of sorbed element (meq/g sorbent);  $q_0$  - maximum sorption capacity (meq/g sorbent);  $c$  - concentration of the element left in the solution (meq/mL);  $c_0$  - initial concentration of solution (meq/mL).

The IR spectra have been recorded on a SPECORD 71 IR spectrophotometer, while the diffuse reflectance spectra on a VSU-2P spectrophotometer equipped with a device for the study of the solid substances.



## RESULTS AND DISCUSSION

Study of the distribution coefficients dependence on pH (Figure 1) evidences that, over the  $pH_e = 2.9$  and  $pH_e = 5.1$  interval an increase of sorption differentiated from one element to another takes place.

On taking  $K_d$  as a comparison criteria, the three elements range in the following order of the sorbent's selectivity

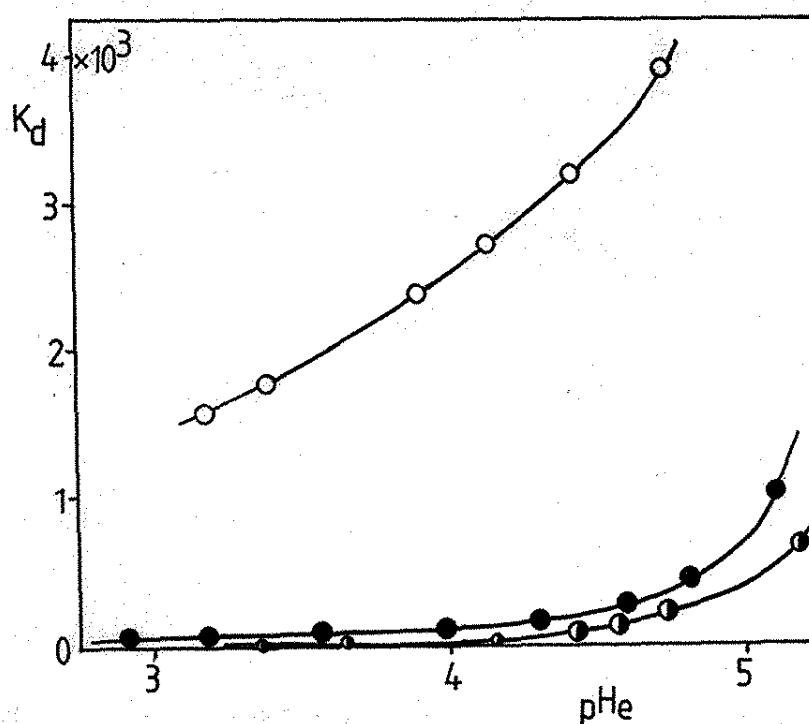


Fig. 1. Dependence of  $K_d$  on pH, at 25°C : o - Cu(II); ● - Ni(II); ● - Co(II).

For all determinations, it was experimentally observed that the  $pH_e$  value was lower than the pH of the initial solutions having contacted the sorbent.

Some observations referring to the mechanism of Cu(II), Co(II), Ni(II) sorption on 1(4'-azobenzylcellulose)-2-naphtol may be drawn from the study of sorption isotherms. The shape of the sorption isotherms (Figure 2) pleads for a combined mechanism of adsorption and chemisorption, the physical sorption being predominant for Co(II), while chemical sorption characterizes mainly Ni(II) and Cu(II), with highest preponderance for the latter element.

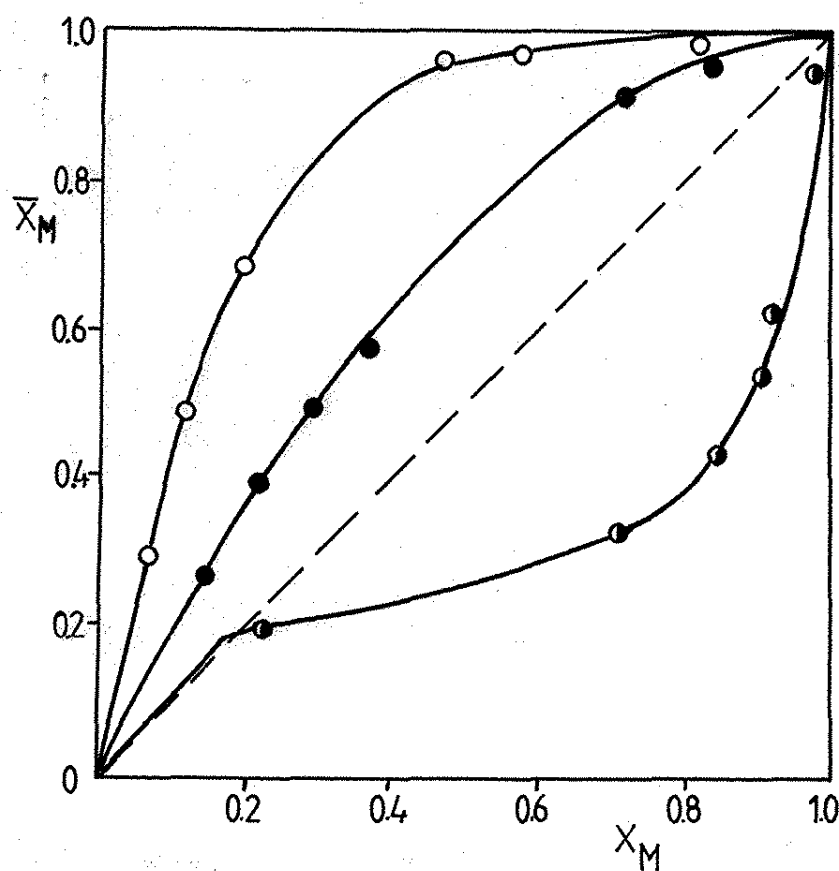


Fig. 2. The sorption isotherms at 25°C: o - Cu(II); ● - Ni(II); ● - Co(II).

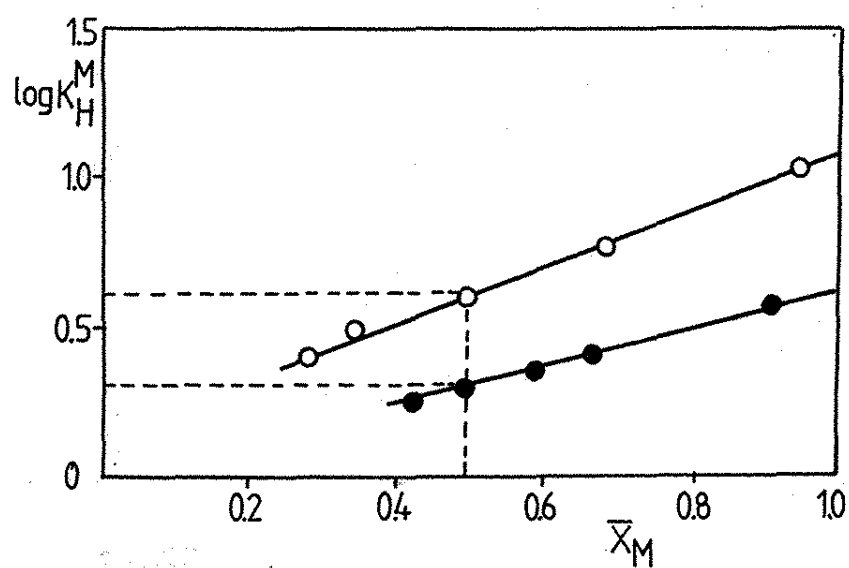


Fig. 3. The evaluation of the exchange reaction constant: o - Cu(II); ● - Ni(II).

The data obtained from isotherms have been employed in the determination of the apparent constants of ionic exchange.

For the reaction of ionic exchange



the exchange constant is:

$$K_H^M = \frac{\bar{X}_M^{1/2} \cdot X_H}{X_M^{1/2} \cdot \bar{X}_H}$$

where  $\bar{X}_M$  and  $\bar{X}_H = 1 - \bar{X}_M$  - the equivalent fractions in the sorbent phase;  $X_M$  and  $X_H = 1 - X_M$  - the equivalent fractions in the solution phase.

Substitution of the corresponding values from the isotherms permits calculation of  $K$  for each experimental point.

For the evaluation of the apparent constants of ionic exchange, the graph of the  $K_H^M = f(\bar{X}_M)$  dependence is built while, through interpolations, the  $K_H^M$  value is found for  $\bar{X}_M = 0.5$  (Figure 3).

The graph evidences that at  $\bar{X}_M = 0.5$ , the values  $K_H^{\text{Cu}} = 3.98$  and  $K_H^{\text{Ni}} = 2.23$  result.

Based on the apparent constants of ionic exchange determined experimentally, the variation of the apparent free enthalpy may be calculated with relation

$$\Delta G = -RT \ln K_H^M$$

the values  $-3421.6$  J/mol for Cu(II) and  $-1985$  J/mol for Ni(II) being found, which pleads for a chemical sorption through ionic exchange, which is more prominent for Cu(II).

Information on chemical sorption may be obtained from the study of IR and respectively diffuse reflectance spectra.

The IR spectra are quite difficult to be interpreted, due to the minor modifications appearing in both the form and position of the absorption bands and peaks. This is due to the low number of functional groups from the cellulose's macromolecule. In the sorbent's IR spectrum, two small peaks appear at  $1600 \text{ cm}^{-1}$  and, respectively  $1050 \text{ cm}^{-1}$  attributed to the  $-\text{N}=\text{N}-$  group. They disappear after the sorption of Cu(II) and Ni(II), or are diminished after Co(II) sorption which evidences the involvement of the azo group in the formation of chelate - type compounds between the sorbent and cations. At the same time, small modifications appear in the band from  $2800\text{-}3000 \text{ cm}^{-1}$  attributed to the  $-\text{OH}$  groups. This band also includes the vibrations of the  $-\text{OH}$  groups from cellulose remained unmodified.

The diffuse reflectance spectra are plotted in Figure 4. The sorbent is red, evidencing an absorption maximum at  $500 \text{ nm}$ , observed as suffering a bathochromic shifting after sorption of Cu(II) at  $521 \text{ nm}$ , of Ni(II) at  $513 \text{ nm}$  and Co(II) at  $505 \text{ nm}$ .

The equilibrium and spectroscopic data led to the conclusion that the physical sorption of Cu(II), Ni(II) and Co(II) on 1(4'-azobenzylcellulose)-2-naphtol is accompanied by a chemical sorption, the latter being prevalent for Cu(II) and Ni(II), and occurs probably by a reaction of ionic exchange with formation of chelates:

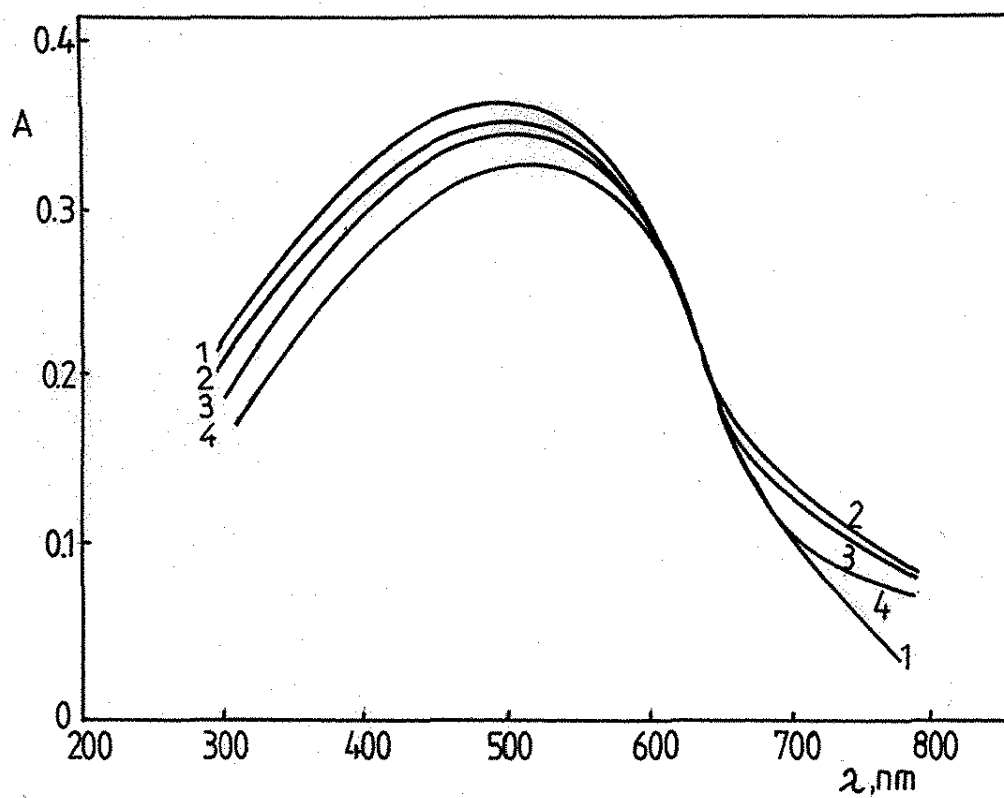


Fig. 4. The diffuse reflectance spectra: 1 - sorbent ; 2 - Cu(II)-compound; 3 - Ni(II)-compound; 4 - Co(II)-compound.

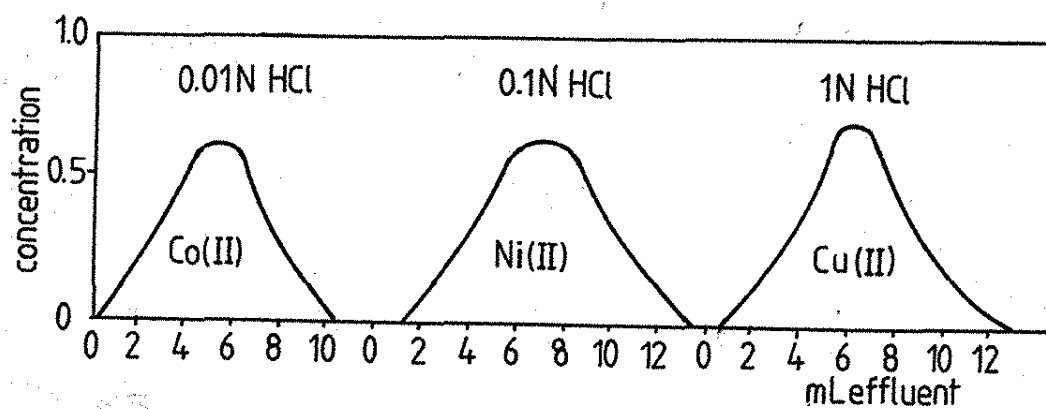
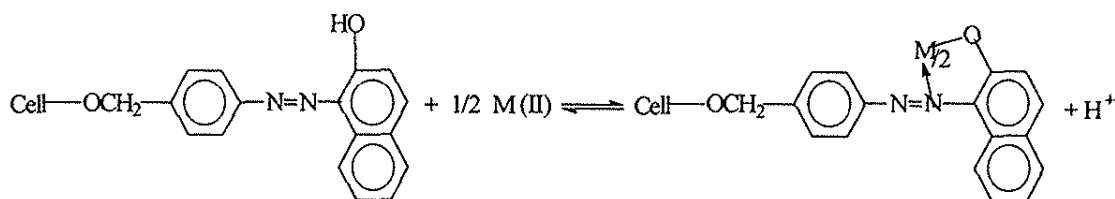


Fig. 5. Separation of Co(II) - Ni(II) - Cu(II).



The data obtained under static conditions suggested the possible separation of the three elements on a column filled with 1(4'-azobenzylcellulose)-2-naphthol. A satisfactory separation of Co(II) - Ni(II) - Cu(II) was obtained on a column with a length of 120 mm and diameter of 20 mm, filled with 4 g sorbent, by successive elution with 0.01 N HCl, 0.1 N HCl and 1 N HCl at the eluent flow rate of 0.1 - 0.12 mL/min (Figure 5).

The obtained results represented in the figure hold true in the domain of a ratio of 1/10 between components (amounts varying from 0.1 to 1 mg).

## REFERENCES

1. G. V. Myasoedova, O. P. Eliseeva and S. B. Savin, *Zhur. Analit. Khim.*, **26**, 2172 - 2187 (1975).
2. G. V. Myasoedova and S. B. Savin, *Zhur. Analit. Khim.*, **37**, 499 - 519 (1982).
3. C. Kantipuly, S. Katragadda, A. Chow and H. D. Gesser, *Talanta*, **37**, 491 - 517 (1990).
4. Jinfan Zhou and Linmei Yu, *Linhua Jianyan Huaxue Fence*, **25**, 2-5 (1989); *Chem. Abstr.* **113**, 33903b (1990).
5. Jinfan Zhou, Meifang Shi, Linmei Yu, Linmei Chen, Jingyao Ying and Xianyao Lu, *Lizi Jiaohuan Yu Xifu*, **6**, 93- 99, (1990); *Chem. Abstr.*, **114**, 258604a (1991).
6. Takehiro Kojima, Takaiuki Sowa and Makoto Sato, *Anal. Chim. Acta.*, **264**, 59-64 (1992).
7. C. P. Trivedi, Deepali Jain and Purnima Kapoor, *Anal. Lett.*, **22**, 2021-2031 (1989).
8. S. Fisel, T. Ungurenasu - Onofrei and I. Gabe, *Anal. Sti.Univ. "Al.I.Cuza" Iasi*, **11**, 51-54 (1965).
9. \*\*\* *Analytical Methods for Atomic Absorption Spectrophotometry PERKIN-ELMER*, Norwalk, Connecticut, USA (1982), Standard conditions, pp 1-2.

**COORDINATION COMPOUNDS OF Cu(II)  
AND Ni(II) WITH SCHIFF BASES DERIVED FROM  
FORMYLCARVONE AND o,p-AMINOBENZOIC ACID**

Adalgiza Ciobanu\*, Florica Zalaru\*\*, D. Albinescu\* and Christina Zalaru\*

\* Faculty of Chemistry, Organic Chemistry Dept., University of Bucharest, 90-92 Panduri Road, Romania.

\*\* Faculty of Chemistry, Inorganic Chemistry Dept., University of Bucharest, 23 Dumbrava Rosie, Romania.

**ABSTRACT**

Copper(II) and nickel(II) complexes employing the Schiff bases derived from formylcarvone and ortho and para aminobenzoic acid (L) have been prepared. The complexes of general formula  $\text{CuL}_2 \cdot 2\text{H}_2\text{O}$  and  $\text{NiL}_2 \cdot 2\text{L}$  have been characterized by elemental analysis, infrared, visible and EPR spectra and thermodifferential analysis. The metallic ion has determined the type of the complex.

**Keywords:** Coordination compounds of Cu(II) and Ni(II), Schiff bases derived from formylcarvone.

**RESUMO**

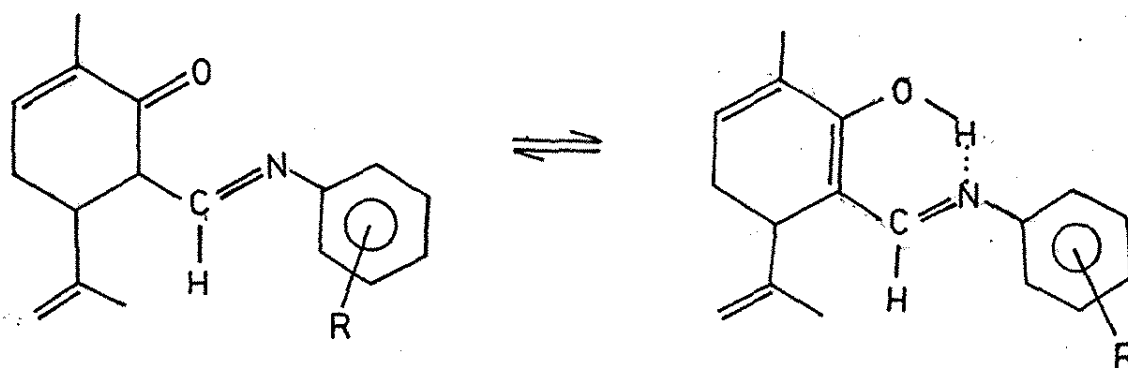
Foram preparados complexos de cobre(II) e níquel(II) usando como ligantes bases de Schiff derivadas de formilcarvona e orto- e para- isômeros do ácido aminobenzoico. Os complexos tem a formula geral  $\text{CuL}_2 \cdot 2\text{H}_2\text{O}$  e  $\text{NiL}_2 \cdot 2\text{L}$  e foram caracterizados através de análise elementar, espectroscopia no infravermelho, visível e REP e análise termodiferencial. O íon metálico determina o tipo de complexo formado.

## INTRODUCTION

Schiff bases represent a versatile series of ligands, the metal complexes of which have been widely studied <sup>/1-5/</sup>. Coordination compounds prepared by the reaction of some Schiff bases derived from formylcarvone and o,m,p-toluidine with Cu(II) and Ni(II) acetates have been previously described <sup>/6/</sup>.

This paper describes analogous compounds prepared by reaction of some Schiff bases derived from formylcarvone and ortho and para benzoic amino acid by the type:

where R = -COOH, ortho and para



The presence of a  $>\text{C}=\text{O}$  group at the 2-position of the carvone ring of the ligand favours a keto-enolic tautomerism (scheme 1). NMR studies have been shown that these Schiff bases exist in solution as the enolic tautomer, and that the tautomer distribution was very strongly solvent dependent <sup>/7,8/</sup>. Such tautomerism has been attributed to intramolecular hydrogen bond formation. Since the oxygen is present as an OH group, these Schiff bases can act as chelating monoanion. The position of the -COOH substituent of the benzen ring and metallic ion might determine the type of the complex.

## EXPERIMENTAL

The ligands were prepared according to the literature and  $\text{Cu}(\text{CH}_3\text{COO})_2 \cdot \text{H}_2\text{O}$  and  $\text{Ni}(\text{CH}_3\text{COO})_2 \cdot 4\text{H}_2\text{O}$  p.a. were used. The complex compounds were prepared by mixing warm methanolic solutions 50% of metal acetate (1 mmole) and ligands (2 mmols and 4 mmols). The resulting precipitates were filtered and washed with aqueous methanol solution 50% and dried at room temperature.

The nickel and copper contents were determined gravimetrically analyses. The water content was calculated from the TG curve.

Diffuse reflectance spectra were obtained on VSU 2-P Zeiss Jena spectrophotometer using MgO as standard.

EPR spectra were recorded at room temperature on polycrystalline powders with an ART 5-IFA Spectrograph. The klystron frequency was 9060 MHz and the modulation of the magnetic field was 100 KHz. The EPR spectral parameters were calculated versus a Mn(II) standard.

Thermodifferential analyses were carried out with a Paulik-Paulik-Erdey derivatograph Q 1500 D MOM. Conditions of measurements: temperature range up to 1000°C, heating program 10 deg/min, sensivity DTA=1/10, s=50, m=0.0180 g; 0.0164 g; 0.024 g; 0.0190 g; atmosphere over sample-air.

IR spectra were recorded within 700-4000  $\text{cm}^{-1}$  range on a Specord 75 Spectrophotometer in KBr pellet.

## RESULTS AND DISCUSSION

The reaction of metallic acetates with the ligands in water-methanol mixture=1:1 and various M:L molar ratios (1:1; 1:2; and 1:4) produces the complex compounds of formulas  $\text{CuL}_2 \cdot 2\text{H}_2\text{O}$  and  $\text{NiL}_2 \cdot 2\text{L}$  (table 1). The isolated compounds contain also molecules of water or ligand either as coordinated and/or as crystalline water.

Table 1: Results of the elemental and thermodifferential analyses.

No.	Ligand	Molar ratio M:L	Complex	M% found/calcd.	H <sub>2</sub> O% found/calcd.	L% found/calcd.	Colour
1.	R=ortho	1:2	$\text{Cu(o-L)}_2 \cdot 2\text{H}_2\text{O}$	8.08/ 9.11	4.94/ 5.46	86.80/ 85.52	light-brown
2.	R=ortho	1:2 and 1:4	$\text{Ni(o-L)}_2 \cdot 2(\text{o-L})$	4.91/ 4.76	-	94.85/ 95.25	ochre
3.	R=para	1:2	$\text{Cu(p-L)}_2 \cdot 2\text{H}_2\text{O}$	8.55/ 9.11	4.44/ 5.46	86.80/ 85.52	light brown
4.	R=para	1:2 and 1:4	$\text{Ni(p-L)}_2 \cdot 2(\text{p-L})$	4.66/ 4.76	-	94.39/ 95.25	ochre

It is noticed that, for nickel(II) ion is obtained the same compound for both Ni:L molar ratio (1:2 or 1:4).

The complex compounds are sparingly soluble in water and soluble in organic solvents (methanol, ethanol, chloroform).

The thermodifferential analyses have been confirmed the formulas. Fig.1 and fig.2 show the decomposition of the compounds 1 and 2 in detail.

It is clear from the thermogravimetric data that, copper compounds contain water, while nickel compounds do not. The mass loss observed within 120-190°C range on TG curve corresponds to the loss of two water molecules per molecule of each of the copper compounds. The thermogravimetric (TG) curve for  $\text{Ni(o-L)}_2 \cdot 2(\text{o-L})$  does not



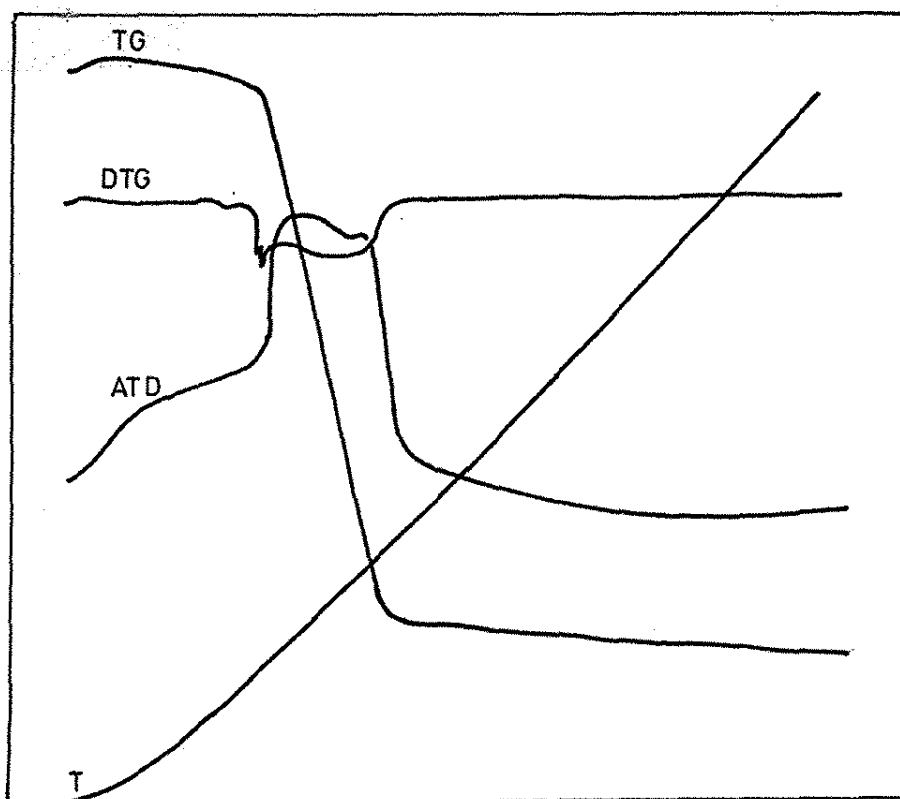


Fig. 1 Thermogravimetric curve of  $\text{Cu(o-L)}_2 \cdot 2\text{H}_2\text{O}$ .

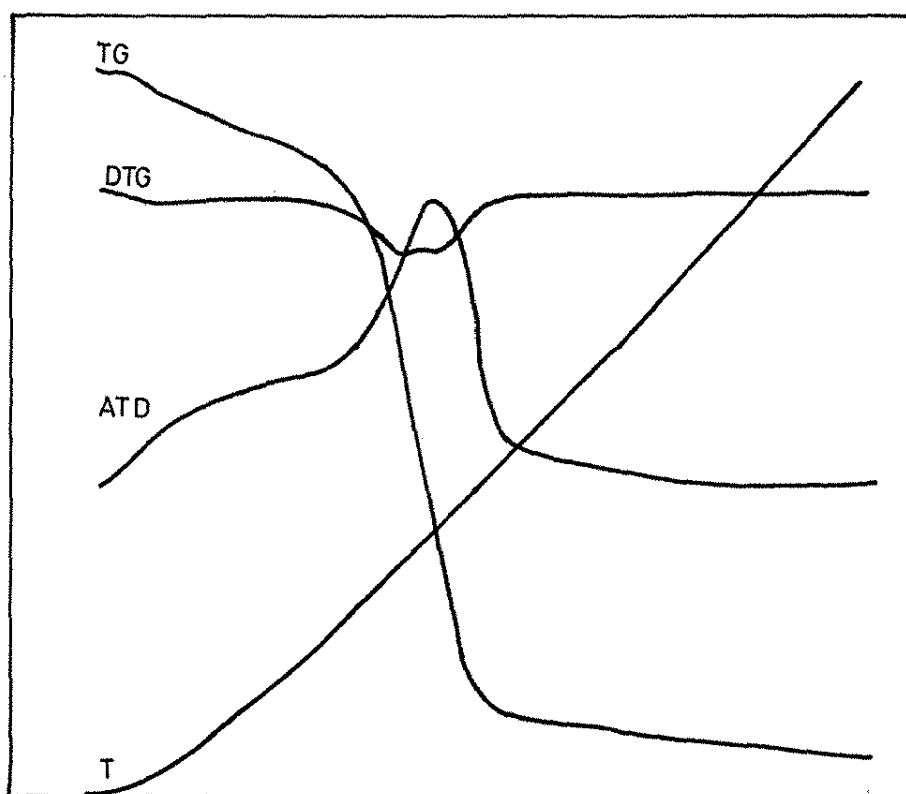


Fig. 2 Thermogravimetric curve of  $\text{Ni(o-L)}_2 \cdot 2(\text{o-L})$ .

show whether or not the ligand molecules are liberated in steps (weight loss at 190°C, found:10.98% calcd., for 2(o-L):47.62%).

Diffuse reflectance electronic spectra of Cu(II) complex compounds are similar; the broad band with a maximum at 700 nm can be assigned to a d-d transition (fig. 3).

This band can be associated with a distorted octahedron axially<sup>9,10/</sup>. The strong broad absorption which occurs at ~ 400 nm is assigned to the ligand. Its "tails off" strongly into the visible range.

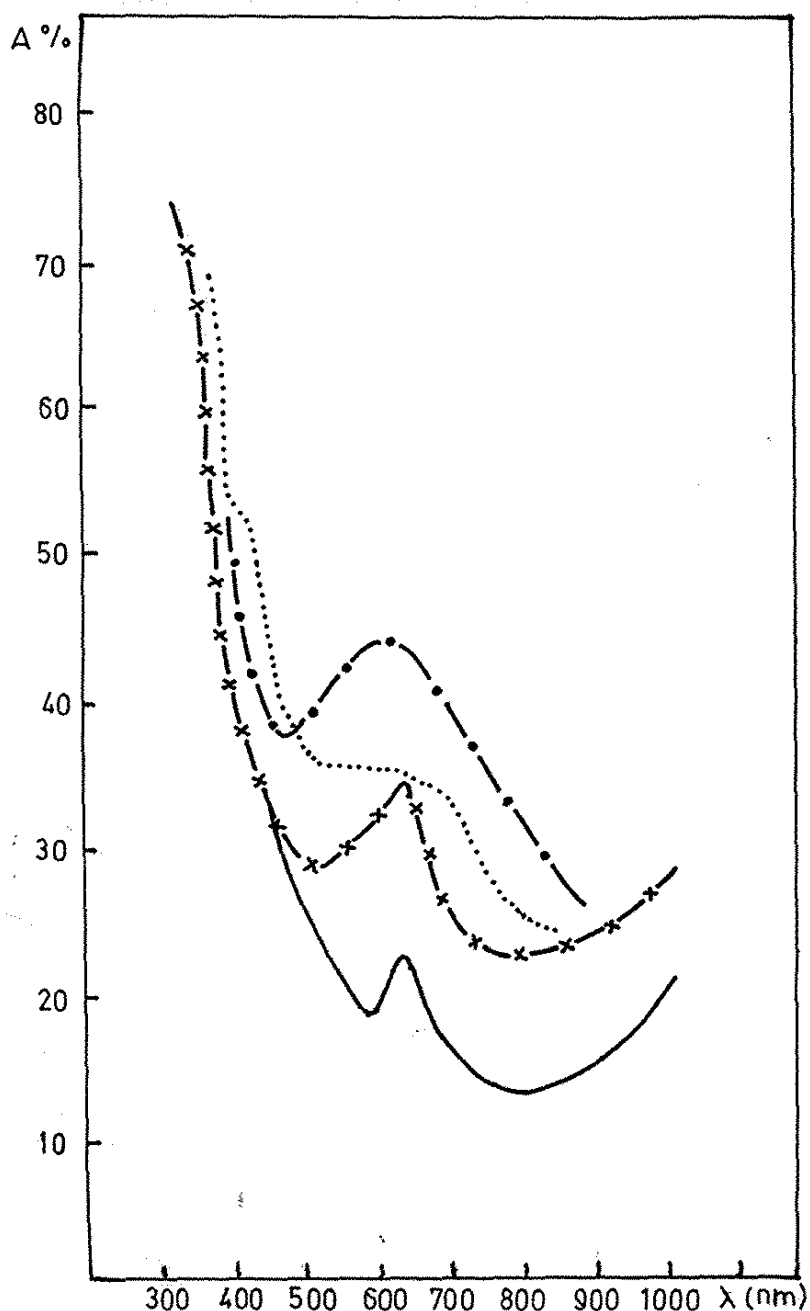


Fig. 3 Electronic reflectance spectra of the compounds:

- - - Cu(p-L)<sub>2</sub> · 2H<sub>2</sub>O; ..... Cu(o-L)<sub>2</sub> · 2H<sub>2</sub>O;  
- x - x - Ni(p-L)<sub>2</sub> · 2(p-L); \_\_\_\_\_ Ni(o-L)<sub>2</sub> · 2(o-L).

The EPR spectra of both Cu(II) complex compounds present a similar EPR signal with two g factors characteristic for the elongated tetragonal octahedral stereochemistry supporting the electronic spectra (fig. 4). The numerical g factors:  $g_{\parallel} \gg g_{\perp} > 2.0$  suggests a bigger distortion for  $\text{Cu}(\text{p-L})_2 \cdot 2\text{H}_2\text{O}$  compound.

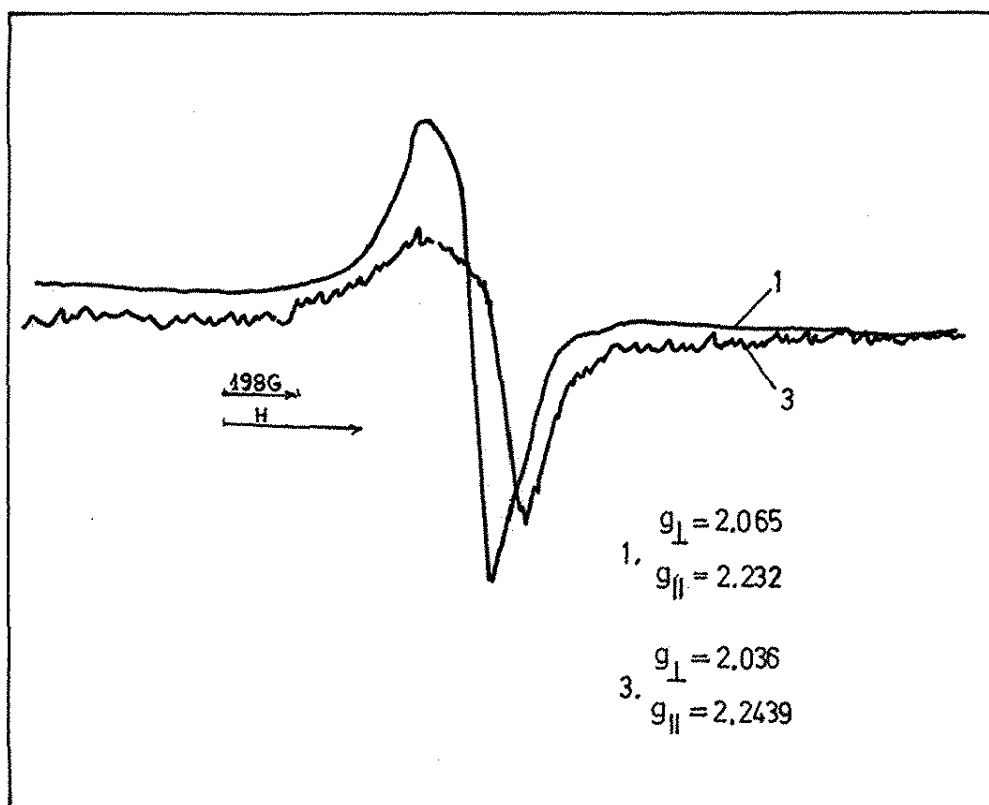


Fig. 4 EPR spectra of the compounds and EPR spectral parameters:  
1.  $\text{Cu}(\text{o-L})_2 \cdot 2\text{H}_2\text{O}$ ; 3.  $\text{Cu}(\text{p-L})_2 \cdot 2\text{H}_2\text{O}$ ;

The electronic spectra of the Ni(II) complex compounds are similar and are consistent with the postulation that Ni(II) ion is essentially hexacoordinate<sup>11/</sup>. The spectra present a band ( $\lambda_{\text{max}} = 730 \text{ nm}$ ,  $740 \text{ nm}$  respectively),  $\nu_2$ , that could be assigned to  ${}^3\text{A}_{2g} \rightarrow {}^3\text{T}_{1g}(\text{F})$  transition. The band  $\nu_3$  ( $\lambda_{\text{max}} \sim 400 \text{ nm}$ ) assigned to  ${}^3\text{A}_{2g} \rightarrow {}^3\text{T}_{1g}(\text{P})$  transition could be covered by the very strong ligand band.

Infrared spectra. The most relevant absorption bands in the IR spectra of the free ligands and their complex compounds are shown in table 2.

The keto-enolic tautomerism is supported by presence of the bands due to  $\nu_{\text{OH}}$  and  $\nu_{\text{C=O}}$ . The spectra of the free ligands are different within  $1700\text{--}1000 \text{ cm}^{-1}$  range. Thus, the stretching frequencies  $\nu_{\text{C=O}}$  ( $1700 \text{ cm}^{-1}$ ) and  $\nu_{\text{C=N}}$  ( $1610 \text{ cm}^{-1}$ ) appear as a strong and broad band with two unresolved peaks ( $1665$  and  $1610 \text{ cm}^{-1}$ ) for the ortho substituted ligand, but as a very strong band ( $1610 \text{ cm}^{-1}$ ) structured in some peaks ( $1680$ ,  $1650$ ,  $1550 \text{ cm}^{-1}$ ) for the para substituted ligand.

The bands due to  $\nu_{OH}$  and  $\nu_{C-OH}$  from the carvone ring and  $-COOH$  group ( $3400$  and  $1200\text{ cm}^{-1}$  respectively) are different, too. These bands are broad for ortho substituted ligand. The electronic and steric effects of the  $-COOH$  substituent may be transmitted to affect the strength of the hydrogen bond  $O-H \cdots N$  modifying the capacity of the nitrogen atom for participating in hydrogen bonding<sup>/8/</sup>. The changes noticed in the infrared spectra of the complex compounds  $Cu(o-L)_2 \cdot 2H_2O$  and  $Ni(o-L)_2 \cdot 2(o-L)$  are similar and involve the  $\nu_{OH}$  and  $\nu_{C=N}$  stretching frequencies. The broad band with two peaks ( $1665$  and  $1610\text{ cm}^{-1}$ ) is shifted to lower values ( $1600\text{ cm}^{-1}$ ).

Table 2: The main bands in IR( $\text{cm}^{-1}$ ) and their assignments

Ligand/ Complex compound	$\nu_{OH}$	$\nu_{C=O}$	$\nu_{C=N}$	$\nu_{C-OH}$
R=ortho	3000-3400 br	-	1610 s } 1665 }*	1200 m, br
$Cu(o-L)_2 \cdot 2H_2O$	3410 s	-	1600 br	1200 vw
$Ni(o-L)_2 \cdot 2(o-L)$	3350-3405 s	-	1600 br	1200 w
R=para	3405 m	1700 vw	1550 } 1610 vs } 1650 } 1680 }*	1160 m 1230 vw 1260 s
$Cu(p-L)_2 \cdot 2H_2O$	3410 s	1700 vw	1560 sh 1600 s 1650 sh	1160 w 1230 vw 1260 s
$Ni(p-L)_2 \cdot 2(p-L)$	3410 s	1700 vw	1580 sh 1600 s 1650 sh	1160 m 1230 sh 1270 s

vs = very strong; s = strong; m = medium; w = weak; vw = very weak; br = broad;  
sh = shoulder.

}\* = multiplet structure of the band.

It is due to  $M \leftarrow N$  bond formation. The band  $\nu_{OH}$  (3400-3000  $\text{cm}^{-1}$ ) lost its broad character and is shifted to higher values suggesting that upon coordination intramolecular hydrogen bond  $O-H \cdots N$  from the ligand (scheme 1) is destroyed and  $O-M \leftarrow N$  bond is formed in the metal chelates.

The IR spectrum of both compounds:  $\text{Cu}(\text{p-L})_2 \cdot 2\text{H}_2\text{O}$  and  $\text{Ni}(\text{p-L})_2 \cdot 2(\text{p-L})$  presents the changes that involve the  $\nu_{OH}$  and  $\nu_{C=N}$  stretching frequencies suggesting the same donor atoms. Very strong band (1610  $\text{cm}^{-1}$ ) appears as a strong band (1600  $\text{cm}^{-1}$ ) with two shoulders (1650 and 1560  $\text{cm}^{-1}$ ).

These Schiff bases containing an N,O donor atoms set, upon coordination to metal ion through both O and N, a decrease of the  $\nu_{C=N}$  frequency and a increase of the  $\nu_{OH}$  frequency are generally noticed<sup>18/</sup>.

These changes correlated with analytical data, electronic and EPR spectra could suggest that ligands are acted bidentately through both O and N donor atoms by the deprotonation of the OH group making evident participation of the ligands in the enolic tautomeric form. Cu(II) coordinates with four strong bond N and O donor atoms in a plane and with weaker bond to axial two molecules of water (Fig. 5).

Octahedral environment of the Ni(II) ion suggested by electronic spectrum could be achieved by the participation of para-substituted ligand to coordination both bidentately in a plane (through both O and N donor atoms) and monodentately axial (through O atom of the -COOH group).

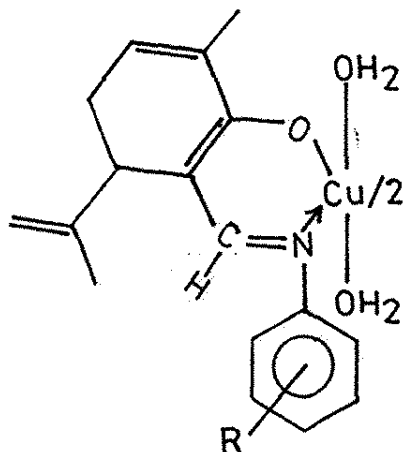


Fig. 5 Structural formula proposed for  $\text{Cu}(\text{o-L})_2 \cdot 2\text{H}_2\text{O}$

## CONCLUSION

Metallic ion determines the type of the compounds and different coordination behaviours of the ligands.

## REFERENCES

1. P.C. Chieh and G.J. Palenik, *Inorg.Chem.*, 11, 816 (1972)
2. J. Drummond and J.S. Wood, *J.Chem.Soc.Dalton Trans.*, 365 (1972)
3. M.Di Vaira, P.L. Orioli and L.Sacconi, *Inorg Chem.*, 10, 553 (1971)
4. B. Chiari, O. Piovesana, T. Tarantelli and P.F. Zanazzi, *Inorg.Chem.*, 23, 2542, 3398 (1984)
5. C.T. Spencer and L.T. Taylor, *Inorg.Chem.*, 10, 2407 (1971)
6. P. Grandclaudeon, F. Zalaru, D. Albinescu, A. Ciobanu and A. Meghea, *Anal.Univ.Buc.Chimie*, III, (1996) in press
7. G.O. Dudek and G.P. Volpp, *J.Am.Chem.Soc.*, 85, 2697 (1964)
8. G.C. Percy, *J.Inorg.Nucl.Chem.*, 34, 3357 (1972)
9. B.J.Hathaway and D.E.Billing, *Coord.Chem.Rev.*, 5, 143 (1970)
10. B.J. Hathaway, *Structure and Bonding*, 57, 85, 109 (1984)
11. H.B.P. Lever "Inorganic Electronic Spectroscopy", 2<sup>nd</sup> Ed. Amsterdam, p.507 (1984)

**REACTIVE EXTRACTION OF DICARBOXYLIC ACIDS**  
**I. MECHANISM, LIMITING STEPS AND KINETICS**

*Dan Cascaval, Radu Tudose and Corneliu Oniscu*

Technical University " Gh. Asachi " Jassy, Faculty of Industrial Chemistry,  
Department of Organic Industries, Bd. Mangeron 71, 6600 - Jassy, Romania.

**ABSTRACT.** In this paper the reactive extraction of some dicarboxylic acids ( oxalic acid, malonic acid, succinic acid, glutaric acid and adipic acid ) have been studied. These acids have been extracted by Amberlite LA-2 in butyl acetate using a modified extraction cell of the Lewis type. Mechanism, limiting steps and kinetic of the mass transfer process have been settled.

**RESUMO** Foi estudada a extração reativa de alguns ácidos dicarboxílicos (oxálico, malônico, succínico, glutárico e adípico). Estes ácidos foram extraídos com Amberlite LA-2 com acetato butílico e usando uma célula de extração modificada do tipo Lewis. Foram determinadas as etapas determinantes, o mecanismo e a cinética do processo de transferência.

**KEYWORDS :** dicarboxylic acids, oxalic acid, malonic acid, succinic acid, glutaric acid, adipic acid, reactive extraction, Amberlite LA-2.

## INTRODUCTION

Since 1970 the advantages offered by the reactive extraction have been determined the extent of applications area on organic compounds separation. In present, the conditions for reactive extraction of some derivatives, namely : carboxylic acids, amino acids, phenolic derivatives, alcohols, antibiotics, are intense studied with a view to industrial scale applying <sup>1</sup>.

For the carboxylic acids separation by reactive extraction different extracting agents have been used :

- organophosphoric agents ( tri-n-octyl phosphine oxid, tri-n-butyl phosphate ) <sup>2-5</sup> ;
- high molecular weight aliphatic amines or amines salts, especially secondary and tertiary amines ( lauryl-trialkylmethylaniline, named Amberlite LA-2, dodecylamine, named Adogen 283, tri-n-octylamine, tri-iso-octylamine, named Adogen 381, tri-n-(octyl - decyl)-amine, named Alamine 336, tri-n-octyl-methyl ammonium chloride, named Adogen 464 ) <sup>2,5-15</sup>.

The carboxylic acids extraction mechanisms are influenced by extraction system nature, being based on a chemical reaction of solvation or ionic exchange type or on a formation of high molecular weight ion - pair compounds.

In this paper the reactive extraction of the series of dicarboxylic acids : oxalic, malonic, succinic, glutaric and adipic acids, by Amberlite LA-2 in butyl acetate medium is studied, with a view to establishing the mechanism, the limiting steps and the kinetic of mass transfer process.

## EXPERIMENTAL

The experimental studies have been made in two separate stages. The first one consists on the study on the reactive extraction mechanism by means



of equilibrium data. The extraction was carried out in batch system in a cylindrical glass vessel, provided with a jacket which the thermosetting agent passes, namely ethylene glycol maintained at 24°C.

The initial concentration of dicarboxylic acids in aqueous phase has been varied as follows :

- oxalic acid : 1.80 - 71.66 g L<sup>-1</sup>;
- malonic acid : 3.43 - 65.33 g L<sup>-1</sup>;
- succinic acid : 4.55 - 54.10 g L<sup>-1</sup>;
- glutaric acid : 5.49 - 81.99 g L<sup>-1</sup>;
- adipic acid : 3.11 - 11.18 g L<sup>-1</sup>.

The organic phase was butyl acetate with a content of 42 g L<sup>-1</sup> Amberlite LA-2. The volume ratio between the aqueous solution and the solvent phase was 1, each phase volume being 25 mL.

The second stage consists in the establishment of the nature of the resistances which can appear in the organic acid overall mass transfer process and the study on reactive extraction kinetic. The laboratory equipment used includes a modified extraction cell of the Lewis type ( Figure 1 ). The extraction cell was made up of two compartment of glass pipe having 750 mL each. The phases have been mixed by two perforated blade stirrers with variable rotation speed ( 0 - 1000 rpm ). The contacting area of the central circular interface was 28.27 cm<sup>2</sup>.

The studies on the limiting steps were carried out in a continuous system, the aqueous phase and the organic phase were separately feed, and the two phases throughputs were :

- aqueous phase : 1.25 - 2.73 L h<sup>-1</sup>;
- organic phase : 1.23 - 2.40 L h<sup>-1</sup>.

Stamps prelevation was carried out from the aqueous phase evacuation tract.

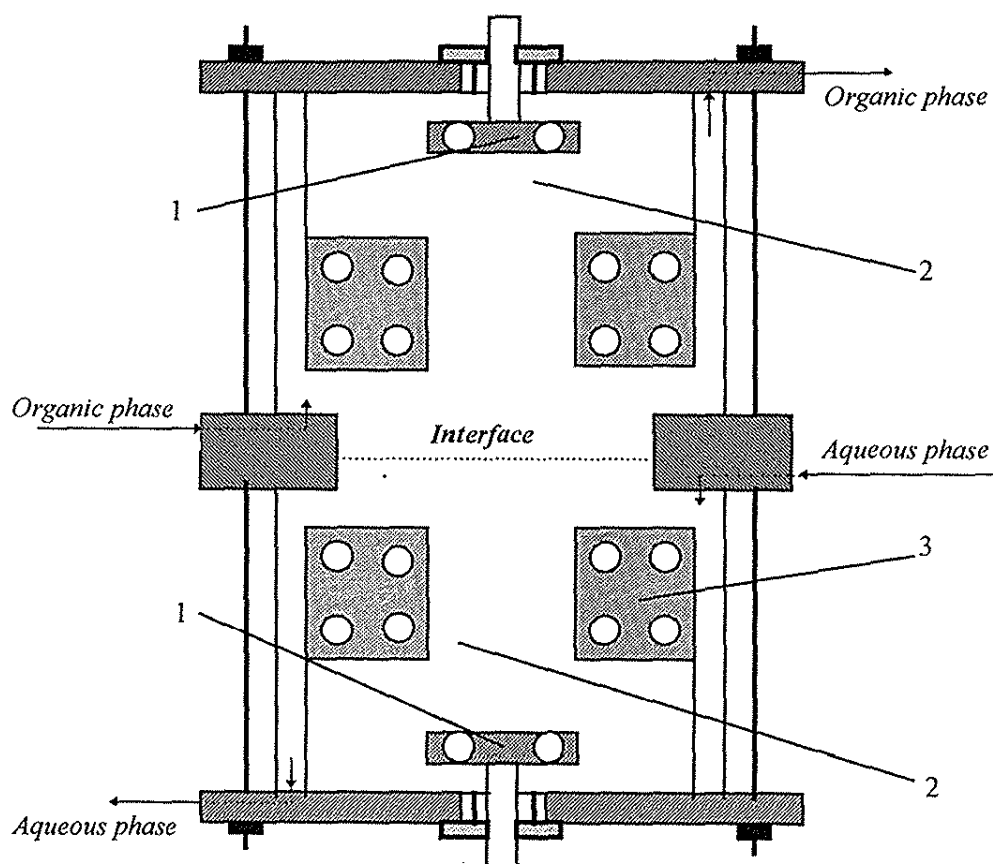


Figure 1. Extraction cell ( 1 - cylindrical compartment, 2 - perforated blade stirrer, 3 - baffle ).

The reactive extraction kinetic was established in a batch system, at 24°C, for kinetic regime ( rotation speed value greater than 1200 rpm, level determined by means of preliminary studies ). Thus, the rotation speed values were between 1.600 and 1.800 rpm for each phase.

The extracting agent concentration in butyl acetate was 80 g L<sup>-1</sup> for the study on limiting steps and 42 g L<sup>-1</sup> for the kinetic study. In both experiments the initial concentration of dicarboxylic acids was 4.50 - 6.78x10<sup>-2</sup> M.

The extraction process development has been followed by titration of initial aqueous solution and raffinate with a sodium hydroxide solution of 3x10<sup>-2</sup> M.

## RESULTS AND DISCUSSION

*a. Reactive Extraction Mechanism*

The reactive extraction of dicarboxylic acids by Amberlite LA-2 can be described by following interface equilibrium :



where  $\text{R(COOH)}_2$  is the dicarboxylic acid and A is the extractant of Amberlite LA-2 type.

For a constant value of the extractant concentration, the structure of the formed complex is determined by the level of the organic acid concentration, as follows :

a. for a molar ratio between dicarboxylic acid and Amberlite LA-2 below 1, the interfacial reaction product is :  $\text{R(COOH)}_2 \cdot \text{A}_2$ ;

b. for a molar ratio nearly 1, the extraction system components react in a equimolecular proportion forming :  $\text{R(COOH)}_2 \cdot \text{A}$ ;

c. at high initial concentration of the organic acids, a third phase of high complex concentration can appeared in non - polar diluents ( butyl acetate, for example ). In this case, the structure of the complex is  $[\text{R(COOH)}_2]_m \cdot \text{A}_p$  <sup>6</sup>.

For establishing the extraction mechanism the variation of the reactive extraction degree with dicarboxylic acids initial concentration in aqueous solution has been represented and compared with the theoretical curves corresponding to the proposed mechanisms ( Figures 2, 3, 4, 5 and 6 where 1 - experimental values, 2 - theoretical values corresponding to mechanism a., 3 - theoretical values corresponding to mechanism b., 4 - theoretical values corresponding to mechanism c. ).

As observed, for the proposed experimental conditions, at a value of the molar ratio between dicarboxylic acid and Amberlite LA-2 of 0.8 - 1 the extraction mechanism was b. The existed differences between theoretical and

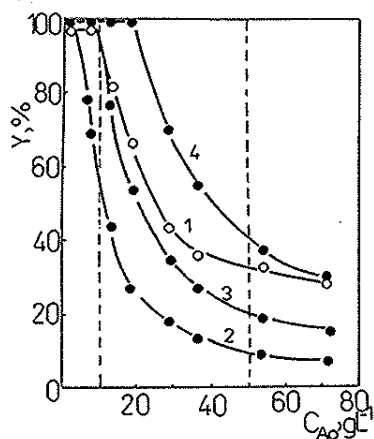


Figure 2. Variation of reactive extraction degree versus initial concentration of oxalic acid in aqueous phase.

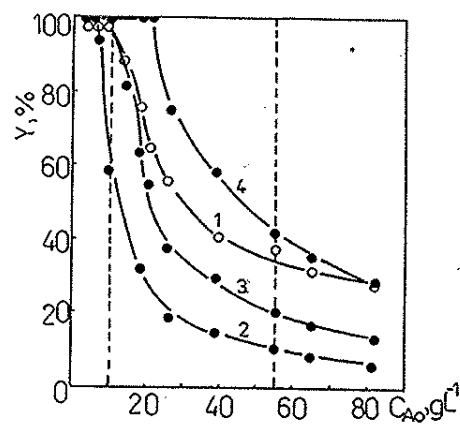


Figure 3. Variation of reactive extraction degree versus initial concentration of malonic acid in aqueous phase.

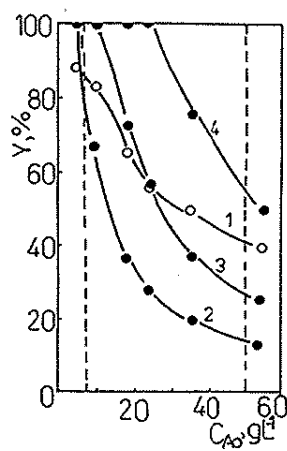


Figure 4. Variation of reactive extraction degree versus initial concentration of succinic acid in aqueous phase.

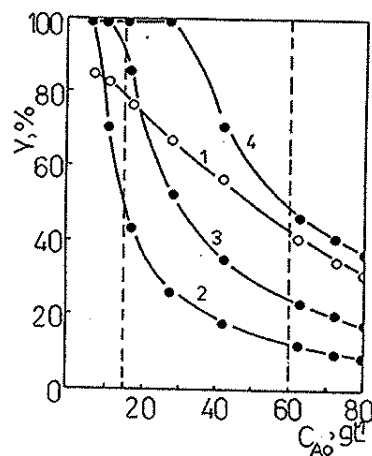


Figure 5. Variation of reactive extraction degree versus initial concentration of glutaric acid in aqueous phase.

real extraction degree values are the result both of the variation of acidic constant for the considered acids and of the resistance to the system components diffusion.

At the initial molar ratio values greater than 4.5, the formation of complexes of c. type is possible. Adipic acid represents an exception because of his low solubility in aqueous phase and low acidity compared with the other dicarboxylic acids, the reactive extraction mechanism being of b. type for all acid concentration range.

Both mechanisms b. and c. are involved simultaneously in mass transfer process for a molar ratio included between the previous values, as seen from the extraction yield variation.

#### *b. Limiting Steps*

The overall reactive extraction process can be determined by two types of resistance : diffusion and/or chemical reaction. For settle the relative importance of one among them the dependence between the transferred solute

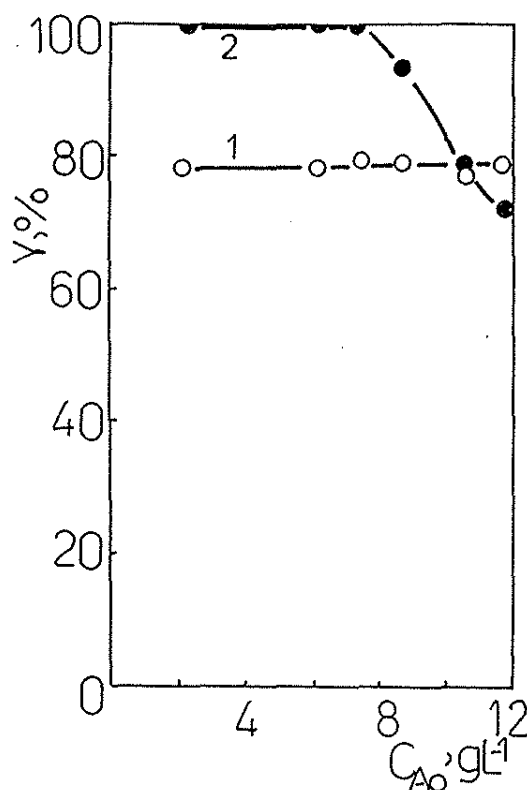


Figure 6. Variation of reactive extraction degree versus initial concentration of adipic acid in aqueous phase.

mass flow and the rotation speed has been studied. Thus, for low values of mixing intensity the reactive extraction process is most likely diffusional limited. By increasing the rotation speed of the stirrer, the overall mass transfer process is gradually controlled by the chemical reaction, so that over a certain rotation speed value specific to each dicarboxylic acid the chemical reaction becomes the limiting step.

As seen in Figure 7 the rotation speed range corresponding to the diffusional regime depends on the acidic constant of dicarboxylic acids ( the values of the acidity for these acids are given in Table 1<sup>16</sup> ). Over the following rotation speed values the chemical reaction controls the overall extraction process :

- oxalic acid : 1000 rpm;

- malonic acid : 960 rpm;

- succinic acid : 900 rpm;

- glutaric acid : 900 rpm;

- adipic acid : 800 rpm, observing a tendency to reduce the rotation speed range in which the diffusion consists the limiting steps with the decrease in acidic strength. These studies have been carried out for a molar ratio value between dicarboxylic acids and Amberlite LA-2 near to 1, so that the interfacial reaction is :



This condition has been used because it offers the possibility to compare the mass transfer behaviour for all acids studied.

### ***c. Reactive Extraction Kinetic***

Considering a reactive extraction mechanism of **b.** type the expression for reaction rate is :

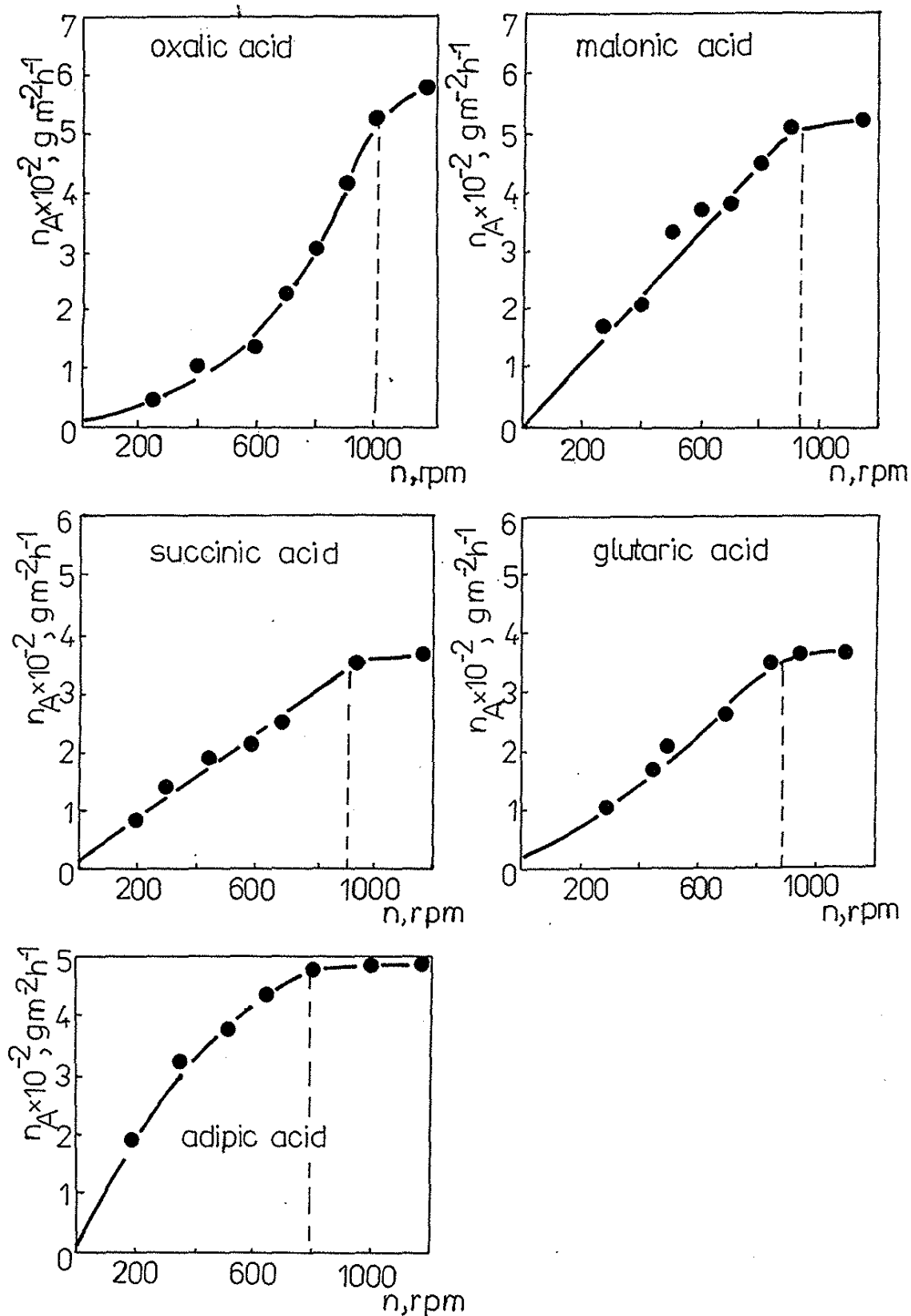


Figure 7. Specific mass flow versus rotation speed.

Table 1. Values of the acidic constants for the extracted dicarboxylic acids.

Dicarboxylic acid	$k_1$	$k_2$
Oxalic acid	$6.5 \cdot 10^{-2}$	$6.1 \cdot 10^{-5}$
Malonic acid	$1.4 \cdot 10^{-2}$	$8.7 \cdot 10^{-7}$
Succinic acid	$6.9 \cdot 10^{-5}$	$2.8 \cdot 10^{-6}$
Glutaric acid	$4.5 \cdot 10^{-5}$	$3.8 \cdot 10^{-6}$
Adipic acid	$3.7 \cdot 10^{-5}$	$3.9 \cdot 10^{-6}$

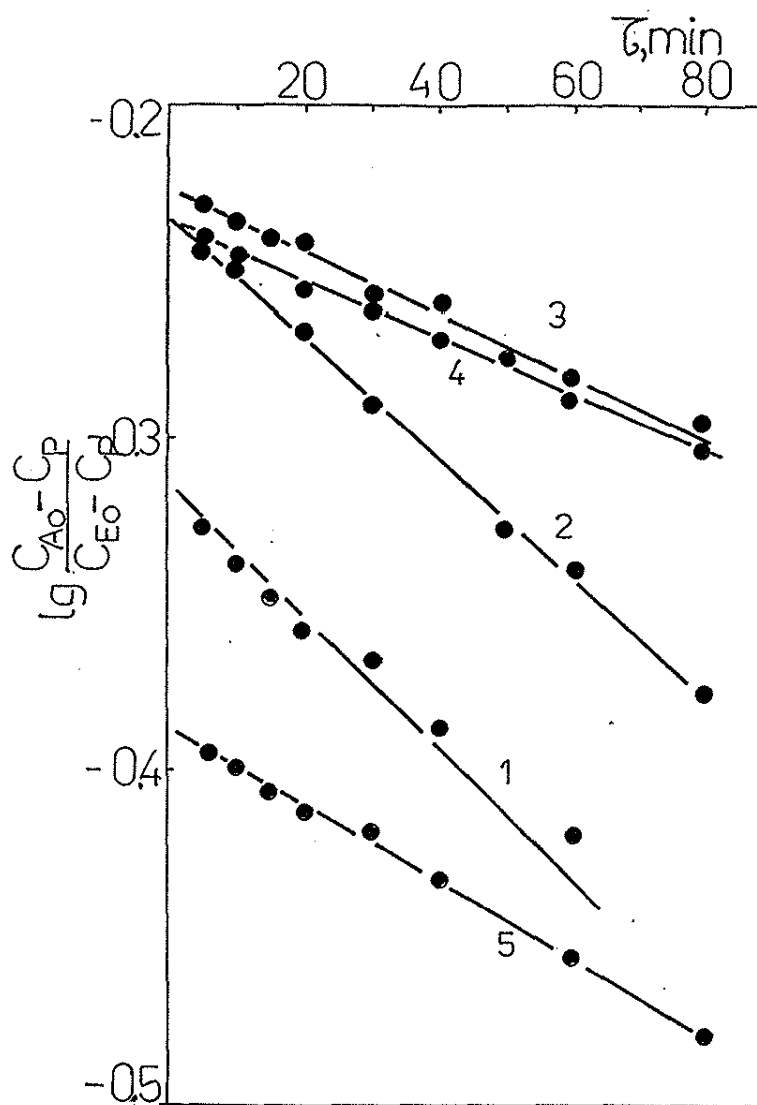


Figure 8.  $\lg [(C_{A0} - C_P)/(C_{E0} - C_P)]$  versus extraction time ( 1 - oxalic acid, 2 - malonic acid, 3 - succinic acid, 4 - glutaric acid, 5 - adipic acid ).



Table 2. Experimental values,  $v_{exp}$ , and theoretical values,  $v_{th}$ , of reaction rate between dicarboxylic acids and Amberlite LA-2.

Dicarboxylic acid	time, min	$v_{exp} \times 10^6$ , $M L^{-1} s^{-1}$	$v_{th} \times 10^6$ , $M L^{-1} s^{-1}$	r, %	$r_{av}$ , %
Oxalic acid	5	8.000	7.643	4.46	3.750
	10	7.000	7.130	1.87	
	15	6.671	6.805	2.00	
	20	6.000	6.400	6.67	
Malonic acid	5	8.889	8.844	0.50	2.592
	10	8.000	8.316	3.95	
	20	7.619	7.305	4.12	
	50	4.762	4.896	2.81	
Succinic acid	6	6.000	5.800	3.33	2.24
	10	5.583	5.396	3.35	
	20	4.889	4.927	0.78	
	30	4.670	4.740	1.50	
Glutaric acid	5	6.061	5.913	2.44	2.70
	10	5.555	5.654	1.78	
	20	5.000	5.284	5.69	
	30	4.667	4.709	0.90	
Adipic acid	15	3.000	3.067	2.23	3.95
	30	2.750	2.875	4.54	
	40	2.666	2.688	0.83	
	60	2.220	2.394	7.83	

$$dC_p / d\tau = k_1 (C_{A_0} - C_p)(C_{E_0} - C_p)$$

This study has been carried out for rotation speed value domain corresponding to the kinetic regime. The specific reaction rate was determined by means of the equation obtained by integration of the former one :

$$\lg [(C_{A_0} - C_p)/(C_{E_0} - C_p)] = f(\tau)$$

which represents the straight line equation. The slope of this straight line is :  $0.434 (C_{A_0} - C_{E_0}) k_1^{17}$ . In Figure 8 are plotted the straight lines for each dicarboxylic acid. Thus, the following values for the specific reaction rate have been obtained :

- oxalic acid :  $1.452 \times 10^{-3} \text{ M L}^{-1} \text{ s}^{-1}$ ;
- malonic acid :  $1.419 \times 10^{-3} \text{ M L}^{-1} \text{ s}^{-1}$ ;
- succinic acid :  $8.227 \times 10^{-4} \text{ M L}^{-1} \text{ s}^{-1}$ ;
- glutaric acid :  $8.686 \times 10^{-4} \text{ M L}^{-1} \text{ s}^{-1}$ ;
- adipic acid :  $6.893 \times 10^{-4} \text{ M L}^{-1} \text{ s}^{-1}$ .

The calculated values are confirmed by the experimental values, as resulted from Table 2.

As it was to be expected, the specific reaction rate decreases from oxalic acid to adipic acid. By means of these results and of their acidity, the organic acids studied can be grouped in three categories : oxalic and malonic acids, succinic and glutaric acids, and adipic acid. The specific rate for the reaction between adipic acid and extracting agent is about 2.11 times lower than those corresponding for the reaction between oxalic acid and extracting agent, and about 1.3 times lower than those for glutaric acid.

## CONCLUSIONS

These studies on separation of dicarboxylic acids by reactive extraction with Amberlite LA-2 in butyl acetate have indicated the significant

influence of the acidic constant variation for the series oxalic acid - adipic acid on extraction degree, on relative importance of the limiting steps and on value of the specific rate of the interfacial chemical reaction between the solute and the extracting agent, even for the similar extraction mechanisms.

### List of Symbols

$C_A$  - dicarboxylic acid concentration in aqueous solution;

$C_{A_0}$  - dicarboxylic acid initial concentration in aqueous solution;

$C_E$  - extracting agent concentration in solvent phase;

$C_{E_0}$  - extracting agent initial concentration in solvent phase;

$C_P$  - complex concentration;

$k_1$  - specific reaction rate;

$n$  - rotation speed;

$n_A$  - specific mass flow of dicarboxylic acid;

$r$  - deviation from experimental values;

$r_{av}$  - average deviation;

$\tau$  - extraction time;

$Y$  - reactive extraction degree.

### REFERENCES

1. M. H. I. Baird, *Can. J. Chem. Engn.*, 69, 1287 (1991).
2. C. Hanson (Ed.), " *Recent Advances in Liquid - Liquid Extraction* ", Pergamon Press, Oxford 1975.

3. R. J. M. Wardell and C. J. King., *J. Chem. Engn. Data*, 23, 144 (1978).
4. T. Hano, *J. Chem. Engn. Jpn.*, 23, 734 (1990).
5. K. Schuegerl, R. Hansel, R. Schlichting and W. Halwachs, *I. Ch. E.*, 28, 393 (1988).
6. H. J. Rehm, G. Reed, A. Puhler and P. Stadler (Eds.), " *Biotechnology* ", vol.3, VCH Weinheim 1993, pp.566.
7. N. L. Ricker, J. N. Michaels and C. J. King, *J. Separ. Process Technol.*, 1, 36 (1979).
8. N. L. Ricker, C. F. Pittmann and C. J. King, *J. Separ. Process Technol.*, 1, 23 (1980).
9. M. Puttemans, L. Dryon and D. C. Massart, *Anal. Chim. Acta*, 130, 307 (1980).
10. M. Puttemans, L. Dryon and D. C. Massart, *Anal. Chim. Acta*, 164, 221 (1984).
11. M. Puttemans, L. Dryon and D. C. Massart, *Anal. Chim. Acta*, 164, 245 (1984).
12. J. A. J. Harris, S. Khan, B. G. reuben and T. Shokaya, *Separ. Biotechnol.* 2, D. L. Elsevier, London 1990, pp.172.
13. C. Oniscu, D. Cascaval, E. Horoba and A. Dumitrascu, *Rev. Chim.*, 44, 1021 (1993).
14. C. Oniscu, R. Tudose and D. Cascaval, *Rev. Roum. Chim.*, 39, 1343 (1994).
15. D. Cascaval, C. Oniscu and A. Dumitrascu, *South. Braz. J. Chem.*, 3, 37 (1995).
16. C. D. Nenitescu, " *Chimie organică* ", vol.1, Editura Didactică si Pedagogica, Bucharest 1980, pp.756.
17. V. Isac and N. Hurdac, " *Chimie fizică - cinetică chimică și cataliză* ", Stiinta, Chisinau 1994, pp.33.

**THE PHOTODEGRADATION REACTION OF SOME  
PORPHYRINS**

111

Dr.Chim.Rodica-Mariana ION , ZECASIN S.A.,Photochemistry Dept.,  
Splaiul Independentei 202,Bucharest,Romania.

Prof. Dr. Cristina MANDRAVEL, Bucharest University, Physical-  
Chemistry Dept.,Bd.Carol I,13,Bucharest,Romania.

**ABSTRACT**

One of the most important, but undesirable properties of the porphyrins is their oxidative photodegradation which can occur in non-polar solvents, under irradiation and in the presence of molecular oxygen. The mechanism of this oxidative photodegradation implies singlet oxygen and different radical species.

This paper is concerned with the mechanism of the photodegradation of some meso-tetra(4-X-phenyl)porphyrins(TXPP) and meso-tetra(4-X-1-naphthyl)porphyrins(TXNP), where X could have different organic structures (-NH<sub>2</sub>, -NO<sub>2</sub>, -SO<sub>3</sub>H, -OH, -OCH<sub>3</sub>, -CH<sub>3</sub>).

Based on different spectral methods (UV-Vis and IR absorption spectroscopy, emission spectroscopy, X-ray diffraction, electronic microscopy and mass spectrometry, we propose a photodegradation mechanism and we evaluated the effect of some scavengers (2,6-di-tert-butyl-phenol (DTBF) for radical species, 1,3-diphenylisobenzofuran (DPBF) for singlet oxygen and nitro-blue tetrazolium (NBT) for superoxide anion) during the porphyrin photodegradation.

**KEYWORDS** porphyrins, photodegradation, spectral analysis, meso-substitution.

## RESUMO

Este trabalho trata do mecanismo da fotodegradação de algumas meso-tetra(4-X-fenil)porfirinas (TXPP) e meso-tetra(4-X-1-naftil)porfirinas (TXNP), onde X corresponde a vários substituintes ( $-NH_2$ ,  $-NO_2$ ,  $-SO_3H$ ,  $-OH$ ,  $-OCH_3$ ,  $-CH_3$ ).

Usando métodos de espectroscopia UV-vísivel, infravermelho, espectroscopia de emissão, difração de raios-X, microscopia eletrônica e espectrometria de massa foi proposto um mecanismo de fotodegradação. O efeito de alguns compostos como 2,6-di-tert-butilfenol (DTBF) sobre radicais como as espécies do 1,3-difenilisobenzofurano (DPBF), oxigênio singlete e do nitro-azul tetrazólio (NBT) sobre ânion superóxido foi também estudado durante a fotodegradação das porfirinas.

## 1. INTRODUCTION

Porphyrins, both as free base and metallocomplexes, play an important role in many energy transfer processes from chemistry and biology <sup>1</sup>.

Porphyrins can be oxidized chemically, electrochemically or photochemically generating porphyrin-ring centered oxidized products, <sup>2-7</sup>.

Competition between singlet oxygen (type II) and electron transfer (type I) photosensitization mechanisms has been observed in homogeneous and heterogeneous model systems, <sup>8-10</sup>.

A possible photodegradation mechanism for different meso-tetra(4-X-phenyl)porphyrins (TXPP) and meso-tetra(4-X-naphthyl)porphyrins (TXNP), where X could have different organic structures ( $-NH_2$ ,  $-NO_2$ ,  $-SO_3H$ ,  $-OH$ ,  $-OCH_3$ ,  $-CH_3$ ) is discussed in this paper.

We could demonstrate this photodegradation mechanism by means of different spectral techniques: UV-Vis and IR absorption spectroscopy, emission spectroscopy, X-ray diffraction, electronic microscopy and mass spectrometry.

The effects of some traps for reactive species of oxygen (1,3-diphenylisobenzofuran (DPBF) for singlet oxygen, 2,6-di-tert-butylphenol (DTBF) for radical species and nitro-blue tetrazolium chloride (NBT) for the superoxide anion) on the photodegradation reaction of meso-substituted porphyrins, were analysed in this paper.

## 2. EXPERIMENTAL PROCEDURE

### 2.1. Materials and Methods

The structure of the meso-tetra(4-X-phenyl)porphyrins(TXPP), of the meso-tetra(4-X-naphtyl) porphyrins (TXNP), and the name of these porphyrins are shown in Tables 1, 2 and Figure 1.

All the porphyrins have been prepared and purified in the laboratory according to the literature data <sup>11-20</sup>, or means of our own methods,<sup>2</sup>.

The singlet oxygen trap, DPBF, obtained from Fluka (Purum grade) was used as received. Also, the superoxide anion trap (NBT) and the radical inhibitor (DTBF) were Fluka products and were used without further purification.

Potassium ferrioxalate, used as a chemical actinometer with a quantum yield of 1.11 at  $\lambda = 420$  nm, was prepared by Parker's method <sup>21</sup>.

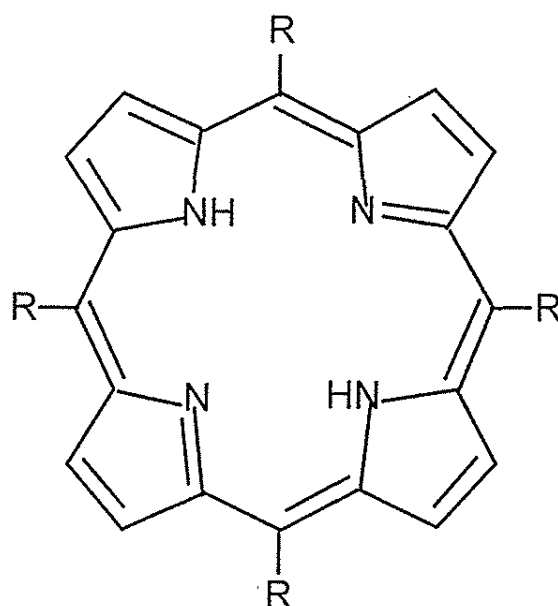


Fig.1. The structure of meso-substituted porphyrins;

Table 1. The structure of meso-substituents and the name of meso-(tetra- X-phenyl)porphyrins

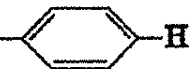
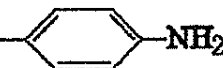
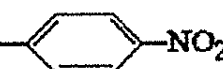



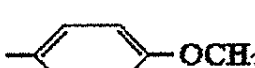
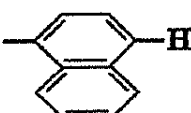
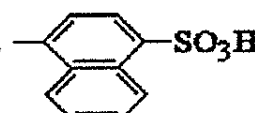
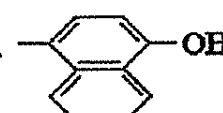
Meso-substituent (R)	Name of porphyrins	Abreviation
1. 	meso-tetra (4-phenyl) porphine	(TPP)
2. 	meso-tetra (4-amino-phenyl) porphine	(TAPP)
3. 	meso-tetra (4-nitro-phenyl) porphine	(TNPP)
4. 	meso-tetra (4-sulphonato-phenyl) porphine	(TSPP)
5. 	meso-tetra(4-hydroxy-phenyl) porphine	(THPP)
6. 	meso-tetra(4-methyl-phenyl) porphine	(TMPP)
7. 	meso-tetra(4-methoxy-phenyl) porphine	(TMOPP)

Table 2. The structure of meso-substituents and the name of meso-(tetra- X-phenyl)porphyrins

Meso-substituent (R)	Name of porphyrins	Abreviation
8. 	meso-tetra (4-naphtyl) porphine	(TNP)
9. 	meso-tetra (4-sulphonato-naphtyl) porphine	(TSNP)
10. 	meso-tetra (4-hydroxy-naphtyl) porphine	(THNP)



## 2.2. Irradiation Conditions and Measurements

The porphyrin ( $10^{-4}\text{M}$ ) was added to a Pyrex flask containing 100 ml of benzene, with magnetic stirring and irradiated through the bottom optimal pyrex windows (transmitting wavelengths greater than 300 nm). The photoreactor was thermostated at  $18^\circ\text{C}$  by a water jacket. Oxygen was bubbled from a bottle at a rate of 3 l/h through a glass frit located inside the reactor. The light was focused by a parabolic reflector on a 420 nm filter (IAUC) which was placed in front of a quartz window.

After photobleaching, the medium was extracted (three times) with chloroform. The chloroform extracts were dried on sodium sulphate, filtered and concentrated before gas chromatography / mass spectrometry analyses.

Mass spectra were obtained with an Hewlett-Packard-5985 spectrometer. The following mass spectrometric operating conditions were employed: electron impact ionization - electron energy: 70 eV; source temperature:  $200^\circ\text{C}$ ; positive chemical ionization - electron energy: 150 eV; source temperature:  $150^\circ\text{C}$ ; methane pressure: 1 torr.

The final product of photodegradation reaction of the porphyrins was identified with an IR Specord M 80 - Carl Zeiss Jena type spectro photometer, from  $\text{CCl}_4$  solution.

All the spectral changes of the porphyrins were analysed by means of the UV-Vis absorption spectra, recorded with a Specord M 400 spectrophotometer (Carl Zeiss Jena).

The chemiluminescence of some intermediate species resulted from the photodegradation reaction were analysed with a proper installation,<sup>22,23</sup>. The device for measuring the chemiluminescence consisted of a cuvette placed in a light-tight compartment situated in front of a sensitive photomultiplier. The photocurrent from the photomultiplier was measured directly by a storage oscilloscope. Since the photodegradation of the porphyrin was very rapid, the photocurrent was integrated by charging a  $1\text{-}\mu\text{F}$  condenser coupled between the input of the oscilloscope and ground. To increase the signal to noise ratio, the photons were collected by a six-branched fiber optics instead of an ellipsoidal light reflector and led to the photomultiplier cathode via a synchronising chopper, lens-assembly and filter cutoff-filters. The apparatus was suitable for recording both total light intensity and

spectra. The minimal light intensity with a signal ratio of 1 is  $10^{-16}$  M, approximately 250 photons/s. The photocathode of the multiplier has been cooled to  $-20^{\circ}\text{C}$  and the temperature of the reaction mixture (5 ml) could be regulated within  $\pm 0.1^{\circ}\text{C}$ . Addition of the sample can be carried out via syringe.

The singlet lifetime (radiative lifetime) of the porphyrins were calculated with an integration method, ruled on a ATARI computer.

The formula used was that given by Bowen and Wokes,<sup>32</sup>

$$1/\tau_r = 2900 n^2 \tilde{\nu}_0^2 \int \epsilon d\tilde{\nu} \quad (\tau_r \text{ in seconds}) \quad (1)$$

where  $\int \epsilon d\tilde{\nu}$  is the area under the curve of molar absorption coefficient plotted against wavenumber ;  
 $\tilde{\nu}_0$  is the wavenumber of the maximum of the absorption band;  
 $n$  is the refractive index of the solvent.

The electronic micrograms were achieved with an apparatus Leitz REM -1600 T, (England). For each measurement, the samples were covered with a one Ag conducting silver film and with a fine Pt layer, by evaporation under high vacuum ( $10^{-6}$  torr)<sup>23</sup>.

The X-ray diffraction measurements were achieved with an apparatus HZG-3 Freiberg PM, the X-ray being  $\text{Cu-K } \alpha$ .

Twinned crystals of porphyrins in the form of purple needles were prepared by allowing methanol to diffuse into a saturated of the compound in toluene, to form hexagonal prisms. Some of these crystals could be cleaved into two nontwinned crystal fragments. A suitable nontwinned crystal fragment with approximate dimensions  $0.05 \times 0.075 \times 0.5$  mm was used for the X-ray studies.

### 2.3. Quantum Yield Measurement

Quantum yield of photochemical degradation of the porphyrins upon excitation of the Soret band (420 nm), was determined using ferrioxalate actinometer<sup>21</sup>.

The photodegradation rate of the porphyrins (designated P), was evaluated by optical measurements using  $\epsilon_{420 \text{ nm}}$  (molar absorption coefficient) ( $\text{M}^{-1} \cdot \text{cm}^{-1}$ ), this value being determined independently,<sup>23</sup>.

$$R = \Delta[P] / \Delta t \quad (2)$$

Quantum yield was calculated from the following equation :

$$\Phi = R / I_a \quad (3)$$

Based on Lambert-Beer law, the intensity of absorbed light,  $I_a$  [ $\text{einstein} \cdot \text{l}^{-1} \cdot \text{s}^{-1}$ ] may be expressed as:

$$I_a = I_0 - I = I_0 - I_0 \exp(-\epsilon l [P]) \quad (4)$$

where  $\epsilon$  is the molar absorption coefficient of the photochemically active component of the porphyrin solution at the wavelength of initiating radiation and  $l$  is the effective length of the photoinitiating beam.

### 3.RESULTS AND DISCUSSION

Table 3 shows the main parameters for the photodegradation reaction of the porphyrins (the reaction rate at  $t=0$  ( $V_R^0$  ( $\text{M} \cdot \text{s}^{-1}$ )), the quantum yield ( $\Phi$ ) and the lifetime for the first excited singlet state ( $\tau(s)$ ).

It can be seen that the TXNP derivatives have a photodegradation rate more higher than those from TXPP derivative. The former have a singlet lifetime for the first excited state much smaller than the latter.

Using X-ray diffraction we determined the spatial dimensions of the porphyrin crystals, by means of the interplanar distances ( $\text{\AA}$ ) and the relative intensity of the diffraction maximum ( $I/I_0$  in %),<sup>23</sup>.

In the case of TXPP derivatives the most intensive diffraction maximum ( $I/I_0$  in %), corresponds to an interplanar distance of  $4.688 \text{ \AA}$ , much less than for TXNP derivatives, where this parameter has two values:  $5.56$  and  $4.448 \text{ \AA}$ . From the two values of this parameter we could estimate the distorted spatial orientation of the naphthyl meso-substituents,<sup>23</sup>.

Table 3. The correlation between the Hammett constants and the photochemical parameters of the photodegradation reaction for the meso-substituted porphyrins (solvent dodecanol) \*

Porphyrin	$\Sigma\sigma_x$	$\tau(s)$	$V_{R^0} (M.s^{-1})$	$\Phi \times 10^2$
TAPP	-2.52	3.15	0.7	1.07
THPP	-1.52	2.6	1.3	2.0
TMOPP	-1.3	0.71	2.01	3.09
TMPP	-1.5	0.38	2.4	3.19
TPP	0	0.33	2.5	3.3
TSPP	1.92	0.22	2.9	3.92
TNPP	3.08	0.16	3.2	4.38
THNP	-1.52	2.1	2.89	4.32
TNP	0	2.0	3.4	5.23
TSNP	1.92	1.422	4.76	7.44

\*

$\Sigma\sigma_x$  =the Hammett constants;

$\tau(s)$  =lifetime for the first excited state;

$V_{R^0} (M.s^{-1})$  = reaction rate;

$\Phi \times 10^2$  = quantum yield.

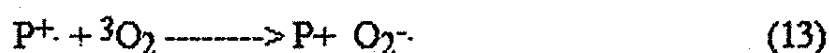
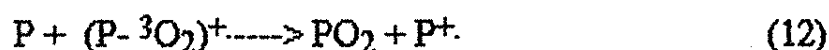
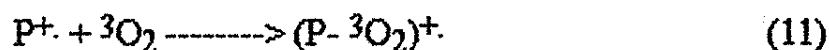
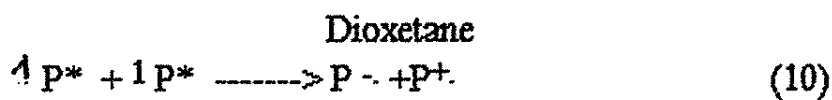
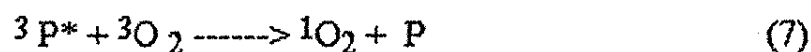
The electronic microscopy data show that the crystal dimensions for TXNP derivatives (50-60  $\mu m$ ) are much less than for TXPP derivatives (200  $\mu m$ ). From all these results we concluded that TXNP derivatives have a more distorted structure than TXPP, in good agreement with our previously published results,<sup>23</sup>.

For both series of porphyrins, the compounds with the Hammett constant smaller than zero, show a less photodegradation because in such cases we have:

- a less intensive hyperconjugation macrocycle-meso-carbons,<sup>29</sup>;
- a smaller inductive effect (from the meso-substituent to the porphyrinic macrocycle) and

-a greater conjugation between the macrocycle and the meso-substituent.

Under these conditions, the photodegradation mechanism for meso-porphyrins (designated P) could be:



To prove the existence of the species that appear in this mechanism we used different spectral methods:

A. From UV-Vis spectra, we could observe the photodegradation of the porphyrin system; some of the initial absorption bands disappeared and new absorption maxima were formed (for example, at TNP, Figure 2). This fact could be an evidence for the photodegradation reaction of these porphyrins which yield to some tetrapyrrolic rings chain (Eq. (12) and Eq. (14)),<sup>23</sup>

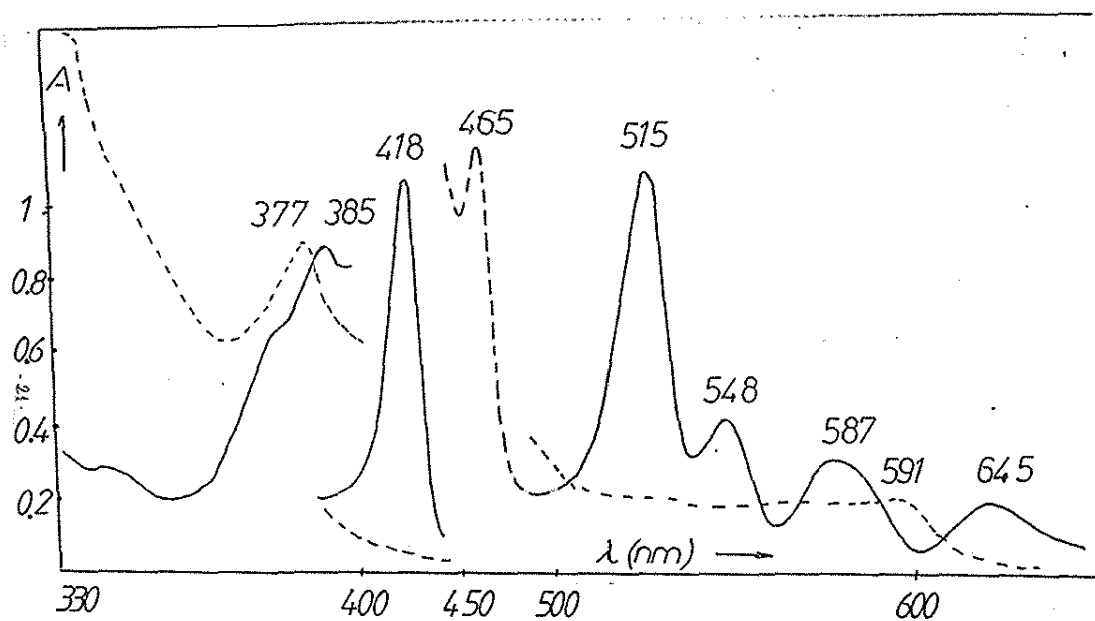


Fig.2. The visible spectra of TNP (—) and its photodegradation product(-----);

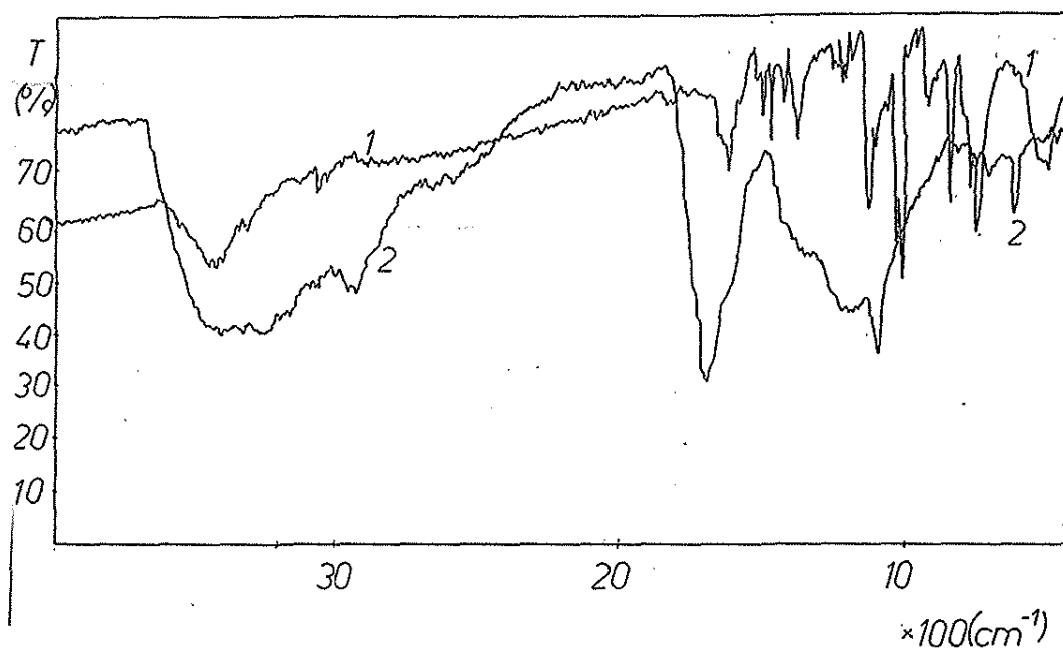


Fig.3. The IR spectra of TNP(1) and its photodegradation product (2);

B. With IR spectroscopy we could observe the ketone products that resulted from the photodegradation reaction (Figure 3). For example, the spectrum for TNP shows the frequency from  $1700\text{ cm}^{-1}$ , attributed to ketone group identified in the photodegradation product. This could be a evidence for Eq.(15);

C. The lability of the meso-substituent is different for different kind of porphyrins: the bond between the meso-substituent and the macrocycle could be break more rapidly for the porphyrins with Hammett positive constant,<sup>28</sup> The mass-fragment for meso-tetra (1-naphtyl)porphyrin is presented in Figure 4, and this could be a evidence for Eq.(15);

D. Wasser and Fuhrhop,<sup>22,23</sup> proposed two ways of the photooxidative destruction of the porphyrins macrocycle; one of these implies a dioxetane state which was detected by chemiluminescence signal in agree with the literature data, Scheme 1.

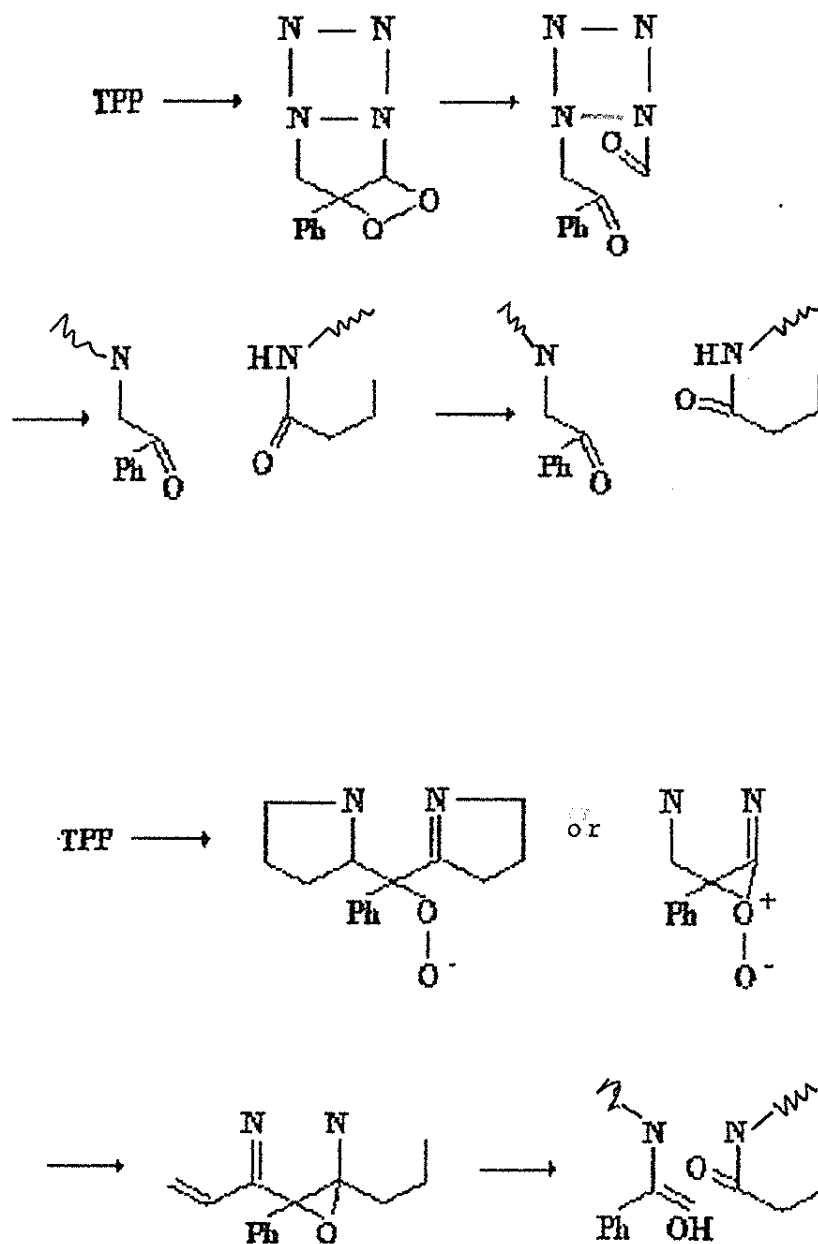
Table 4. The correlation between the Hammett constants, the reaction rate and the ketone and peroxide concentration generated during the photodegradation reaction of the meso-substituted porphyrins\*

Porphyrin	$\Sigma\sigma_x$	$V_R^0$ ( $\text{M.s}^{-1}$ )	Ketone (mg/ml)	Peroxide (mg/ml)
TAPP	-2.52	0.7	5.12	3.13
THPP	-1.52	1.3	7.16	8.90
TMOPP	-1.3	2.01	23.46	17.45
TMPP	-1.5	2.4	34.15	12.15
TPP	0	2.5	43.12	34.00
TSPP	1.92	2.9	44.39	39.05
TNPP	3.08	3.2	50.80	69.07
THNP	-1.52	2.89	23.46	17.45
TNP	0	3.4	23.45	19.78
TSNP	1.92	4.76	46.21	68.00

\*

$\Sigma\sigma_x$  = the Hammett constants;

$V_R^0$  ( $\text{M.s}^{-1}$ ) = reaction rate;

*Photodegradation of Porphyrins*

Scheme 1. The photodegradation products of the porphyrins.

All these species were quantitative detected by spectrophotometric methods,<sup>33</sup>(Table 4). From this table we can observe that the ketone and peroxides concentrations increase in the same way with the Hammett constants and the photodegradation rates for each class of meso-substituted porphyrins (TXPP and TXNP).



Table 5. Quantum yields of  $^1\text{O}_2$  formation, standardized by taking  $\Phi_\Delta$  for all studied porphyrins (TPP or TNP as references).

Porphyrin	$\Phi_\Delta$
TPP(ref)	0.89
TAPP	0.69
THPP	0.70
TMOPP	0.77
TMPP	0.85
TSPP	0.85
TNPP	0.89
TNP(ref)	0.90
THNP	0.78
TSNP	0.80

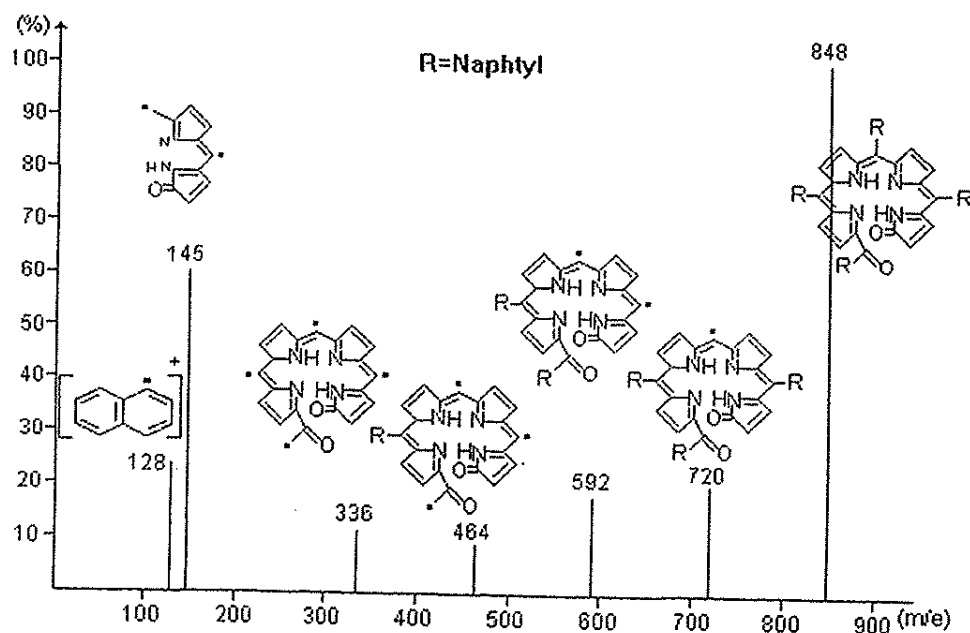


Fig.4. The mass spectrum of the photodegradation product of TNP;

As we know, the porphyrins having no central metal atom had no chemiluminescence activity.<sup>30</sup> But, the photodegradation reaction of these compounds generates dioxetanes as chemiluminescent species. The decomposition of the dioxetane must produce one of the carbonyl products in an excited state. The wavelength maximum of the chemiluminescence is at 430-440 nm, this showing that the decomposition of the dioxetane is a concerted electrocyclic reaction which forms a carbonyl compound in the excited singlet state, and confirms the suggestion that the chemiluminescence is due to the decomposition of 1,2 dioxetanes, Scheme 1.

E. We tried to demonstrate the mechanism of the photodegradation reaction of the porphyrins. As we know, the photodegradation reaction of the porphyrins is preponderantly radical. We have studied the reaction between a meso-tetra(p-X-phenyl)porphyrin and a radical trap, DTBF. The photodegradation rate of TNP, measured at  $t=0$ , is very small than in the absence, Figure 5. This plot is specific for a radicalic reaction (with a proper induction period) and we could observe that the induction period for this plot is bigger than in its absence and than in the presence of only singlet oxygen trap. This fact could be an experimental evidence for the presence of radical states in this reaction. These radical states could come from the porphyrin or from the oxygen during the photodegradation, Eqs. (13), (11), (10), (8), (12);

F. Also, as we know the photodegradation reaction of the porphyrins is a concerted mechanism of singlet oxygen and radical species,<sup>31</sup> The presence of singlet oxygen was demonstrated by means of the reaction between the porphyrin and a singlet oxygen trap, DPBF, Figure 5. The optimum concentration of the scavenger for this photodegradation reaction was  $10^{-5}$  M, as we already published.<sup>31</sup> In the presence of this scavenger, the photodegradation rate of the porphyrin is smaller than in its absence, this conclusion being a proof for the Eq. (7).

The explanations for this observation are:

- the porphyrins have a very strong absorption at 410 nm (and a very big molar absorption coefficient ( $100,000-400,000 \text{ M}^{-1}.\text{cm}^{-1}$ ) by comparison with the scavenger at the same wavelength ( $25,000 \text{ M}^{-1}.\text{cm}^{-1}$ );
- in such conditions the porphyrin will generate less excited states and less singlet oxygen than the scavenger;
- the scavenger will be firstly destroyed, and the porphyrin will be degraded more slower in the presence of the scavenger. From Fig. 5, we can observe that the induction period of the plot  $c_{\text{porphyrin}} \times 10^{-5} \text{ (M)}$  vs.

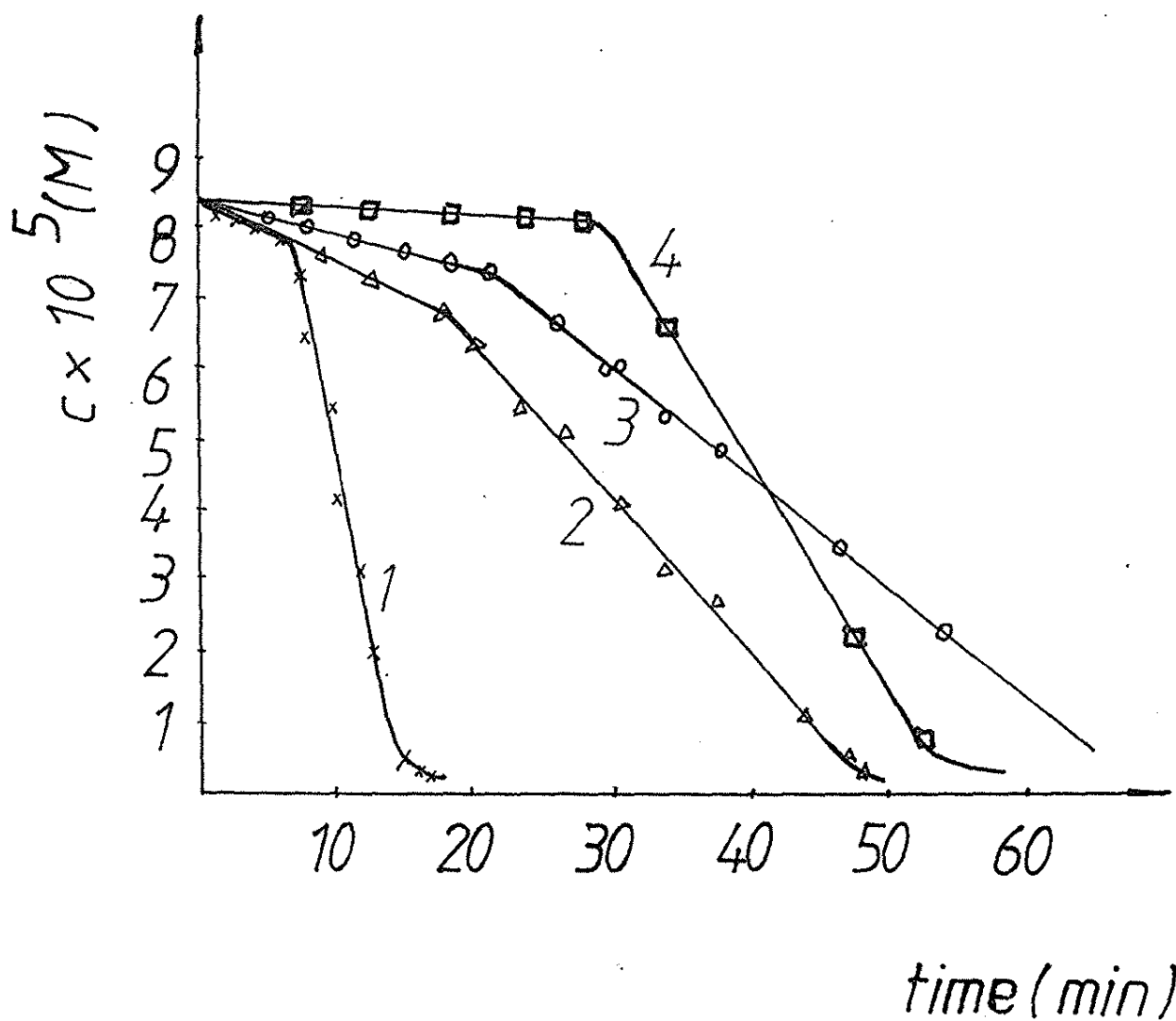
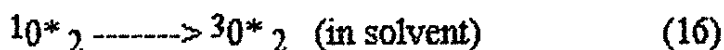


Fig.5. The variation of the porphyrin concentration during its photodegradation reaction in different conditions:

1. TNP  $10^{-5}$  M in benzene;
2. TNP  $10^{-5}$  M in benzene and in the presence of NBT  $10^{-3}$  M;
3. TNP  $10^{-5}$  M in benzene and in the presence of DPBF  $10^{-5}$  M;
4. TNP  $10^{-5}$  M in benzene and in the presence of DTBF  $10^{-4}$  M.

t (min) ,in the presence of the scavenger is two times and half bigger than in its absence. The scavenger will firstly absorb the incident photons and the singlet oxygen generated will attack the porphyrin. This is the well known filter effect of the scavenger,<sup>31</sup>.

In the presence of DPBF, the singlet oxygen is desactivated as follows:



During a continuous irradiation process, the singlet oxygen has been observed from the absorption spectra of DPBF with the formula,<sup>24-27</sup>.

$$-1/\Delta A = 1/\epsilon \cdot l [\text{DPBF}] + (\beta/[\text{DPBF}]) \cdot (1/A) \quad (18)$$

where  $\Delta A$  is the absorption changes of DPBF during the irradiation process measured at 410 nm ( $\epsilon = 25000 \text{ M}^{-1} \cdot \text{cm}^{-1}$  being the molar absorption coefficient and  $l = 1 \text{ cm}$ ;

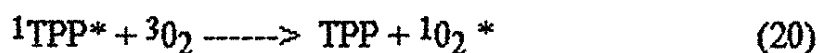
$[\text{DPBF}]$  is the mole number of DPBF oxidated in an unit of volume, where  $A \longrightarrow \infty$ ,  $\beta = k_d/k_r$  ( $k_d$  being the constant for the physical quenching of singlet oxygen, and  $k_r$  being constant for the chemical quenching of singlet oxygen).

The plot of  $1/\Delta A = f(1/A)$  gives us  $\beta$  and  $[\text{DPBF}]$ ;  $\beta$  values are in agreement with the literature data,<sup>26</sup>.

The quantum yield for singlet oxygen generation has been determined by comparison with this value for TPP and TNP, Table 5.

$$\Phi_{\Delta} = \Phi_{\Delta \text{ref}} [\text{DPBF}] / [\text{DPBF}]_{\text{ref}} \quad (19)$$

Where  $[\text{DPBF}]_{\text{ref}}$  and  $\Phi_{\Delta \text{ref}}$  correspond to the unsubstituted meso-porphyrin. Under our conditions, the singlet oxygen is generated by an intermolecular process of energy transfer.



From this table, we can observe that for all porphyrins studied the photodegradation rate changes in the same way as  $\Phi_{\Delta}$ .

The presence of the radical species was evaluated by means of a specific scavenger, 2,6-di-*tert*-butyl-phenol (DTBF).

In the presence of this scavenger, the porphyrin radicals, generated during of the photodegradation reaction (see the eqs. 10-14), are quickly trapped. As we can see from the Figure 5, the induction period for the reaction in the presence of this scavenger is four time bigger than in its absence.

G. The superoxide anion that appeared in Eq. 8 also participates in the photodegradation reaction. To demonstrate this fact, we demonstrated the reaction between the porphyrins and NBT, Figure 5. The conclusion was the same: in the presence of this scavenger the photodegradation rate is smaller than in its absence. So, under these conditions it was evident that the superoxide anion participate in this reaction.

Doing this reaction in the presence of all three scavengers, we have observed that the photodegradation rate is twenty time smaller than in their absence (Figure 5).

Even qualitatively, all these experimental proofs are very useful for the application fields where the porphyrin solutions needs to be very photostable.

H. The eqs. (5) and (6) were considered from the literature data,<sup>34</sup>.

#### 4. CONCLUSIONS

In this paper we tried to elucidate a few of the complex aspects of the photodegradation reaction of the meso-substituted porphyrins.

As we saw, this reaction is a concerted process, the main active species of oxygen being singlet oxygen, superoxide anion, and different excited and radical states derived from the porphyrins and also from oxygen.

An important conclusion is that: when the Hammett constant for the meso-substituent has a positive value, the porphyrin undergoes a faster photodegradation reaction.

In this paper we have summed the results from different spectral technics, the cuantic and experimental photochemical methods to proof the intermediate states which concure to this reaction.

In this paper we have combined the experimental results from different spectroscopic techniques, photochemical methods, and quantum yields to prove the presence of intermediate states that participate in this reaction.

## 5. REFERENCES

1. P. Hambright, *Coord. Chem. Rev.*, 6, 247-258(1971);
2. R.M. Ion and L. Teodorescu, *Rev. Chim.*, 41,4,312-315 (1990).
3. R.M. Ion, L. Teodorescu, C. Mandravel, E. Volanschi and M. Hillebrand, *Rev. Chim.*, 2,129-133(1990).
4. R.M. Ion, L. Ceafalau, F. Moise and A. Iosif, *Anal. Univ. Buc.*, 1,51-58(1992).
5. R.M. Ion, *Rev. Chim.*, 44,11,957-960(1993);
6. R.M. Ion, S. Coca and D. Mardare, *Progr. Catal.*, 1,54-61(1993).
7. R.M. Ion, *Rev. Chim.*, 44,5,431-434(1993);
8. G.S. Cox, D.G. Whitten and G. Gianotti, *Chem. Phys. Lett.*, 67,511-512(1979);
9. M. Shopova, G. Braschiev and T. Ivanov, *Lasers Med. Sci.*, 2,91-96 (1987);
10. R.M. Ion, F. Moise, V. Gazdaru, C. Bercu and V. Badescu, *Progr. Catal.*, 1-2,9-14(1994);
11. R.G. Little, J.A. Anton, P.A. Loach and J.A. Ibers, *J. Heterocycl. Chem.*, 12,343-349(1975);
12. A.M.D'A. Rocha Gonsalves and M.M. Pereira, *J. Heterocycl. Chem.*, 22,931-933(1985);
13. C.M. Badger, R.A. James and R.L. Laslett, *Austr. J. Chem.*, 19,1928-1935 (1964);
14. K. Rousseau and D. Dolphin, *Tetr. Lett.*, 48,4251-4254(1974);
15. J.R. Miller and G.D. Dorough, *J. Amer. Chem. Soc.*, 74,20,3977-3981 (1952).
16. G.D. Dorough and F.M. Huennekens, *J. Amer. Chem. Soc.*, 74,20,3974-3976(1952);
17. R.H. Ball, G.D. Dorough and M. Calvin, *J. Amer. Chem. Soc.*, 68,2278-2281(1946);
18. P. Rothmund and A.R. Menotti, *J. Amer. Chem. Soc.*, 70,1808-1812(1948);
19. G.D. Dorough, J.R. Miller and F.M. Huennekens, *J. Amer. Chem. Soc.*, 73, 4315-4320(1951);
20. A.D. Adler, F. Longo, J.D. Finarelli, J. Golmacher, J. Assour and L. Korsakoff, *J. Org. Chem.*, 32,476(1976).
21. C.A. Parker, "Luminescence of Solutions", Acad. Press, New York(1968), pp.208-214;
22. R.M. Ion and A. Ureche-Fotea, *Rev. Chim.*, 47,11,1064-1072(1996).
23. R.M. Ion, "Ph.D Thesis", (Bucharest University)1994, pp.38-44.

24. P.B. Merkel and D.R. Kearns, *J. Amer. Chem. Soc.*, **97**, 462-463 (1975).
25. C. Tanelian, L. Golder, C. Wolff, *J. Photochem.*, **25**, 117-125 (1984).
26. J.B. Verlhac, A. Gaudemer and J. Kraljic, *Nouv. J. Chim.*, **8**, 6, 401-406 (1984).
27. G. Roissbroich, N.A. Garcia and S.E. Braslavski, *J. Photochem.*, **31**, 37-47 (1985).
28. R.M. Ion and C. Mandravel, *Anal. Univ. Buc.*, **5**, 51-53 (1996).
29. J.A. Shelnutt and V. Ortiz, *J. Phys. Chem.*, **89**, 4733-4739 (1985).
30. M. Motsenbocker, Y. Ichimori and K. Kondo, *Anal. Chem.*, **65**, 397-402 (1993).
31. R.M. Ion, *Roum. J. Biophys.*, **6**, 3-4, 207-214 (1996).
32. E.J. Bowen and F. Wokes, *Fluorescence of solutions*, Longmans Green Co., London, 1953.
33. R.D. Arasasingham and T.C. Bruice, *Inorg. Chem.*, **29**, 1422-1427 (1990).
34. W. Busch, *Ph. D. Thesis*, Stuttgart, 1992.

Dumitru Fatu\* and Maria Muscalu\*\*

\*Department of Physical Chemistry,  
Faculty of Chemistry, University of  
Bucharest, Bul. Carol No. 13.

\*\*Hidrojet Breaza, Str. Grivitei No. 18

## ABSTRACT

In this study thermal analysis has been used to characterize thermal behaviour and oxidation resistance of some nodular cast iron.

One has studied samples of nodular cast iron, in several stages of elaboration, with different chemical compositions. The samples have been heated in air, in the temperature range : 18 - 1000°C and the thermal (TG, DTG and DTA) curves have been recorded.

A group of samples, with low silicon content, shows similar behaviour : a continuous increase of weight, some peaks and exothermal effect up to 850°C. The thermal peaks correspond to iron oxides ( $\text{Fe}_3\text{O}_4$ ,  $\text{FeO}$ ,  $\text{Fe}_2\text{O}_3$ ) formation. At high temperatures ( $T > 850^\circ\text{C}$ ) one can see a decrease of weight and an endothermal effect. A superficial decrease of carbon content by combustion ("decarburization" effect) takes place in the range of high temperatures. The two effects : oxidation-decarburisation depend on the structural changes of cast iron, which take place at high temperatures.

The decarburisation process has been modeled and the kinetical parameters have been determined (reaction order  $n=0.76$ ; activation energy  $E=141.5$  kJ).

Kinetical study of oxidation process has been achieved by nonisothermal methods using two mechanisms : bidimensional transport - for low temperatures and three-dimensional transport through a sphere - for high temperatures. The activation energies have been calculated : 67.7 kJ-for low temperatures and 122.5 kJ-for high temperatures.

## RESUMO

O comportamento térmico de ferros fundidos foi estudado com análise térmica. Amostras de vários ferros fundidos foram aquecidas no intervalo de 18° - 1000°C e curvas de termogravimetria, termogravimetria diferencial e análise térmica diferencial foram determinadas. Foram observados dois efeitos: um de oxidação e outro de decarburização que dependem de mudanças estruturais que acontecem a temperaturas elevadas. Estudos cinéticos do processo de oxidação foram também realizados. À temperaturas baixas foi usado o mecanismo de transporte bidimensional e à temperaturas mais elevadas o transporte tridimensional. A energia de ativação para decarburização é 141,5 kJ e para oxidação é 67.7 kJ para temperaturas baixas e 122.5 kJ para temperaturas altas.



### Introduction

High mechanical properties, good casting properties and special oxidation resistance are the main features of nodular cast iron. Generally nodular cast iron has a good oxidation resistance up to 650°C, higher than that of grey cast iron or low alloy steel<sup>1</sup>.

The oxidation resistance of nodular cast iron is related to nodular shape of graphite and it is dependent on chemical composition and microstructural features of the material.

The nodular shape of graphite is the result of a special treatment of molten metal before casting. It consists of two processes: the addition of a (MgFeSi) alloy ("modification") and the addition of (FeSi) alloy ("postmodification" or "inoculation")<sup>2,3</sup>

One has studied nodular cast iron (F<sub>1</sub> - F<sub>3</sub>) samples after modification process, without ferro-silicon addition and the F<sub>4</sub> sample, after modification and inoculation (final stage of elaboration).

The samples of nodular cast iron were powders, resulted by breaking some plates, with "white" structure, the particles having no more than 0,5 mm. These plates have a rapid solidification when cooling and therefore the structure is "white" (iron carbide Fe<sub>3</sub>C = cementite is the main structural component).

Chemical composition of the samples is given in the table 1.

Table 1. Chemical composition of cast iron samples

Sample	C	Si	Mn	P	S	Cu	Mg	C.E.
F <sub>1</sub>	3.78	0.74	1.20	0.020	0.026	0.026	0.027	4.03
F <sub>2</sub>	3.79	0.88	1.25	0.021	0.024	0.370	0.028	4.09
F <sub>3</sub>	3.94	1.45	1.00	0.021	0.034	0.046	0.026	4.43
F <sub>4</sub>	3.50	2.80	0.50	0.021	0.032	0.450	0.050	4.44

C.E. = carbon equivalent =  $C \% + 1/3 (Si + P) \%$

Primary solidification of hypoeutectic samples (F<sub>2</sub>, F<sub>3</sub>) has as its result austenitic dendrites and ledeburitic eutectic (with carbon content 4.3%), in accordance with Fe-Fe<sub>3</sub>C diagram. When cooling goes on, the austenite turns into pearlite and secundar cementite. The microstructure of these samples consists of: acicular crystals of cementite and some pearlite. The microstructure of hypereutectic samples (F<sub>3</sub>, F<sub>4</sub>) consists of primary cementite and ledeburite<sup>4</sup>.

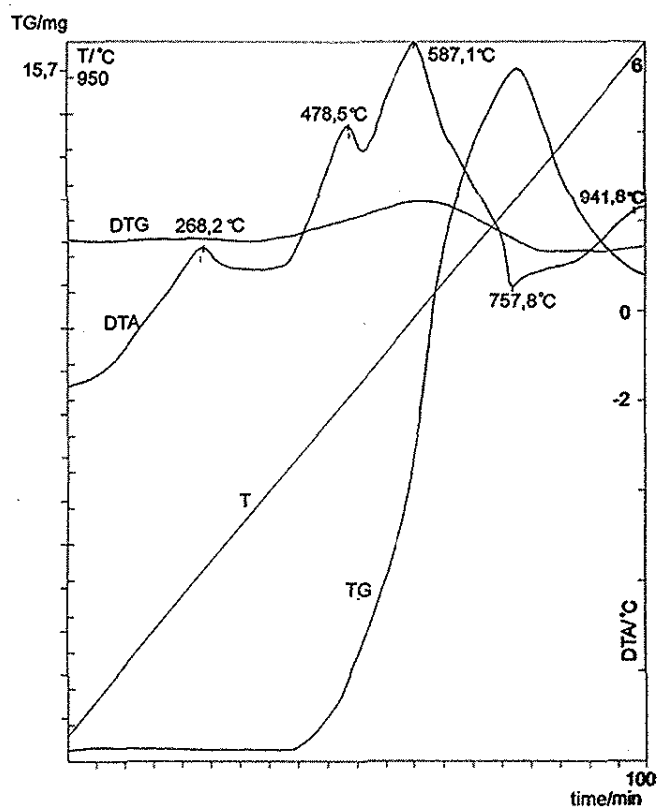
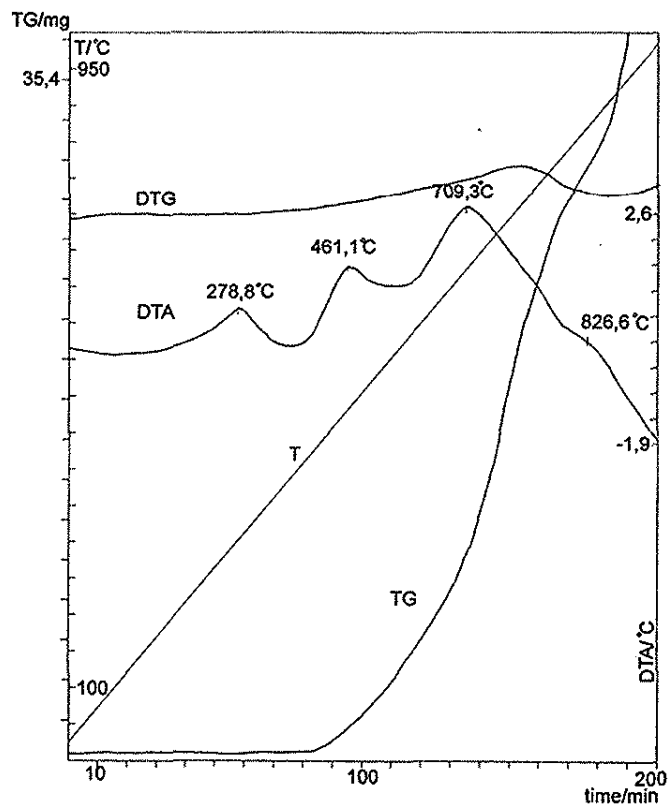
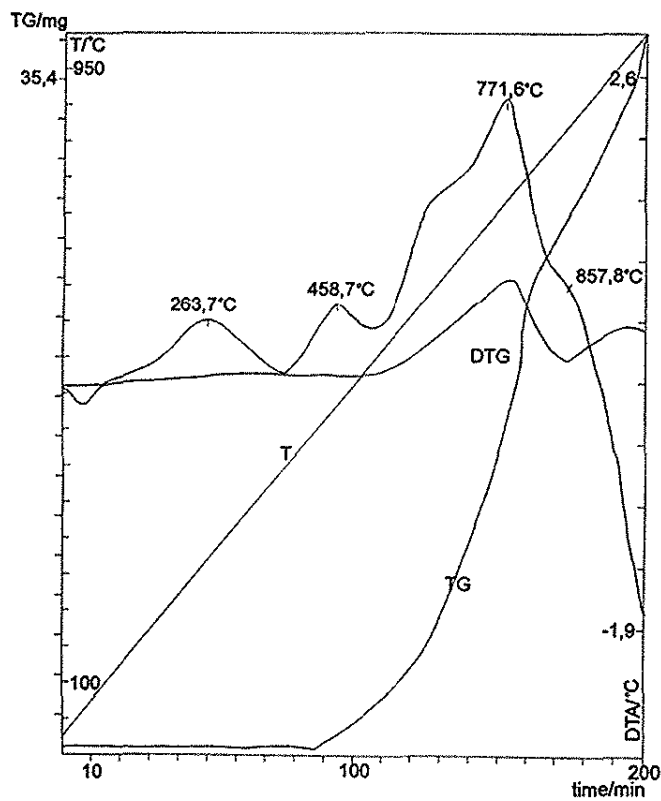
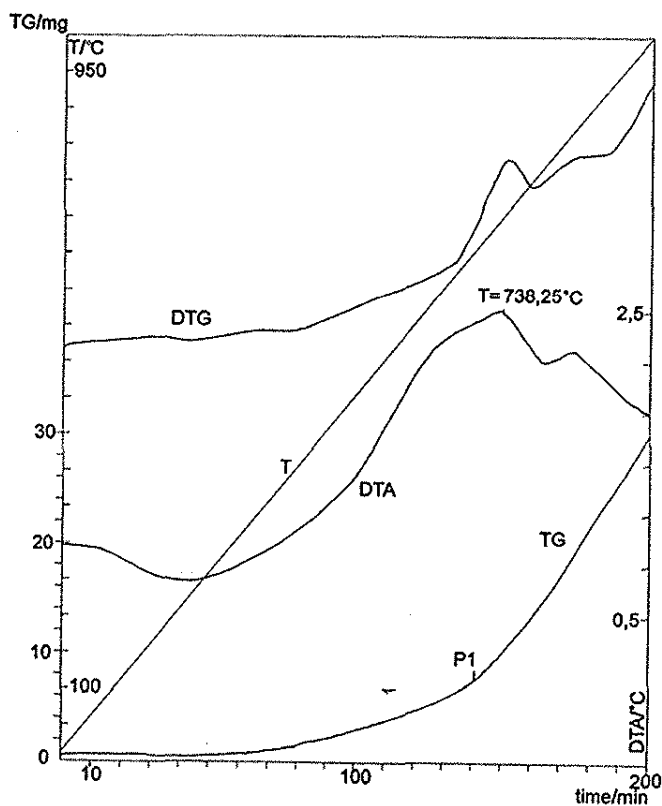
### Experimental

The powdered samples of cast iron have been heated from room temperature to 1000°C with a linear heating rate of 10°C/min. The experimental conditions and total weight variation are given in the table 2.

The instrument used was a derivatograph MOM Paulik Paulik C Budapest with null thermobalance and air statical atmosphere of the sample chamber; reference material was Al<sub>2</sub>O<sub>3</sub>.

Fig. 1-4 give the thermal curves for F<sub>1</sub> - F<sub>4</sub> cast iron samples.

Besides that, the powders and the corresponding plates have been kept in a furnace, at the temperatures, which are peaks on thermal curves. Then the samples have been examined by a microscope.

Fig.1. Thermal curves for F<sub>1</sub> sampleFig.2. Thermal curves for F<sub>2</sub> sampleFig.3. Thermal curves for F<sub>3</sub> sampleFig.4. Thermal curves for F<sub>4</sub> sample

## Results and Discussion

The  $F_1 - F_3$  samples have a similar behaviour, while the  $F_4$  sample shows a different behaviour.

Table 3 gives complete data from thermal curves : temperatures of interest, the weight variation  $\Delta m$  and the temperature variation  $\Delta T$ .

A. The result of linear heating of  $F_1 - F_3$  samples is a continuous increase of the weight up to 850 °C, then a decrease of the weight takes place. The DTA curves show an exothermal effect up to about 850°C and some thermal peaks.

-At low temperature (260-270°C) a change without weight variation takes place, perhaps an oxidation of nonmetallic components (S,P).

-At the temperature of about 460°C - the iron oxidation begins, the iron saturated with oxygen and  $Fe_3O_4$  occur, according with Fe-O diagram; the exothermal effect and the weight variation increase.

-At the temperature  $T > 570$  °C, the iron FeO oxide occurs;

-The oxidation process proceeds, the next important temperature is 750°C; at this temperature a large amount of  $Fe_2O_3$  occurs;

-The maximum oxidation effect is at the temperature  $T > 820$ °C- for  $F_2$  and  $F_3$  samples.

The differences between  $F_1 - F_3$  samples are related to silicon element. So  $F_2$  and  $F_3$  samples, with higher silicon content, have the same peaks at higher temperatures; the end of the exothermal effect is also at higher temperatures : 826.6°C - for  $F_2$  sample, 857.8°C - for  $F_3$  sample and 757.8°C for  $F_1$  sample.

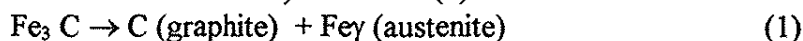
On the other hand microscopical observations are given below :

-At low temperature - the samples do not show structural changes.

-At the temperature of 460°C one can see a thin oxide layer on the surface of the powders; no structural changes of the plates occur.

-For the temperature range 600-700°C : the amount of oxide enlarges; concerning microstructure of the plates - the particles of cementite become smaller.

-An important structural change of  $F_1$  sample takes place at the temperature of 941°C (the cementite transformation)<sup>5</sup> - reaction (1) :



The austenite phase is stable only at high temperatures; when cooling it will turn into pearlite and ferrite. The final microstructure of  $F_1$  sample consists of : graphite (nodular shape), pearlite and ferrite.

-The  $F_2$  plate, kept at the temperature of 830°C, shows some transformation concordant with reaction (1). The microstructure consists of : graphite and a few sections with pearlite and ferrite.

The powdered samples show an intensive tendency to sinter at high temperatures; the graphite appearance favours it.

At the same time we must take into account superficial decrease of carbon content produced by carbon combustion (for  $T > 870$ °C). This "decarburisation" effect leads to a loss of weight which can exceed the increase of weight resulted by iron oxidation.

Table 2. Experimental conditions for thermal analysis of nodular cast iron samples

Sample	Temperature range (°C)	Heating time (min)	Heating rate (°C/min)	Total weight variation (mg)
F <sub>1</sub>	18 - 1000	100	10	15.25
F <sub>2</sub>	18 - 1000	200	10	37.07
F <sub>3</sub>	18 - 1000	200	10	36.34
F <sub>4</sub>	17 - 1000	200	10	30.00

Table 3. Data from thermal curves

Sample	T (°C)	268.19	478.48	587.06	757.75	941.83	
F <sub>1</sub>	ΔT (°C)	+0.11	+3.93	+5.98	+1.50	-2.52	
	Δm . 10 <sup>3</sup> (g)	0	2.0	7.3	15.3	11.3	
Sample	T (°C)	278.84	461.06	620.01	709.31	826.61	
F <sub>2</sub>	ΔT (°C)	+0.86	+1.41	+1.60	+2.46	+0.69	
	Δm . 10 <sup>3</sup> (g)	0	1.8	7.6	15.4	26.4	
Sample	T (°C)	263.73	458.78	670.81	771.62	857.84	
F <sub>3</sub>	ΔT (°C)	+0.42	+0.59	+1.35	+1.83	+2.41	
	Δm . 10 <sup>3</sup> (g)	0	1.1	5.8	10.3	17.0	
Sample	T (°C)	326.36	691.51	738.25	794.53	822.32	919.68
F <sub>4</sub>	ΔT (°C)	+0.02	+2.33	+2.51	+1.99	+2.14	+1.54
	Δm . 10 <sup>3</sup> (g)	0	6.0	9.3	13.7	15.8	24.0

Table 4. Thermal data for F<sub>1</sub> sample

T (°C)	$\Delta m \cdot 10^3$ (g)
749.1	15.25
758.4	15.23
767.2	15.16
777.3	15.03
786.6	14.87
796.0	14.70
806.6	14.51
816.1	14.30
825.2	14.07
834.8	13.86
844.2	13.62
854.2	13.37

863.6	13.12
873.1	12.82
882.9	12.51
893.1	12.20
902.3	11.89
911.8	11.60
921.1	11.37
931.1	11.20
939.4	11.06
950.5	10.99
959.6	10.95

The speed of decarburisation process of nodular cast iron depends on two factors: dissolution of graphite into the matrix and carbon diffusion through the matrix to surface<sup>1</sup>.

The combination of two effects : oxidation-decarburisation is more interesting in the case of F<sub>1</sub> sample. We have determined kinetical parameters of the process for the last section of TG curve (fig. 1), where a loss of weight, by carbon combustion, took place (from 15,5 mg at T= 755.5°C to 10.95 mg at T=958.08°C)

Table 4 gives the data from TG and T curves for F<sub>1</sub> sample. A program (in Basic language) allowed to determine kinetical parameters. The pattern of a sphere which contracts, based on the equation (2), has been used<sup>6</sup>.

$$1 - (1 - \alpha)^{1/3} = kt \quad (2)$$

$$\frac{d\alpha}{dt} = k (1 - \alpha)^{2/3} \quad (3)$$

where  $\alpha$  is the degree of reaction;  $t$  is time and  $k$ ,  $k$  are constant.

The following kinetical parameters have been obtained :

-activation energy - 141.5 kJ/mol;

-reaction order -0.76;

-preexponential factor - 199.5 s<sup>-1</sup>.

**B.** The F<sub>4</sub> sample, with a typical chemical composition of nodular cast iron, has a particular oxidation resistance.

The DTA curve shows an important peak at T= 738.25°C; the oxidation practically begins at T= 525°C and it proceed slowly up to T= 715.6°C. The P1 point corresponding to T=715.6°C, delimits two sections on TG curve, which are characterized by different oxidation kinetics.

Nodular cast iron oxidation has been studied using nonisothermal kinetics of heterogeneous reactions, which involve solid phases. They are described by special equations (without reaction order)<sup>7,8</sup>.

Integral kinetical equation for nonisothermal conditions, using Coats-Redfern approximation, is :

$$\log \frac{F(\alpha)}{T^2} = \log \frac{AR}{aE} \left( 1 - \frac{2RT}{E} \right) - \frac{E}{2,303R} \cdot \frac{1}{T} \quad (4)$$

where  $F(\alpha)$  is integral of conversion, given by :

$$F(\alpha) = \int_0^{\alpha} \frac{d\alpha}{f(\alpha)} \quad (5)$$

where  $\alpha$  is the degree of conversion ;  $f(\alpha)$  is a function which shows the dependence of the reaction rate on the conversion degree;

$A$  is preexponential factor ;  $E$  is activation energy;

$a = dT/dt$  is constant heating rate;

$T$  is absolute temperature;  $R$  is perfect gas constant.

Table 5. Thermal data for F<sub>4</sub> sample - part I

No.	T (°C)	(1/T).10 <sup>4</sup> (K <sup>-1</sup> )	$\Delta m \cdot 10^4$ (g)	-log [F( $\alpha$ )/T <sup>2</sup> ]	$\alpha$
1.	38.9	15.2	0.13		0.00044
2.	39.6	14.9	0.53		0.00176
3.	40.8	14.7	1.00		0.00334
4.	41.5	14.5	1.64		0.0055
5.	42.3	14.3	2.35		0.0078
6.	43.1	14.1	3.19		0.0106
7.	44.0	13.9	4.02		0.0130
8.	454.7	13.7	4.98		0.0170
9.	464.4	13.6	5.97		0.0200
10.	474.3	13.4	7.09		0.0240
11.	484.5	13.2	8.38		0.0280
12.	494.4	13.0	9.78		0.0325
13.	505.0	12.9	11.05	8.272	0.0370
14.	514.9	12.7	11.94	8.270	0.0400
15.	524.9	12.5	14.71	8.246	0.0490
16.	534.7	12.4	17.03	8.200	0.0570
17.	544.6	12.2	18.96	8.160	0.0632
18.	554.4	12.1	21.56	8.146	0.0718
19.	564.8	11.9	24.28	8.097	0.0809
20.	574.6	11.8	27.33	8.034	0.0910
21.	584.7	11.7	30.24	7.987	0.1010
22.	594.5	11.5	33.24	7.933	0.1110
23.	604.7	11.4	36.54	7.850	0.1220
24.	614.8	11.3	39.96	7.830	0.1330
25.	624.9	11.1	43.44	7.788	0.1450
26.	635.0	11.0	46.80	7.740	0.1560
27.	645.2	10.9	50.13	7.695	0.1670
28.	655.3	10.8	53.48	7.652	0.1780
29.	665.3	10.7	56.95	7.613	0.1900
30.	675.4	10.5	60.60	7.578	0.2020
31.	685.6	10.4	64.41	7.535	0.2150
32.	695.6	10.3	68.41	7.495	0.2280
33.	705.5	10.2	72.88	7.449	0.2430

Table 6. Thermal data for F<sub>4</sub> sample - part II

No.	T (°C)	(1/T).10 <sup>4</sup> (K <sup>-1</sup> )	Δm .10 <sup>4</sup> (g)	-log [F(α)/T <sup>2</sup> ]	α
34.	715.6	10.1	78.01	7.399	0.260
35.	725.7	10.0	84.16	7.801	0.281
36.	736.0	9.9	91.15	7.730	0.304
37.	746.2	9.8	98.96	7.630	0.329
38.	756.1	9.7	107.27	7.580	0.358
39.	766.2	9.6	115.32	7.510	0.384
40.	776.2	9.5	123.41	7.440	0.411
41.	786.3	9.4	131.00	7.400	0.437
42.	796.4	9.3	138.39	7.350	0.461
43.	806.7	9.25	146.03	7.280	0.487
44.	816.8	9.2	153.98	7.240	0.513
45.	826.9	9.1	162.30	7.200	0.541
46.	836.9	9.0	170.88	7.140	0.570
47.	847.1	8.9	179.58	7.085	0.598
48.	857.0	8.8	188.33	7.029	0.628
49.	867.2	8.75	196.89	6.977	0.656
50.	877.2	8.7	205.32	6.930	0.684
51.	887.6	8.6	213.56	6.890	0.712
52.	897.8	8.55	221.81	6.850	0.739
53.	908.1	8.5	230.12	6.800	0.767
54.	918.4	8.4	238.77	6.750	0.796
55.	928.4	8.3	248.11	6.680	0.827
56.	938.7	8.25	258.28	6.630	0.861
57.	949.0	8.2	269.42	6.545	0.898
58.	959.0	8.1	281.83	6.450	0.939
59.	969.3	8.0	295.41	6.263	0.985

Table 7. Kinetic parameters for F<sub>4</sub> sample

Temperature range (°C)	E (kJ/mol)	A (s <sup>-1</sup> )
385.9 - 715.6	67.7	3803.8
715.6 - 969.3	122.5	2913.3

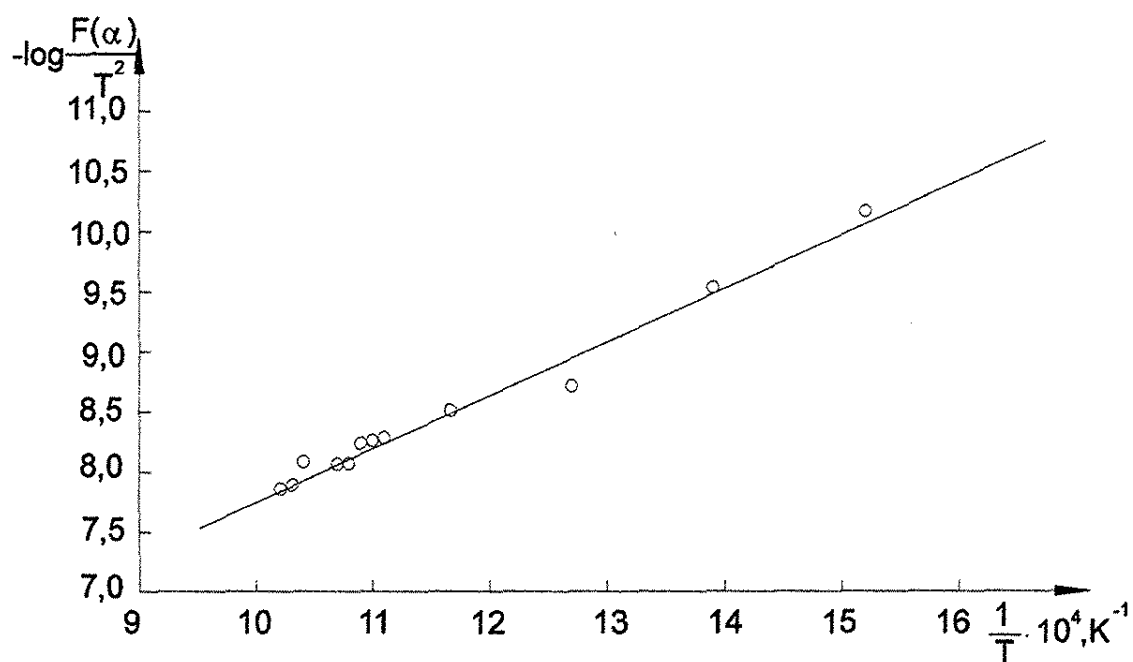


Fig.5. The dependence  $[\log \frac{F(\alpha)}{T^2}, \frac{1}{T}]$  for low temperatures (Jander equation)

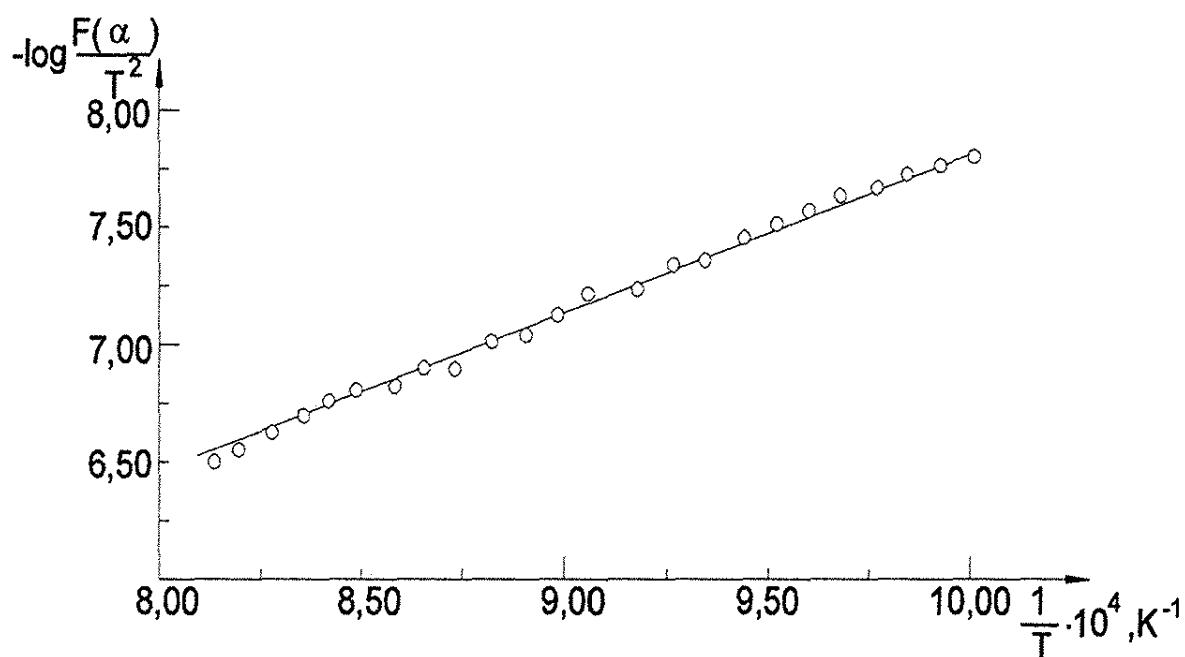


Fig.6. The dependence  $[\log \frac{F(\alpha)}{T^2}, \frac{1}{T}]$  for high temperatures (Jander equation)



The plotting of the dependence  $\left[ \log \frac{F(\alpha)}{T^2}, \frac{1}{T} \right]$  is a straight line, which gives

Arrhenius parameters (A and E).

The model of reaction controlled by diffusion and two mechanisms have been used :

- a) Bidimensional transport ;
- b) Threedimensional transport through a sphere.

The integral of conversion is:

$$a) F(\alpha) = \alpha + (1 - \alpha) \ln(1 - \alpha) - \text{for bidimensional transport} \quad (6)$$

$$b) F(\alpha) = \frac{3}{2} \left\{ \frac{1}{2} [1 + (1 - \alpha)^{2/3}] - (1 - \alpha)^{1/3} \right\} \quad (7)$$

-for threedimensional transport.

The corresponding equations are:

$$a) \log \frac{1}{T^2} [\alpha + (1 - \alpha) \ln(1 - \alpha)] = \log \frac{AR}{aE} (1 - \frac{2RT}{E}) - \frac{E}{2,303R} \cdot \frac{1}{T} \quad (8)$$

$$b) \log \frac{3}{T^2} \left\{ \frac{1}{2} [1 + (1 - \alpha)^{2/3}] - (1 - \alpha)^{1/3} \right\} = \log \frac{AR}{aE} (1 - \frac{2RT}{E}) - \frac{E}{2,303R} \cdot \frac{1}{T} \quad (9)$$

Relation (9) is Jander equation.

Tables 5,6 give data from thermal curves : the weight variation and the degree of conversion.

First we have tried to describe oxidation kinetics using Jander equation for the two temperature range (fig.5,6). One can see that Jander equation better describe the oxidation kinetics for the second temperature range ( $T = 715,6 \dots 1000^\circ\text{C}$ ). This equation is not appropriate for the first temperature range, where small oxidation takes place.

The model of bidimensional transport is better for the first temperature range ( $T < 715,6^\circ\text{C}$ ) - fig.7.

Kinetical parameters calculated using the two mechanisms are given in the table 7

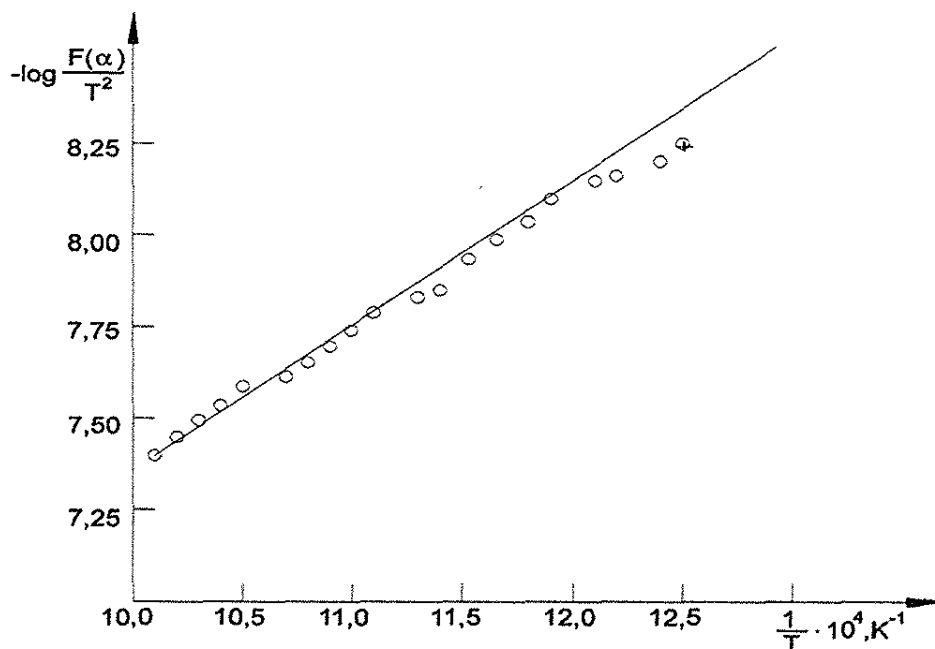


Fig.7. The dependence  $\left[ \log \frac{F(\alpha)}{T^2}, \frac{1}{T} \right]$  for low temperatures (bidimensional transport)

### Conclusions

1. Thermal methods of analysis and microscopical observations have been used to characterize some less studied features of nodular cast iron : thermal behaviour and oxidation resistance.

The study is an application of thermal analysis based on heating curves ; usually cooling curves are recorded for metallurgical studies of iron-base alloys.

2. Generally all the samples (which are nodular cast iron melts) have a good oxidation resistance up to 600-670°C. This property depends on silicon content. The ( $F_1 - F_3$ ) samples, modified with magnesium alloy and without ferro-silicon addition, show similar features on thermal curves: some thermal peaks, corresponding to iron ( $Fe_3O_4, FeO, Fe_2O_3$ ) oxides. The  $F_1$  sample (with lower silicon content) has smaller oxidation resistance.

The  $F_4$  sample, having specific nodular cast iron composition, shows a good oxidation resistance up to 715,6°C.

3. The decarburisation process must be taken into account at high temperature ( $T > 870^\circ C$ ). It is correlated with phase transformation (reaction 1).

4. The kinetics of decarburisation and oxidation have been modeled and the kinetical parameters of these processes have been calculated.

The model of a sphere which contracts has been used for decarburisation process; two mechanisms (bidimensional transport and threedimensional transport through a sphere) have been used to describe oxidation kinetics of nodular cast iron, as a function of temperature.

### References

1. Sofroni, L., Stefanescu, D. M., Vincenz, C., Nodular Cast Iron, Technical Publishing House Bucharest, 1978.
2. Sofroni, L., Stefanescu, D. M., Modified Cast Iron, Technical Publishing House, Bucharest, 1971.
3. Taloi, D., Orea, F., Constantin, I., Roman, R., Metallurgic Process Theory, Didactical and Pedagogical Publishing House, Bucharest, 1978.
4. Gadea, S., Petrescu, M., Physical Metallurgy and Study of Metals, Didactical and Pedagogical Publishing House, Bucharest, 1981.
5. Geru, N., Physical Metallurgy, Didactical and Pedagogical Publishing House, Bucharest, 1981.
6. Murgulescu, I., G., Segal, E., Oncescu, T., Chemical Kinetics and Catalysis, Academy Publishing House, Bucharest, 1980.
7. Segal, E., Fatu, D., Introduction to Nonisothermal Kinetics, Academy Publishing House, Bucharest, 1983.
8. Charlsley, E., L., Warrington S., B., Thermal Analysis (Techniques and Applications), Royal Society of Chemistry, Cambridge, 1992.

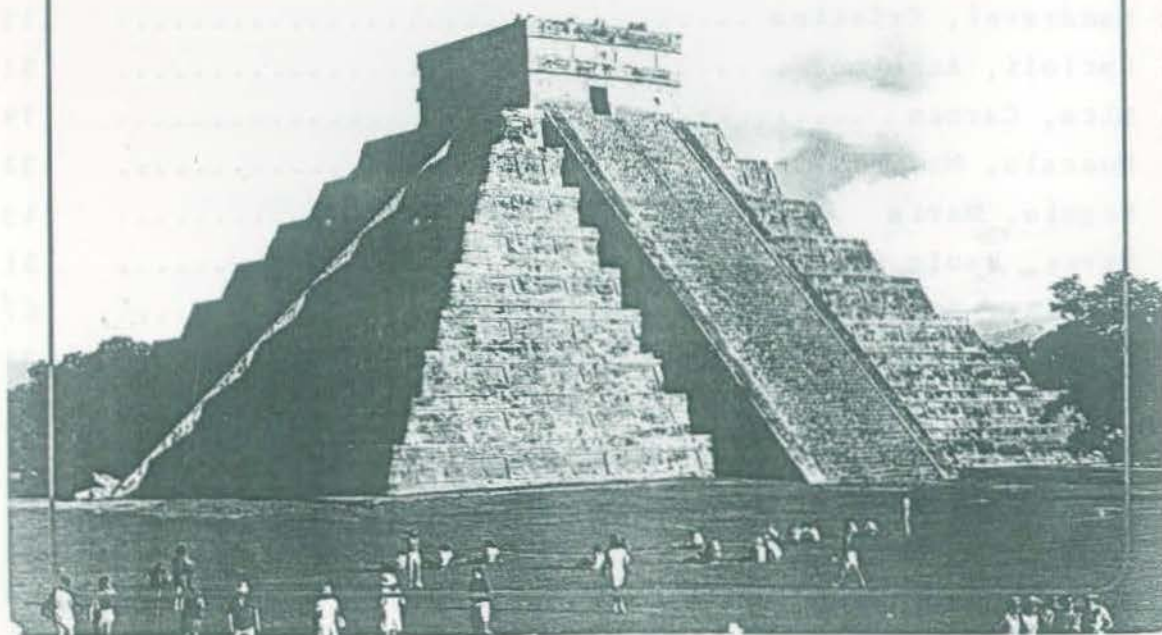
## AUTHOR INDEX / ÍNDICE DE AUTORES

Albinescu, D. ....	87
Arsene, Cecilia ....	79
Badicu, Niculina ....	43
Branco, Pércio de Moraes ....	51
Calinescu, Mirela ....	21
Cârcu, Viorel ....	43,67
Carneiro, Manuel ....	7
Cascaval, Dan ....	97
Ciobanu, Adalgiza ....	87
Emandi, Anca ....	21
Fatu, Dumitru ....	131
Fiedler, Haidi D. ....	7
Garcia, Rosangela G. ....	35
Ionescu, Lavinel G. ....	1
Ion, Rodica Mariana ....	111
Júnior, Arnaldo D.S. ....	35
Kriza, Angela ....	67
Maior, Ovidiu ....	43
Mandravel, Cristina ....	111
Matioli, Anselmo ....	51
Mita, Carmen ....	79
Muscalu, Maria ....	131
Negoiu, Maria ....	43
Neves, Paulo César Pereira das ....	51
Nicolae, Anca ....	67
Nozaki, Jorge ....	35
Oniscu, Corneliu ....	97
Onofrei, Tinca ....	79
Paruta, Lidia ....	21
Rodrigues, Dina G. ....	35
Rosu, Tudor ....	21,43,67
Teixeira, Elba C. ....	7
Tudose, Radu ....	97
Zalaru, Florica ....	87
Zalaru, Christina ....	87



MEXICO CITY. CRISTOPHER COLUMBUS SQUARE AND LA REFORMA BOULEVARD.  
CIDADE DO MÉXICO. PRAÇA CRISTOBAL COLON E PASEO DE LA REFORMA.

## *Chichen-Itzá*



THE AMAZING EQUINOX NATURAL SPECTACLE: THE SERPENT COMING DOWN THE  
PYRAMID. CHICHEN-ITZÁ, YUCATÁN, MEXICO.

O ASSOMBROSO ESPETÁCULO NATURAL DO EQUINÓCIO: A SERPENTE DESCENDO  
A PIRAMIDE. CHICHEN-ITZÁ, YUCATÁN, MÉXICO.

# SOUTHERN BRAZILIAN JOURNAL OF CHEMISTRY

ISSN 0104-5431

The *SOUTHERN BRAZILIAN JOURNAL OF CHEMISTRY* is an international forum for the rapid publication of original scientific articles dealing with chemistry and related areas. At the present there are no page charges and the authors will receive twenty five free reprints of their papers.

## SPECIAL COMBINATION OFFER FOR NEW SUBSCRIBERS!

### SUBSCRIPTION INFORMATION

PRICE: Brazil and Latin America: US\$ 35.00 per issue.

Other Countries: US\$ 50.00 per issue, including  
air mail delivery.

Persons or institutions outside Brazil should send  
subscription fee payable to Dr. L. G. Ionescu, c/o SBJC  
8532 Howard Circle, Huntington Beach, California, USA  
92647

---

### ORDER FORM

- ☐ Please enter my subscription for \_\_\_\_\_ issues of  
Southern Brazilian Journal of Chemistry.
- ☐ Please send me \_\_\_\_\_ copies of the Southern Brazilian  
Journal of Chemistry Vol. 1,2,3,4,5,6 (1993-1998)  
(Circle desired copies.)
- ☐ I enclose a check or money order in the amount of \$ \_\_\_\_\_
- ☐ Please send me a Pro Forma Invoice for the above  
order.

### SOUTHERN BRAZILIAN JOURNAL OF CHEMISTRY

Lavinel G. Ionescu, B.S., M.S., Ph.D., Editor  
Caixa Postal 15032, Agronomia  
Porto Alegre, RS BRASIL 91501-970

TEL. 55 51 485-1820 FAX 55 51 320-3612 or 55 51 477-1313

EMail: LGIPUCRS @ MUSIC.PUCRS.BR  
LAVINEL @ MOZART.ULBRA.TCHE.BR



## INFORMATION FOR AUTHORS

The Southern Brazilian Journal of Chemistry - SBJC will publish review articles, original research papers and short communications dealing with chemistry and interdisciplinary areas such as materials science, biotechnology, bioengineering and other multidisciplinary fields.

Articles report the results of a complete study. They should include an Abstract, Introduction describing the known art in the field Experimental or Materials and Methods, Results and Discussion, Acknowledgments (when appropriate) and References.

Short Communications should be limited to 1500 words, including the equivalent space for figures and/or tables and should include an Abstract and concise Experimental.

Manuscripts may be submitted on-line or in triplicate (original and two copies by registered mail) and are received with the understanding that the original has not been submitted for publication elsewhere. It is implicit that all the persons listed as authors have given their approval for the submission of the paper and that permission has also been granted by the employer, when necessary.

Manuscripts must be written in American or British English, single spaced, on A4 sheets (21 cm x 29.5 cm) and one side only and should be numbered beginning with the title page. Type must be 12 Arial or Times New Roman.

Margins of at least 3 cm should be left at the top and bottom and both sides of each page. The first page of the paper should contain only the title of the paper, the name(s) and addressees of the author(s), an abstract of not more than 250 words and 4-8 keywords. We reserve the right to translate the abstract in Portuguese. Abstracts are required of all papers including reviews and short communications.

Figures and Tables with short explanatory titles, each on a separate sheet, should be adequate for direct reproduction and identified in pencil on the back of each page by Arabic numerals, corresponding to the order they appear in the manuscript. Tables and Figures (BMP or JPG format) may also be included directly in the text when convenient and the article may submitted in a quasi-final form in order to facilitate editorial work.

References should be numbered in the sequence they appear in the text, cited by superior numbers and listed at the end of the paper in the reference section in the numerical order they appear in the text. The style for references is shown below:

1. L. G. Ionescu and D. S. Fung, *J. Chem. Soc. Faraday Trans. I*, 77, 2907-2912 (1981).
2. K. L. Mittal, Ed., "*Solution Chemistry of Surfactants*", Plenum Press, New York (1984), Vols. 1-3, pp. 1-2173.

IUPAC Rules should be used for the name of chemical compounds and preference should be given to 51 units.

Authors are invited to send manuscripts by registered air mail to the EDITOR - SBJC, C.P. 15032, Agronomia, Porto Alegre, RS BRASIL 91501, or by e-mail to [lavinel@ibest.com.br](mailto:lavinel@ibest.com.br) or [lavinel@pop.com.br](mailto:lavinel@pop.com.br).

**VISIT OUR SITE:** <http://www.sbjchem.he.com.br>



# SCIENCO SOUTHERN BRAZILIAN JOURNAL OF CHEMISTRY

ISSN 0104-5431

The *SOUTHERN BRAZILIAN JOURNAL OF CHEMISTRY - SCIENCO* publishes original research articles in chemistry and related interdisciplinary areas and is intended to fill a gap in terms of scientific information for Southern Brazil.

Occasionally the journal will include review papers and articles dealing with chemical education and philosophy and history of science. It will be published mainly in English, with abstracts in Portuguese and only occasional papers in other languages. At the present there are no page charges and the authors will receive twenty five reprints of their papers free of charge.

We have set high standards for the articles to be published by ensuring strong but fair refereeing by at least two reviewers. We hope that this journal will provide a forum for dissemination of high quality research in chemistry and related areas and are open to any questions and suggestions.

The Editor

## SUBSCRIPTION INFORMATION

Brazil and Latin America:  
US\$ 35.00 per issue.

Other Countries: US\$ 50.00 per issue,  
including air mail delivery. Persons or  
institutions outside Brazil should send  
subscription fee payable to Dr. L. G. Ionescu,  
c/o SBJC, 8532 Howard Circle, Huntington Beach,  
California, USA 92647

## MAILING ADDRESS

*SOUTHERN BRAZILIAN JOURNAL OF CHEMISTRY - SBJC*  
Lavinel G. Ionescu, B.S., M.S., Ph.D., Editor  
C.P. 15032, Agronomia  
Porto Alegre, RS BRASIL 91501-000  
Tel. (051) 485-1820 FAX (051) 339-1564

## FINANCIAL SUPPORT

SARMISEGETUSA RESEARCH GROUP

SANTA FE, NEW MEXICO, U.S.A.



Endless Column, 1937, cast iron  
CONSTANTIN BRĂNCUȘI